BSc. Andreas Schranzinger

Modeling of Long-Fiber-Reinforced Composites in ABAQUS

Master Thesis

submitted in fulfillment of the requirements for the degree of
Diplom-Ingenieur (Dipl. Ing.)
Master of Science (MSc.)

Master's program Mechanical Engineering
at
GRAZ UNIVERSITY OF TECHNOLOGY

Supervisor:
Univ.-Prof. Dipl.-Ing. Dr. mont. Thomas Antretter
Institute for Mechanics
MONTAN UNIVERSITY OF LEOBEN

Graz, October 2014

In collaboration with:

MONTAN UNIVERSITY OF LEOBEN

Institute for Mechanics

Franz-Josef-Strasse 18

A-8700 Leoben

Contact:

Univ.-Prof. Dipl.-Ing. Dr. mont. Thomas Antretter

AVL List GmbH

Engineering and Technology Powertrain Systems

Hans-List-Platz 1

A-8020 Graz

Contact:

Dr. Christopher Huber

WAYNE STATE UNIVERSITY

Department of Mechanical Engineering

Advanced Composite Research Leboratory

42 W Warren Ave

Detroit, MI 48202, USA

Contact:

Prof. Golam Newaz

Eidesstattliche Erklärung

Affidavit

Ich erkläre an Eides statt, dass ich die vorliegende Arbeit selbstständig verfasst, andere als die angegebenen Quellen/Hilfsmittel nicht benutzt, und die den benutzten Quellen wörtlich und inhaltlich entnommenen Stellen als solche kenntlich gemacht habe. Das im TUGRAZonline hochgeladene Textdokument ist mit der vorliegenden Masterarbeit identisch.

I declare that I have authored this thesis independently, that I have not used other than the declared sources/resources, and that I have explicitly indicated all material which has been quoted either literally or by content from the used sources used. The text document uploaded to TUGRAZonline is identical to the present master's thesis

Graz, am _____ _____

Datum / Date Unterschrift / Signature

Abstract

The present work deals with the stress analysis of structures made of composites. Composite materials such as fiber-reinforced plastics (FRPs) are commonly used in lightweight engineering. The anisotropic mechanical behavior of these materials gives rise to some difficulties concerning the simulation of composites in comparison to metal designs. The numerical simulation of these materials was under investigation using the commercial Finite Element software ABAQUS.

As the main part of this work, a universal simulation workflow for FRPs was developed. The workflow covers the entire analysis process starting from the information gathering and ending with the assessment of laminates with respect to failure. The preparation of the geometry is an important step in the simulation process of composites. It determines the quality of the analysis results as well as the time consumed by the whole simulation. Since the geometry is usually provided as volume geometry and the computation of composite structures is often carried out using shell elements, the transformation process from 3D to 2D geometry is shown.

Furthermore, sub-workflows for the material definition and the selection of finite elements for the analysis are generated. Depending on the stress state, the element has to be chosen properly. The sub-workflows are meant to guide the engineer through these difficult parameter definition steps.

For the verification of the workflow, the results of the World Wide Failure Exercise (WWFE) are employed. On basis of the published experimental data within the WWFE, the best failure criteria for anisotropic materials are compared against each other. For the failure theories implemented in ABAQUS, polar plots for different stress states are created to highlight the criterion with the best practice for each stress ratio. The plots will support the analysis engineer to choose the proper criterion for the present stress state.

Due to the complex failure behavior of composite materials, the assessment of composites is a challenging task within the workflow. A sub workflow is created to support the engineer within this process. Beginning from First-Ply Failure (FPF) to Last-Ply Failure (LPF) and linear to nonlinear simulation for different fiber types, the sub workflow acts as a detailed guideline within this task.

Two FRP components, one using glass fibers, another one comprising carbon fibers, have been chosen to demonstrate the features of the workflow.

Kurzfassung

Die vorliegende Arbeit behandelt die Spannungsanalyse von Bauteilen aus Verbundstrukturen. Verbundmaterialen wie faserverstärkte Kunststoffe werden häufig im Leichtbau eingesetzt. Das anisotrope mechanische Verhalten solcher Materialien bringt Schwierigkeiten bei der Simulation mit sich, welche im Vergleich mit Metallen nicht entstehen. Die numerische Simulation solcher Materialien wurde mit Hilfe der kommerziellen Finite Elemente Software ABAQUS untersucht.

Der Hauptteil dieser Arbeit beschäftigt sich mit der Erstellung eines durchgängigen Simulationsworkflows. Der Workflow beinhaltet den gesamten Analyseprozess angefangen von der Informationsbeschaffung bis zum Auswerten der Laminate. Die Geometrieaufbereitung ist ein wichtiger Schritt im Simulationsprozess von Verbunden. Sie entscheidet über die Qualität der Analyseergebnisse wie auch über den Zeitbedarf der Simulation. Da die Geometrie zumeist als Volumengeometrie zu Verfügung steht, die Simulation jedoch häufig mit Schalenelementen durchgeführt wird, wurde der Umwandlungsprozess von 3D in 2D Geometrien gezeigt.

Des weiteren wurden Teilabläufe zur Materialdefinition und zur Elementauswahl generiert. Abhängig vom Spannungszustand müssen die Elemente entsprechend gewählt werden. Die Teilabläufe unterstützen den Berechnungsingenieur bei dieser schwierigen Parameterwahl.

Zur Verifizierung des Workflows wurden die Ergebnisse der "worldwide failure exercise" (WWFE) herangezogen. Auf Basis der experimentellen Ergebnisse der WWFE wurden die besten Versagenskriterien miteinander verglichen. Für die in ABAQUS implementierten Versagenskriterien wurden Polardiagramme für verschiedene Spannungszustände generiert, um das beste Kriterium für einen bestimmten Spannungszustand herauszufinden. Die Diagramme unterstützen den Berechnungsingenieur bei der Auswahl der passenden Kriterien.

Aufgrund des komplexen Versagensvorganges von Verbundwerkstoffen ist die Auswertung der Ergebnisse eine herausfordernde Aufgabe im Analyseprozess. Ein Teilablaufplan zur Auswertung wurde generiert um den Ingenieur bei diesem Prozessschritt zu unterstützen. Angefangen vom Erstschichtversagen (FPF) und Letztschichtversagen (LPF) bis hin zur linearen und nichtlinearen Analyse stellt der Teilablaufplan eine Richtlinie dar.

Zwei Faserverbundbauteile, einer aus Glasfasern, ein anderer aus Carbonfasern, wurden gewählt, um die Einzelheiten des Workflows zu demonstrieren.

Contents

List of Figures

List of Tables

Abbreviations

2D	two-dimensional
3D	three-dimensional
CAD	Computer-Aided Design
CAE	Computer-Aided Engineering
CDM	Continuum Damage Mechanic
CDS	Characteristic Damage State
CFRP	Carbon Fiber Reinforced Plastic
CL	Composite Layup
CLT	Classic Lamina Theory
COS	Coordinate System
CS	Continuum Shell
DOF	Degree of Freedom
FEA	Finite Element Analysis
FEM	Finite Element Method
FF	Fiber Failure
FRP	Fiber Reinforced Plastic
FSDT	First Order Shear Deformation Theory
GFRP	Glass Fiber Reinforced Plastic
GT	Glass Temperature
HDT	Heat Deflection Temperature
IFF	Inter Fiber Failure
KLuB	Konstruktiver Leichtbau und Bauwesen
MS	Margin of Safety or Safety Margin
NFC	Non-Crimp Fabrics
RTM	Resin Transfer Molding

SA	Section Assignment
SD	Section Definition
SDV	State Dependent Variable
TC	Test Case
UD	Unidirectional
WF	Woven Fabric

Symbols

$[A]$	extensional stiffness matrix of the laminate	
$[B]$	coupling stiffness matrix of the laminate	
$[D]$	bending stiffness matrix of the laminate	
$[H]$	shear stiffness matrix	
$[K]$	stiffness matrix of the laminate	
$[Q]$	stiffness matrix of a lamina	
$[\bar{Q}]$	stiffness matrix referred to the laminate COS	
$[S]$	compliance matrix of a lamina	
$[T]$	transformation matrix	
E_1, E_2	Young‘s modulus in fiber and transverse fiber direction	N/mm^2
f_E	stress exposure	
f_S	stretch factor	
G_{12}	in-plane shear modulus	N/mm^2
$\hat{A}$	initial cross section	m^2
$\hat{E}$	initial Young's modulus	N/mm^2
$\hat{N}$	laminate resultant force	N
$\hat{M}$	laminate resultant moment	Nm
$\hat{V}$	laminate resultant transverse force	N
$\hat{n}$	laminate resultant force per unit length	N/m
$\hat{m}$	laminate resultant moment per unit length	Nm/m
$\hat{v}$	laminate resultant transverse force per unit length	N/m
d	damage variable	
t	laminate thickness	m
w	width of the laminate	m

α	angle of fiber direction	$\circ$
$\kappa_x, \kappa_y, \kappa_{xy}$	laminate curvatures and twist	
$\nu_{\perp\parallel}$	Poisson‘s ratio of a lamina	
$\{\sigma\}$	stress vector	N/mm^2
$\{\varepsilon\}$	strain vector	
η, η_R	reduction factor	
η_v	viscosity factor	

Subscripts: k	k-th ply
x, y, z	laminate coordinate system
$1, 2, 3$	lamina coordinate system

Chapter 1

Introduction

1.1 Background

Over the last decades fiber-reinforced composites became increasingly important in engineering applications. Nevertheless, the concept of using fibers as the load carrying reinforcement for structural components is quite old. It is, as often seen nowadays, copied from nature or simply bionic engineering. Wood, for example, as a natural product uses the strength of fibers to carry high loads caused by wind. Composites as a natural material can also be found in the human body. Bones, for example, use the very hard and brittle hydroxyapatite and the soft and flexible substance collagen, as building components.
Humanity started using fiber reinforcements approximately in 6000 B.C. to increase the resistance of their clay huts. However, in the last century the implementation of fiber-reinforcements became increasingly important to almost every technological application. In civil engineering the use of steel ropes to increase the strength of concrete under tension was a big step forward for the development of bridges. Asbestos was used for many years to improve the mechanical properties of roof tiles.

A few decades back from now fiber-reinforced plastics (FRPs) started to experience a big boost. Due to their desirable strength and stiffness properties, plastic composites are an integral part in lightweight engineering. The high strength-to-density value makes FRPs very suitable for structural applications. Boat manufacturers, for example, started using glass fiber composites for the hull of the boat. Furthermore, the mast of boats

and windsurf boards are often made of composites. Nowadays, there is a wide range of sport equipment made of fiber composites including skiers and bicycles.

In civil aircrafts, plastic composites were introduced in the middle of the last century. With the introduction of Airbus A380, plastic composites, especially carbon fiber reinforced laminates for aircraft structures, received additional attention. Approximately 30% of the aircraft's interior and exterior structures are made of fiber composites. The latest developments of the two big aircraft manufacturers Boeing and Airbus are the Boeing 787 and the A350. More than 50% of the structural weigth will be either glass or carbon fiber plastics.

Due to the high cost of plastic composites, these materials were for a long time limited to aviation applications only. Except for sports cars, the integration of FRPs in passenger vehicles was simply too expensive. Recently, the strict CO_2 emission regulations led to a boost of composites in the automotive industry. A target emission of $95gCO_2/km$ until 2020 can only be reached by improving the efficiency of future power trains as well as by simultaneously reducing the mass of the vehicle. A 200-300kg mass reduction will be required to meet the target values [14]. Therefore, the use of light materials such as carbon fiber composites is necessary for future developments. In 2014 BMW introduced the new BMW i3. This is the first mass produced car which contains a frame made of carbon composites. The weight and subsequently the fuel consumption could be reduced dramatically. To make cars as the i3 affordable, a reduction of the production costs is necessary. As a result, many companies are investing money in the development of new production methods. In order to reduce the development costs of these projects, the expenses for experimental testing have to be lowered. This can only be achieved if the numerical simulation and verification is good enough to predict failure of FRPs accurately. In addition, the more accurately failure can be predicted, the lighter the structure can be designed. Consequently, it is the motivation for researchers all over the world to invest their energy to improve the simulation of fiber-reinforced composites. Still, keeping in mind the words of Prof. Golam Newaz (head of the Advanced Composite Research Laboratory at Wayne State University in Detroit):

> *There is no fiber composite part development without testing. Simulation doesn't replace testing. It rather assists the engineer to understand the phenomena during failure.*

1.2 Scope

The objective of this work is the development of a universal workflow for the modeling of long-fiber-reinforced plastics. Specifically, the focus is on the modeling of components with the commercial finite element software ABAQUS^{TM}[1].

The main goals are to:

- Collect the basics of fiber reinforced plastics with emphasis on the simulation of composites with ABAQUS.
- Show in detail the specific techniques for the preparation of the 3D CAD model provided from the design engineer as well as a guideline for the selection of the proper element types used for the simulation.
- Understand the mechanics and failure mechanisms of fiber composites.
- Find the proper failure criteria for the assessment of the composite component using experimental data available from work prior to this thesis.
- Develop an appropriate FE modeling workflow for long-fiber reinforced composites under quasi-static loading based on best practice.
- Demonstrate the simulation methodology using already existing projects from the project partners.

The simulation of dynamic loads e.g. impact loads are not part of the investigation in this work. Furthermore, stability problems as they are relevant for thin walled components are not taken into account either. The influence of moisture and temperature to plastic composites is also neglected in this thesis.

[1] ABAQUS^{TM} is a registered trademark of Dassault Systèmes. ABAQUS is developed by SIMULIA.

1.3 The Strength of Fiber Composites

The following section provides an overview of the strength of fiber composites. Although fibers have superior mechanical properties, they have to be embedded in a matrix in order to form a suitable design material. The tasks of each constituent are well defined. The fiber provides the strength and the stiffness for the compound, while the matrix material is responsible for the load transfer in-between the fibers and for the protection of the fiber from external influences. In combination, these two materials form a composite with extraordinary properties considering strength, stiffness and weight. Thus, for lightweight load-carrying structures, fiber reinforced plastics are the perfect choice.

There are four phenomena which lead to the special mechanical properties:

- Size effect
- Orientation
- Freedom of defects/notches
- Residual stresses

One of the parameters determining the strength of a material is the number of deficiencies inside a certain volume. According to the "weakest link theory", the fewer defects are apparent in a volume, the lower the risk of failure. Statistically, the number of defects increase with the volume of the material. Therefore, it seems obvious to reduce the volume as much as possible. One way to approach this is to produce fibers with a very high surface area to volume ratio. A cube with an edge length of 1mm has a surface area of 6mm^2. A fiber, for example, with the same volume (1mm^3) but a fiber diameter of $10\mu m$ yields a surface of 400mm^2. This would lead to a surface ratio of 66.7 to 1. Figure 1.1 shows the strength of a material with respect to its dimension. The limiting strength value is the bonding force of the molecular chains in a defect-less fiber. The curve depicted in figure 1.1 reflects this tendency.

For some manufacturing processes it is necessary to stretch the fiber during the production. This step leads to an orientation of the molecular chains within the fiber and hence to a strength enhancement. The drawback of this mechanism is that the fiber

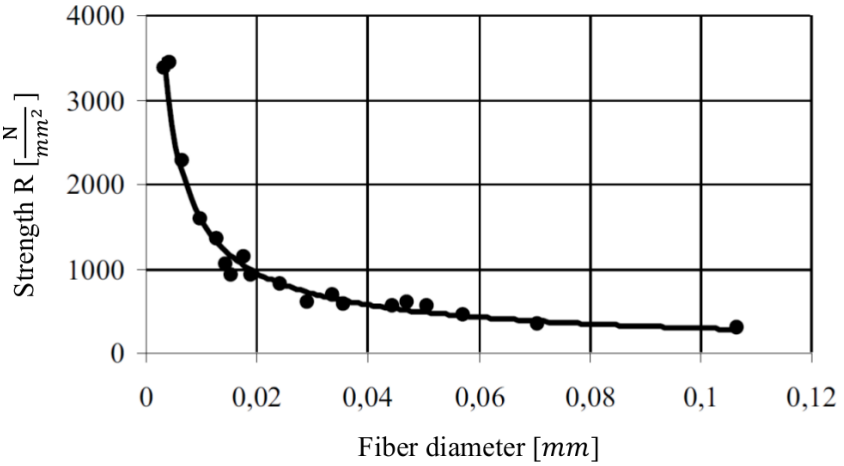

FIGURE 1.1: Influence of the fiber volume represented by the fibers diameter [1].

will lose its strength and stiffness in the transverse direction. That is the reason for the anisotropic material behavior of some fibers.

Notches, especially located on the surface of a part/fiber, can reduce the strength of the material. In particular for brittle materials, these defects will lead to abrupt failure of the component. For fibers the manufacturing process is once again advantageous considering this aspect. Due to the pulling of the fibers, notches will, if at all, only occur in longitudinal direction. This is the preferred orientation since the fiber will keep most of its strength. Surface defects can be reduced by etching the fiber.

The last strengthening effect for fibers has only been observed for glass fibers. During manufacturing the fiber starts solidifying at the surface. Because the core of the fiber takes longer to fully solidify, compressive residual stresses are induced on the fiber surface due to the cool down process. This side effect introduces residual stresses into the fiber and further increases the strength of the fiber material.

In figure 1.2, the strength and the Young's modulus of common fiber materials are compared to standard engineering materials. One has to keep in mind that these property values are specific values considering the density. The differences between fibers and metals considering absolute values would be much smaller or show even a reversed tendency.

As mentioned above, the fiber needs to be in a compound with a matrix material. The high strength of a fiber can not be reached with the compound. Similarly, the ultimate elongation of the composite is lower than that of the matrix material. Figure 1.3 shows

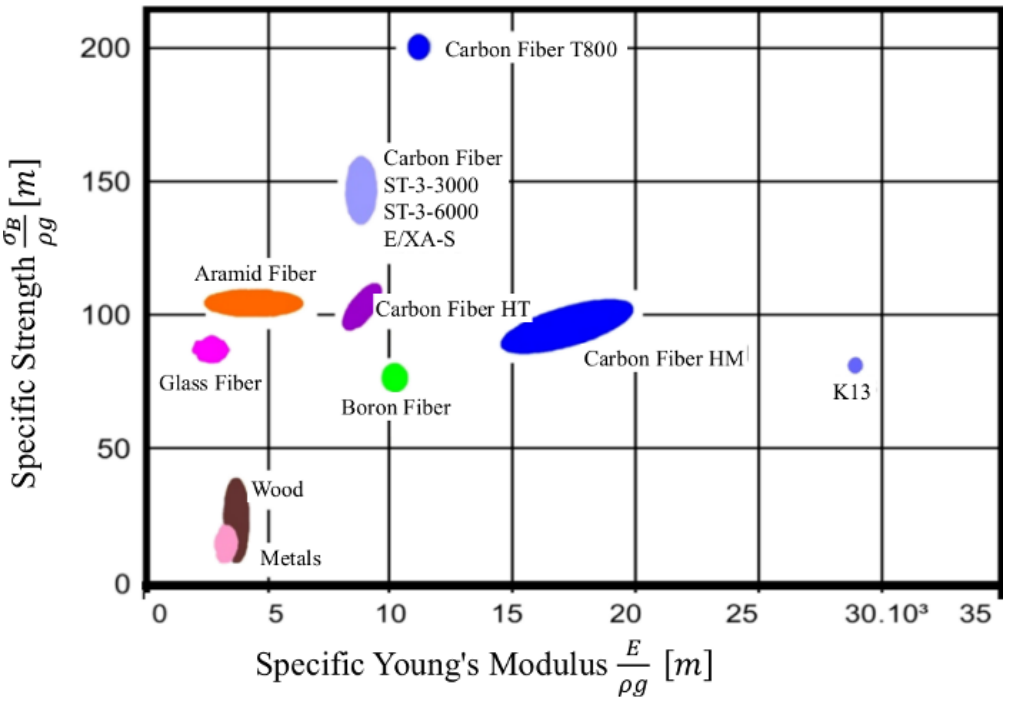

FIGURE 1.2: Specific strength and Young's Modulus of different engineering materials.

qualitatively how the mechanical behavior of the constituents change compared to the composite in terms of the stress-strain curve.

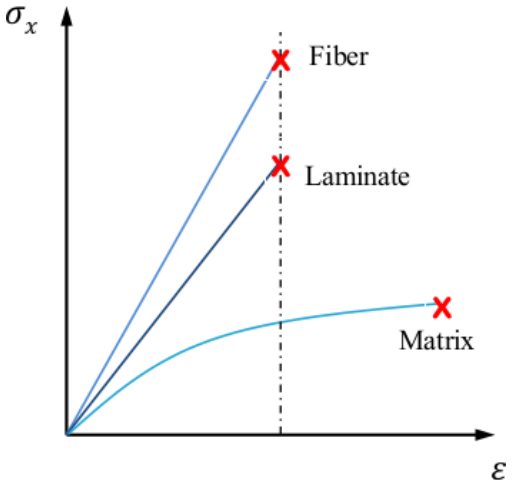

FIGURE 1.3: Qualitative change of the material properties in a compound of two constituents.

Overall, the compound has more advantages than disadvantages considering the mechanical behavior. If, for example, a fiber is broken, the load on the fiber before and after the crack will be redistributed by the matrix as long as the bonding between fiber and matrix is intact. More information about the properties of fiber composites can be found in [1, 15–17].

1.4 Materials

This section deals with the different constituents of fiber composites. Any combination of a fiber type with a matrix material leads to a compound with specific material properties. Thermal, mechanical, volumetric or optical material characteristics can be tailored with the materials available on the market. Below, the most commonly used fiber and matrix types as well as their semifinished products are discussed.

1.4.1 Fiber Types

Fibers are responsible for the load transfer in the composite component. The fiber types have different mechanical properties and show different mechanical behavior. The knowledge of the detailed characteristic is of importance for an accurate simulation.

There are four different types of fibers employed in today's applications as reinforcement material:

- Natural fibers: hair, wool, silk,...
- Organic fibers: basically all plastic fibers (PAN, PE, PP,...)
- Inorganic fibers: glass, basalt, boron,...
- Metal fibers: steel, aluminum, copper, tungsten

In this work only the two main fiber types are discussed in detail. Today, the carbon fiber production is with 47.220 tons/year much smaller than the glass fiber production with 4.33 million tons/year [15]. Both experience huge growth rates and the forecast especially for carbon fibers is remarkedly high.

1.4.1.1 Glass Fiber

Glass fibers are the most commonly used reinforcements for plastics. The combination of the low density and the high strength of the fibers led to their wide popularity. Compared to other fibers, the costs for glass reinforcements are relatively low. Glass fibers feature different cross sections, with circular and ring cross sections being the

most frequently used products. Elliptic shapes provide a better bonding to the matrix material. The bonding enhancement is due the increased surface in comparison to the circular fibers. Depending on the chemical configuration, an engineer can choose from 8 different glass fibers (E-, ECR- , C- AR, R-, S-, D-, and Quartz-glass). The most commonly used glass type for engineering application is the E-glass. The basis for E-glass is a calcium alumino-silicate. For higher strength requirements, typically S- and R-glass fibers (S-strength, R-resistance) are chosen [15].

The favorable material properties of glass are as listed below:

- high ratio of tensile strength to specific mass,
- very good draping behavior,
- inflammable,
- and cheap in production.

On the negative side, a comparatively low Young's modulus, no special material orientation and brittle material failure must be mentioned. The mechanical material behavior of glass fibers is isotropic. It has a very large linear elastic range and is therefore suitable for applications where high failure strain values are needed. If glass fiber is subjected to increased temperature over a long time, the strength values drop. The highest strength is reached at $-180°C$. Low temperatures are uncritical for glass fiber [1]. More information on glass fibers can be found in [15, 16, 18]

1.4.1.2 Carbon Fiber

Carbon fibers as a high-tech material are considered as one of the top ten emerging materials for the future [14]. The superior properties have long been well known. Today, researchers all over the world are looking for more efficient and cheaper ways to manufacture carbon products.

Base material for the production of C-fibers are PAN (Polyacrylnitril) fibers. The high strength and high Young's modulus are reached after the carbonization of the PAN in carbon atmosphere. Depending on the desired Young's modulus, a special graphitization method combined with an elongation of the fiber is applied. A final surface treatment

increases the adhesion between matrix and fibers. During this production process, stable oxides are built at the surface of the fibers. This substances protect the fiber against environmental influences.

The atomic structure of graphite is assembled in layers. This property leads to theoretically very high mechanical values ($E_{||} = 1050000 N/mm^2$ and $R_{||} = 100000 N/mm^2$ (the parallel subscript denotes the property in fiber direction)) [1]. In reality, defects lower these properties as known from other materials. Different groups of carbon fiber types have been developed according to their strength and stiffness values. Six of them are listed below and their strength and Young's modulus are depicted in figure 1.4

- High-Tensile – HT
- Ultrahigh-Tensile - UT
- Intermediate Modulus/Strength – IMS
- High-Modulus – HM
- High-Modulus / Strength – HMS
- Ultrahigh-Modulus/ Strength – UMS

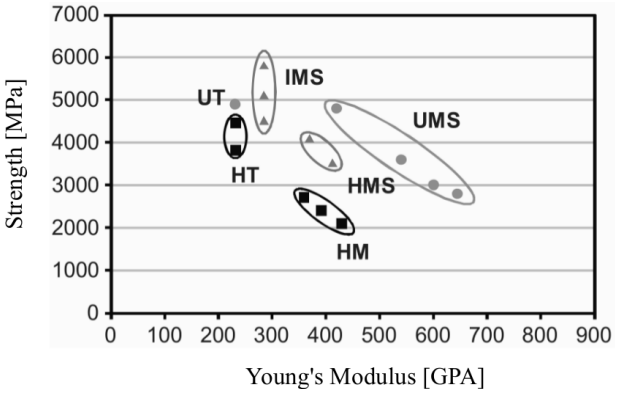

FIGURE 1.4: Strength and Young's modulus for different carbon fiber types [2].

For the analysis of carbon composites it is important to mention that carbon fibers show anisotropic material behavior. The Young's modulus in fiber direction is one magnitude higher than that of the transverse direction. Another rather unusual characteristic can be observed concerning the thermal expansion. The Poisson ratio in transverse direction is positive whereas in longitudinal direction it is negative. This leads to increased thermal stresses if the composite is subjected to heat. Furthermore, the cracking behavior is profoundly brittle and the elongation at fracture very low.

As mentioned earlier, there are many more fiber types available today. Figure 1.5 below shows a comparison of stress-strain curves of different fibers. As can be seen, the higher the Young's modulus of a fiber, the lower the final strain. One exception is the T700 (also T7.0) carbon fiber which shows a very high deformation capability even at high strength and intermediate elastic modulus.

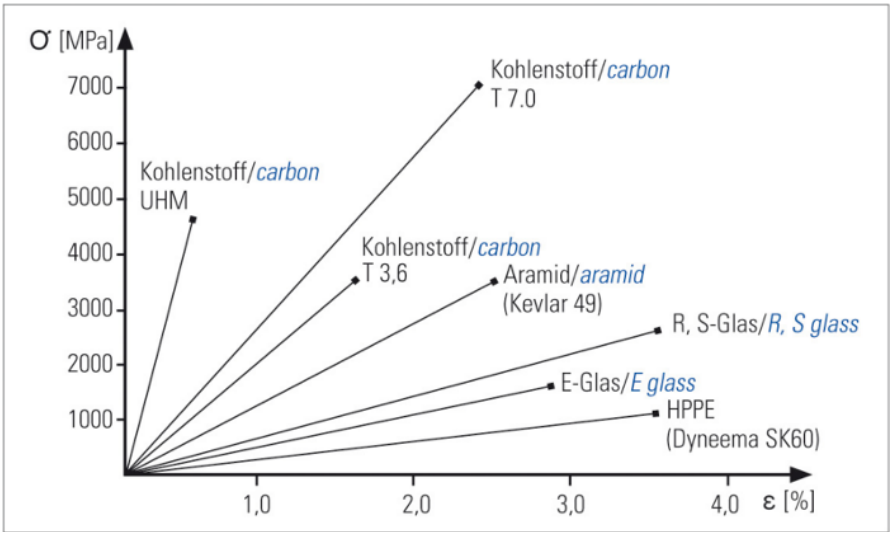

FIGURE 1.5: Stress-strain curves of different fiber types [3].

1.4.2 Semifinished Products

Arranging the unprepared fibers according to the design schematic is almost impossible. Therefore, different types of semifinished products are available. Depending on the manufacturing method of the composite part, the product has to be chosen adequately. The finite element (FE) modeling of the composite is also influenced by the product. The mechanical behavior, as for example isotropy or anisotropy, is highly dependent on the manufacturing process and method.

The simplest form of a semifinished product is the roving. It can be used for the production of filament winded components, but is also the precursor of other products. Typical products are for example unidirectional (UD) tapes and woven fabrics (WF). The big advantage of these products is that they can be assembled in a very simple way. Cutting and the usual frazzling is not a problem for these fabrics. Due to the weaving it is ensured that the fiber direction remains the same.
The big drawback of WFs is the loss of strength due to the undulation of the fibers. Three main types of WF with different properties are available, i.e., plain weave, as the simplest representative, twill weave, as often seen in design components, and satin weave, which shows the best mechanical properties due to its weaving method.

Due to the strength and stiffness loss of WF, multidirectional (multiaxial) tapes consisting of non-crimp fabrics (NCF) were developed. The individual yarns of the NCF

are stitched together using small threads. Up to 8 layers with different orientations can be manufactured. Due to the favorable properties, these semifinished products are used very often in aircraft engineering. Figure 1.6 demonstrates the principle of a multiaxial tape and a real stitched carbon tape.

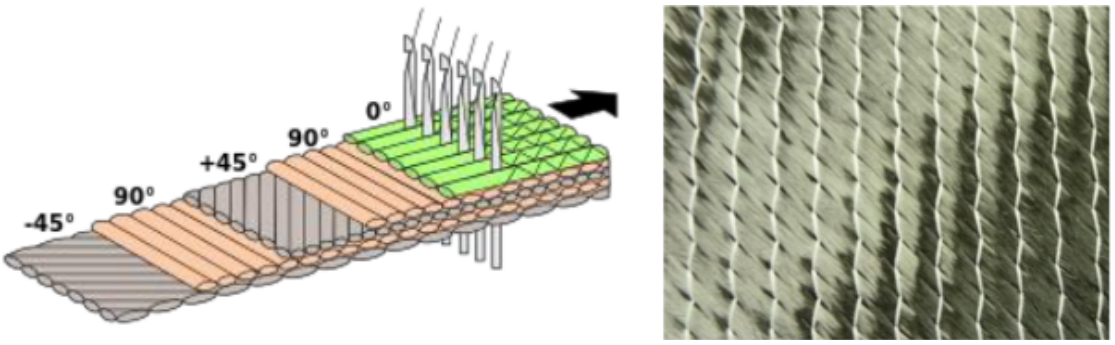

FIGURE 1.6: Left: Principle of a multiaxial tape. Right: Real tape with carbon fiber bundles (black) and stitch yarn (white) [4].

Another rather new production method for semifinished fabrics is the manufacturing of 3D fabrics. The above mentioned fabrics are all manufactured in one plane. Three-dimensional fabrics have yarns in the out of plane direction as well. This is very beneficial concerning the delamination of composites.

The above mentioned products are all considered as long-fiber reinforcements. The two other nomenclatures for fiber dimensions are endless- and short-fiber reinforcements. A part is considered as endless fiber reinforced if the length dimension of the fiber is of the same dimension as that of the component. Fibers with a length below 50mm are referred to as short fibers. Endless-fiber reinforcement is therefore a subgroup of long-fiber products.

Another characteristic of composite parts can be found in the fiber orientation. Be-

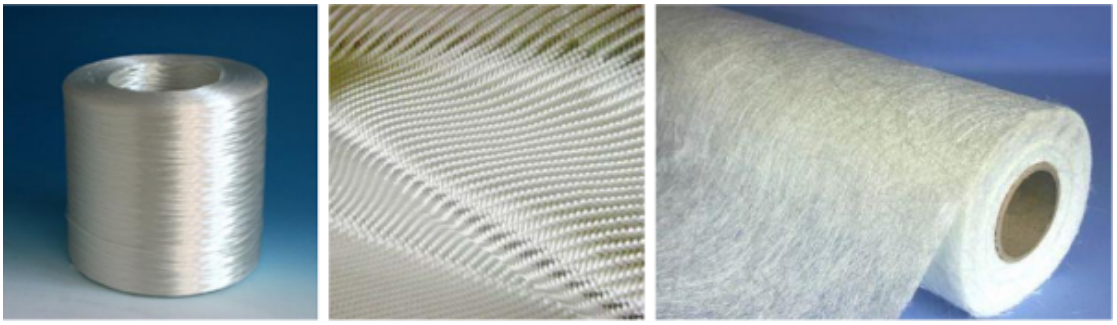

FIGURE 1.7: Semifinished products of glass fiber. Roving (left), woven fabrics (center) and randomly oriented mat (right) [4].

.

sides the products with one or more distinct directions, fabrics with randomly oriented fibers are commonly used. Different types of semifinished products are shown in figure 1.7. This work is dedicated to long-fiber reinforced composites with determined fiber orientation. More information of woven fabrics and semifinished products in general can be found in [1] and [15].

1.4.3 Matrix Materials

As mentioned earlier in this work, the matrix plays an essential role within the compound. Beside the load transfer between the fibers, the matrix has many different tasks. It keeps the fibers in their initial position and supports them during compression load. The matrix links adjacent layers with each other and transfers the load forth and back. If a crack appears in a layer, the matrix has the ability to stop it from further propagation. Especially for transverse and shear loading, the matrix is highly loaded and therefore responsible for the strength of the component. The last noteworthy task of a matrix material is to protect the fibers from environmental influences as radiation, chemical substances and abrasive wear. Plastic materials which are capable of performing all these duties are mostly thermosets, thermoplastics and occasionally elastomers. The first two materials will be described in this work.

1.4.3.1 Thermosets

Thermosets solidify through a chemical cross-linking process. After the curing process when all cross-links are formed, the thermoset polymers cannot be melted and reshaped by the use of temperature and pressure. Therefore, welding of thermosets is not possible at all. The material is characterized by a low viscosity which is beneficial for the wetting of fiber and matrix. Another advantage of these polymers is that they show almost no creep and stress relaxation in comparison to thermoplastics [19].

The weakness of thermoset plastics is their long manufacturing time. Especially for the automotive industry this is the biggest drawback concerning the use of composites for passenger vehicles. However, the low failure strain and impact strength have to be mentioned as well.

A very important material parameter for thermoset plastics is the Glass Temperature (GT) or also called Heat Deflection Temperature (HDT). The GT defines the dimensional stability under heat and can be determined by a simple torsion vibration test [15]. Popular thermoset matrices for fiber composites are Epoxy and Polyester resins.

1.4.3.2 Thermoplastics

Due to their ductile nature and larger failure strain, thermoplastics offer some advantages over thermosets. The manufacturing time is low and hence the production of the composite is cheaper. Furthermore, the handling of thermoplastics is easier and a post thermoforming after initial manufacturing is allowed. However, due to the high melting temperature, it is almost impossible to produce pre-impregnated products of thermoplastic materials [19].

Recently, manufacturers of injection molding equipment developed so called organo-sheets. These thermoplastic components mostly have woven fabrics integrated in a plastic component. The fibers provide the stiffness and strength of the component while the plastic can form attachments, ribs or boreholes. One example is shown in figure 1.8.

FIGURE 1.8: Organo-sheets made by ENGEL AUSTRIA GmbH.

The most common thermoplastic materials for composite structures are polypropylene (PP), polyethylene terephthalate (PET) and polyamide (PA).

1.5 Mechanics of Laminates

In this section, the mechanics of a single lamina as well as the mechanics of the whole laminate are discussed. Many special phenomena arise due to the unique material properties of composites.

1.5.1 General Comments

As mentioned earlier in this work, a lamina (single ply, single layer) consists of fibers and a matrix system. The fiber direction (longitudinal direction or ||-direction) is declared as the local 1-direction of a lamina. The 2-direction is the transverse direction (also $\perp$-direction) of the ply and the 3-direction represents the out-of-plane direction. Usually, a composite structure consists of more than just one ply. Layers with different orientations (layup) are stacked over each other. A position inside the laminated structure is defined by the global x-y-z coordinate system. Figure 1.9 shows the coordinate system corresponding to lamina and laminate configuration respectively.

For the stacking sequence a special coding concept was developed. The orientation for each ply is written in brackets. The number given in the sequence represents the angle between the longitudinal direction (1-direction) of the individual layer and the global x-direction. A positive angle means a positive rotation and a negative value a negative rotation respectively. Superscripts denote the fiber type (G for glass and C for Carbon), whereas the subscript denotes either the number of layers or the alignment type (f for fabrics). If the letter S is subscripted at the end of a stacking sequence, it means the laminate is symmetric about the x-y-plane. An example sequence is demonstrated in Fig. 1.9 (center).

1.5.2 Anisotropy of Composites

A lamina, containing fibers and matrix as depicted in figure 1.9, is mechanically treated as a homogeneous continuum with anisotropic material behavior.
For a three-dimensional element three normal stresses $\sigma_1, \sigma_2, \sigma_3$ and six shear stresses components $\tau_{23}, \tau_{32}, \tau_{13}, \tau_{31}, \tau_{21}, \tau_{12}$ can be defined (see figure 1.10). Considering linear elastic material behavior, *Hooke's Law* (see Eqn. 1.1) links the stresses with the strains

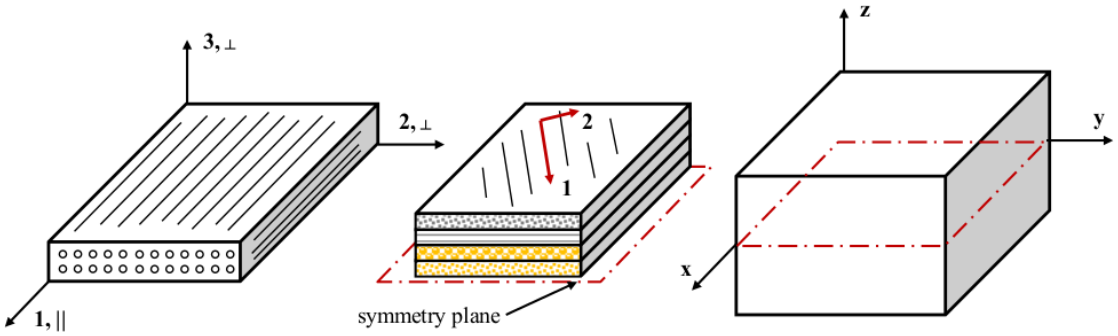

FIGURE 1.9: Lamina with local coordinate system (left), $(45, 90, 0^G, -45^G)_S$ stacking sequence of an example laminate (center) and total laminate with global coordinate system (right).

using 81 coefficients. Knowing from the equilibrium equation and kinematics that $\tau_{23} = \tau_{32}, \tau_{13} = \tau_{31}, \tau_{21} = \tau_{12}$, the coefficients are reduced to 36. This is commonly known as triclinic anisotropy. Considering energy equalities, it can be shown that the stress and strain tensor are symmetric, thus the constants are reduced to 21. The compliance matrix is shown in Voigt notation in Eqn. 1.2

$$\varepsilon_{ij} = C_{ijkl}\sigma_{kl} \tag{1.1}$$

$$\begin{Bmatrix} \varepsilon_1 \\ \varepsilon_2 \\ \varepsilon_3 \\ \gamma_{23} \\ \gamma_{13} \\ \gamma_{12} \end{Bmatrix} = \begin{bmatrix} S_{11} & S_{12} & S_{13} & S_{14} & S_{15} & S_{16} \\ S_{21} & S_{22} & S_{23} & S_{24} & S_{25} & S_{26} \\ S_{31} & S_{32} & S_{33} & S_{34} & S_{35} & S_{36} \\ S_{41} & S_{42} & S_{43} & S_{44} & S_{45} & S_{46} \\ S_{51} & S_{52} & S_{53} & S_{54} & S_{55} & S_{56} \\ S_{61} & S_{62} & S_{63} & S_{64} & S_{65} & S_{66} \end{bmatrix} \begin{Bmatrix} \sigma_1 \\ \sigma_2 \\ \sigma_3 \\ \tau_{23} \\ \tau_{13} \\ \tau_{12} \end{Bmatrix} \tag{1.2}$$

If a symmetry plane can be found in the element (monoclinic anisotropy), the coefficients are reduced even further to a number of 9.

In case of three symmetry planes perpendicular to each other, the material behavior is called orthotropic. Nine independent constants remain. With the introduction of 3 symmetry planes, the coupling between normal strains and shear strains vanishes as illustrated in Eqn. 1.3. Only the coupling between longitudinal strain and transverse strain remains.

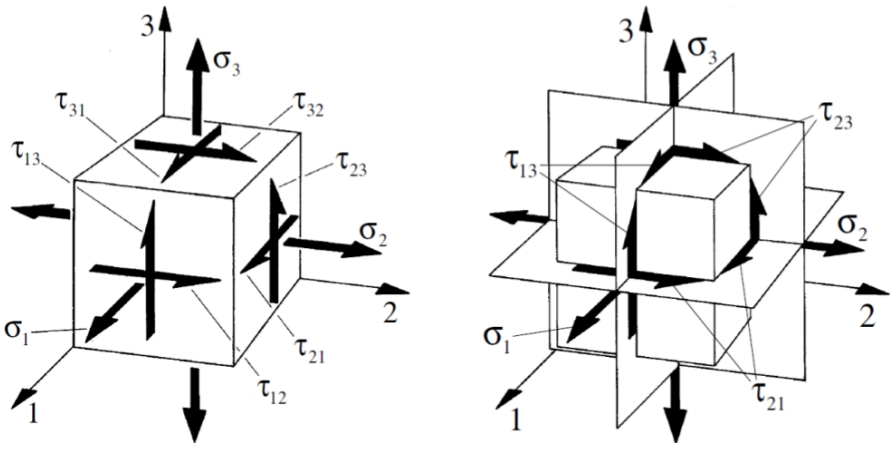

FIGURE 1.10: Triclinic anisotropy (left) and orthotropic material behavior (right) [1].

$$\begin{Bmatrix} \varepsilon_1 \\ \varepsilon_2 \\ \varepsilon_3 \\ \gamma_{23} \\ \gamma_{13} \\ \gamma_{12} \end{Bmatrix} = \begin{bmatrix} S_{11} & S_{12} & S_{13} & 0 & 0 & 0 \\ S_{12} & S_{22} & S_{23} & 0 & 0 & 0 \\ S_{13} & S_{23} & S_{33} & 0 & 0 & 0 \\ 0 & 0 & 0 & S_{44} & 0 & 0 \\ 0 & 0 & 0 & 0 & S_{55} & 0 \\ 0 & 0 & 0 & 0 & 0 & S_{66} \end{bmatrix} \begin{Bmatrix} \sigma_1 \\ \sigma_2 \\ \sigma_3 \\ \tau_{23} \\ \tau_{13} \\ \tau_{12} \end{Bmatrix} \tag{1.3}$$

A UD lamina shows the same transverse properties for every direction. Therefore, an isotropic plane, which leads to a special case of orthotropic material behavior, can be drawn. Perpendicular to this isotropic plane an infinite number of symmetry planes can be created. The isotropic plane is perpendicular to the fiber direction. On every symmetry plane the material has the same properties. This assumption is correct as long as the fibers are homogeneously distributed in the matrix.

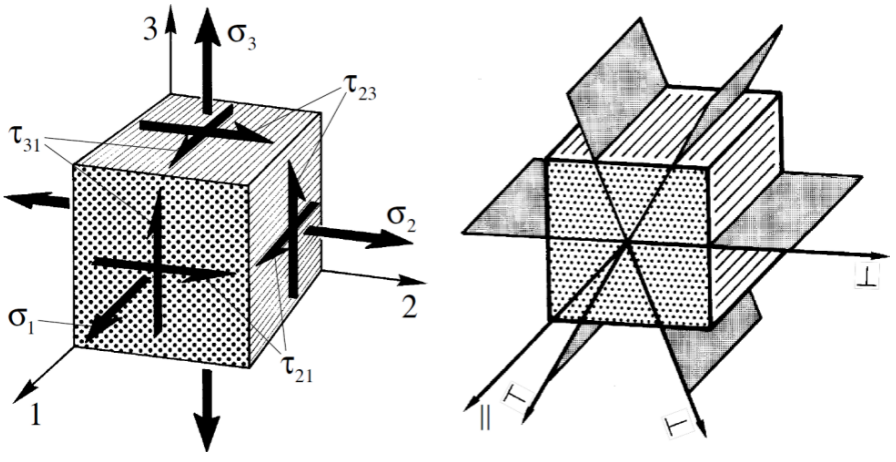

FIGURE 1.11: Volume element of a transverse isotropic material with the stress components (left) and the representative symmetry planes (right) [1].

The presence of an isotropic plane has an effect on the coefficients as well. Some of the constants become equal:

$$\begin{aligned} E_2 &= E_3 = E_\perp \\ G_{31} &= G_{21} = G_{\perp||} \\ \nu_{31} &= \nu_{21} = \nu_{\perp||} \end{aligned} \tag{1.4}$$

According to the geometric relations for isotropic materials, $G_{\perp\perp}$ can be calculated as:

$$G_{\perp\perp} = \frac{E_\perp}{2(1+\nu_{\perp\perp})} \tag{1.5}$$

The symmetry of the compliance matrix yields the following relationship for the Poisson ratio:

$$\frac{E_{||}}{\nu_{\perp||}} = \frac{E_\perp}{\nu_{||\perp}} \tag{1.6}$$

Therefore, only one Poisson ratio has to be determined for a plane state of stress. With the above mentioned relations, the compliance matrix reduces to:

$$\begin{Bmatrix} \varepsilon_1 \\ \varepsilon_2 \\ \varepsilon_3 \\ \gamma_{23} \\ \gamma_{13} \\ \gamma_{12} \end{Bmatrix} = \begin{bmatrix} S_{11} & S_{12} & S_{12} & 0 & 0 & 0 \\ S_{12} & S_{22} & S_{23} & 0 & 0 & 0 \\ S_{12} & S_{23} & S_{22} & 0 & 0 & 0 \\ 0 & 0 & 0 & S_{44} & 0 & 0 \\ 0 & 0 & 0 & 0 & S_{55} & 0 \\ 0 & 0 & 0 & 0 & 0 & S_{55} \end{bmatrix} \begin{Bmatrix} \sigma_1 \\ \sigma_2 \\ \sigma_3 \\ \tau_{23} \\ \tau_{13} \\ \tau_{12} \end{Bmatrix} \tag{1.7}$$

For a transverse isotropic material only five independent coefficients are necessary. The stresses for a transversely isotropic material can be calculated by means of the equation below:

$$\begin{Bmatrix} \sigma_1 \\ \sigma_2 \\ \sigma_3 \\ \tau_{23} \\ \tau_{13} \\ \tau_{12} \end{Bmatrix} = \begin{bmatrix} C_{11} & C_{12} & C_{12} & 0 & 0 & 0 \\ C_{12} & C_{22} & C_{23} & 0 & 0 & 0 \\ C_{12} & C_{23} & C_{22} & 0 & 0 & 0 \\ 0 & 0 & 0 & C_{44} & 0 & 0 \\ 0 & 0 & 0 & 0 & C_{55} & 0 \\ 0 & 0 & 0 & 0 & 0 & C_{55} \end{bmatrix} \begin{Bmatrix} \varepsilon_1 \\ \varepsilon_2 \\ \varepsilon_3 \\ \gamma_{23} \\ \gamma_{13} \\ \gamma_{12} \end{Bmatrix} \tag{1.8}$$

The fourth and fifth row of the equation above form the system below:

$$\begin{Bmatrix} \tau_{23} \\ \tau_{13} \end{Bmatrix} = \begin{bmatrix} C_{44} & 0 \\ 0 & C_{55} \end{bmatrix} \begin{Bmatrix} \gamma_{23} \\ \gamma_{13} \end{Bmatrix} \tag{1.9}$$

These equations are used for the calculation of the H-matrix as described under chapter 3.

Usually, the law of elasticity is written using engineering constants (Young's Modulus E, shear modulus G and Poisson's ratio ν). For simplicity reasons this formulation will be left out in this work.

1.5.2.1 Plane Stress State

In a plane stress state, the third, fourth and fifth row of the matrix above become trivial because of $\sigma_3 = \tau_{13} = \tau_{23} = 0$. Row 1,2 and 6 form the reduced compliance matrix of an orthotropic material subjected to a plane stress state.

$$\begin{Bmatrix} \varepsilon_1 \\ \varepsilon_2 \\ \gamma_{12} \end{Bmatrix} = \begin{bmatrix} S_{11} & S_{12} & 0 \\ S_{21} & S_{22} & 0 \\ 0 & 0 & S_{66} \end{bmatrix} \begin{Bmatrix} \sigma_1 \\ \sigma_2 \\ \tau_{12} \end{Bmatrix} \tag{1.10}$$

The stress components can be computed from the in-plane strains as demonstrated in the equation below:

$$\begin{Bmatrix} \sigma_1 \\ \sigma_2 \\ \tau_{12} \end{Bmatrix} = \begin{bmatrix} Q_{11} & Q_{12} & 0 \\ Q_{21} & Q_{22} & 0 \\ 0 & 0 & Q_{66} \end{bmatrix} \begin{Bmatrix} \varepsilon_1 \\ \varepsilon_2 \\ \gamma_{12} \end{Bmatrix} \tag{1.11}$$

Note that in general $\varepsilon_3 \neq 0$.

The equations for a plane stress state are the basis for the classical laminate theory and first order shear deformation theory described in chapter 3. Note that the entries in eqn. 1.11 are denoted by a capital Q which indicates that the entries are from the reduced stiffness matrix. Usually, the entries of the stiffness matrix are denoted using a capital C as in eqn. 1.9.

Detailed information about this topic is reported in [20].

Chapter 2

Failure of Composites

This chapter is dedicated to the failure mechanisms and analysis approaches of composites. In detail, the failure of a single lamina and its corresponding failure criteria as well as the failure of a whole laminate are discussed. Lamina fracture has to be understood entirely before one is able to account for the complex failure mechanism of laminates.

2.1 Lamina Failure

Compared to metal materials, FRPs show totally different and many more failure modes. In order to predict the failure of composite materials, it is necessary to know which stress state causes which specific failure mode, respectively This section provides an overview of the failure mechanisms of fiber reinforced composites. The most important modes for plastic composites will be discussed in detail.

Crack initiation follows the same laws as for metal materials. The crack starts growing from imperfections in the material, such as broken fibers, debonding of matrix and fiber, micro cracks, voids, inclusions and air bubbles. Further imperfections, especially seen in FRPs, are the nonuniform distribution and misalignment of fibers in the matrix [1, 21, 22]. Due to the lower strength the cracks usually grow in the matrix materials.

2.1.1 Fiber Failure (FF)

Fiber failure is the most fatal failure mode of FRPs. A composite component with a ply damaged by fiber failure is of high risk for its intentional use. As mentioned above, the fiber is mainly responsible for the load transfer in a laminate. If a ply is subjected to fiber failure, the entire composite part loses its loading capacity. The breakage of a single fiber is considered as an imperfection of the laminate. Statistically, every lamina contains a certain amount of broken fibers. Fiber failure means the breakage of many fibers, usually thousands of fibers at the same time. The length scale of a fiber failure crack is in the cm- dimensions. Three different fiber failure modes are distinguished:

- Fiber ruptures caused by longitudinal tension of the lamina.
- Fiber micro buckling (kinking) due to longitudinal compression.
- Transverse fiber breakage; Theoretically, there is a possibility of fiber breakage through transverse-longitudinal shear stress. Practically, the corresponding shear stress will lead to a matrix failure before the fiber breakage occurs.

Fiber rupture and fiber kinking are shown in figure 2.1.

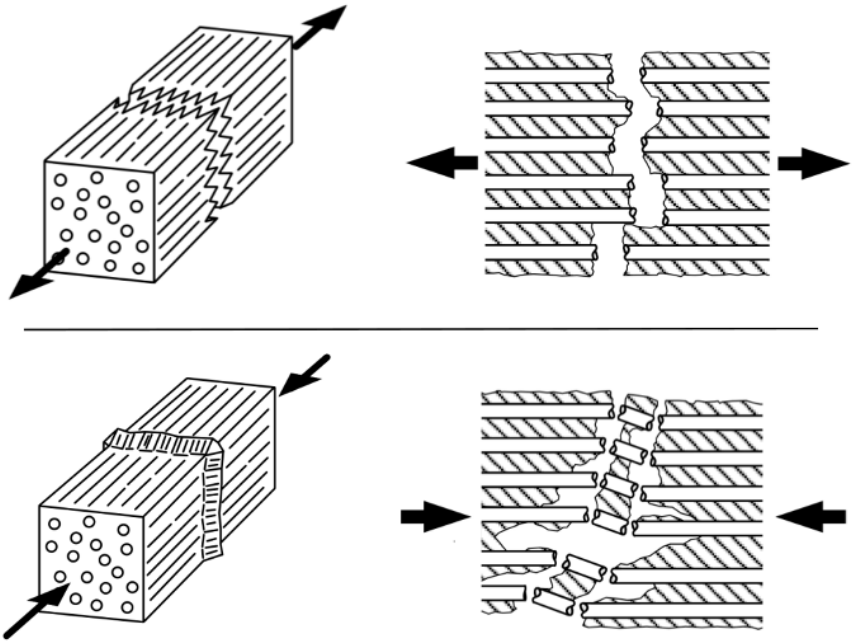

FIGURE 2.1: Fiber failure modes: fiber fracture (top) and fiber micro buckling (bottom) [1].

Although a laminate with more than three plies could bear even higher loads than the load reached at the time of first fiber failure [11], this load is regarded as the fracture load of the laminate. It is highly recommended to replace the composite component if such an initial fiber fracture has occurred.

2.1.2 Inter Fiber Failure (IFF)

Inter Fiber failure is a complex failure mode and difficult to understand. Since the strength of the matrix material is usually much lower than the strength of the fibers, cracks appear at an early stage of loading of the laminate. These cracks are not considered as a fatal damage of the laminate since the capacity of the fibers in the load direction is still at a high level. Nevertheless, matrix cracks caused by tension lead to another phenomenon of FRP components. The stiffness of the laminate varies continuously with an increasing number of cracks in the matrix material, i.e. it exhibits degradation (see section 2.3.2.1). In order to describe this rather complex behavior of laminates under stress, a detailed description of the stress state and the associated IFF mode is required. Figure 2.2 and 2.3 depict the different matrix failure modes and the stresses responsible for them.

For an in-plane stress state Puck [5] introduced 3 relevant failure modes for inter fiber failure. Mode A and B are less important than mode C. Mode A is a simple tension of the lamina combined with a transverse-longitudinal shear stress. The corresponding failure will be a crack running in the longitudinal direction of the lamina. This matrix failure, as mentioned above, is harmless to laminates with usually more than two layers. Mode B is a combination of transverse compression and transverse-longitudinal shear stress. A crack will develop in fiber direction similar to mode A.

Mode C is a very dangerous failure mode due to its inclined fracture plane. The inclination leads to a force component perpendicular to the in-plane stress state. This component can cause a so-called "explosion effect" which can lead to delamination and therefore to fatal failure of the component due to the stiffness loss. The difference between mode B and mode C is simply the ratio between σ_2 and τ_{21}. In one of Puck's newer works, he described the transition point between mode B and C depending on two constants, $R^A_{\perp\perp}$ and τ_{12c}. More details can be found in section 2.2.3.

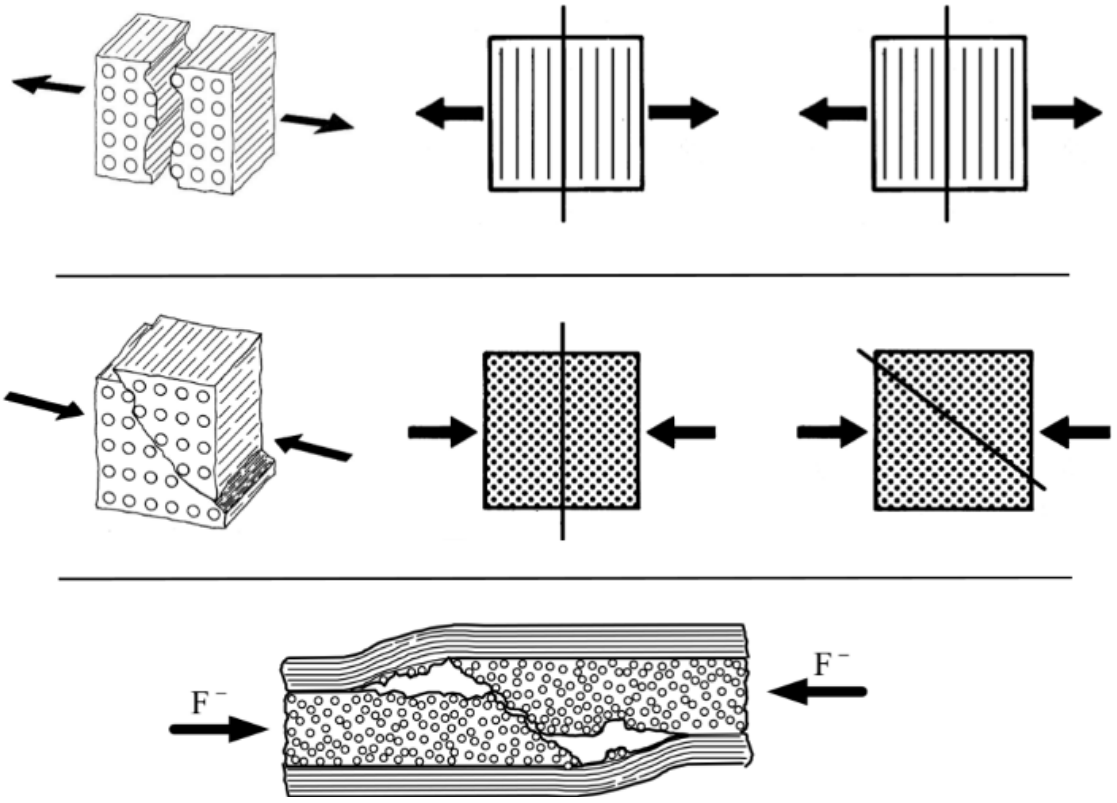

FIGURE 2.2: Matrix failure under tension (top), compression (middle) and compression in a laminate (bottom) [1].

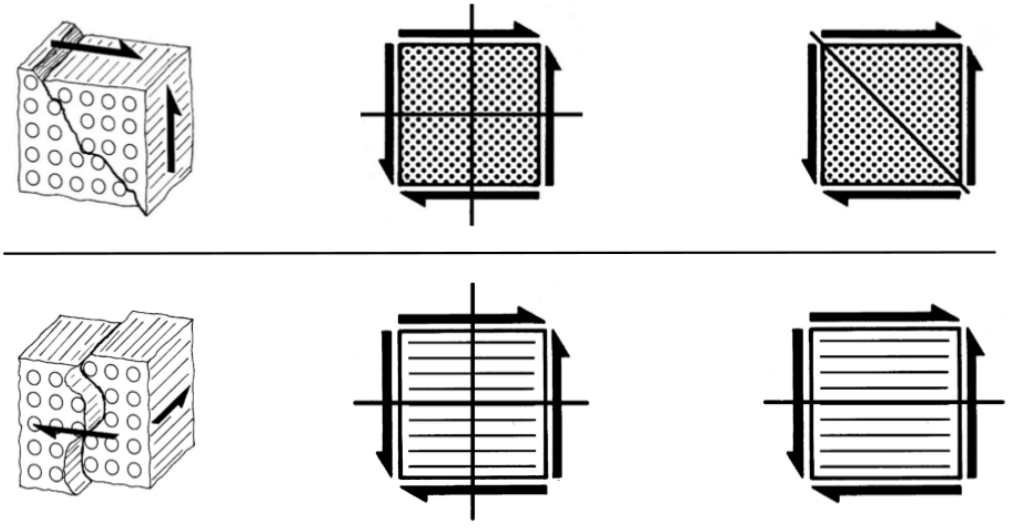

FIGURE 2.3: Matrix failure under transverse-transverse shear (top) and transverse-longitudinal shear (bottom) [1].

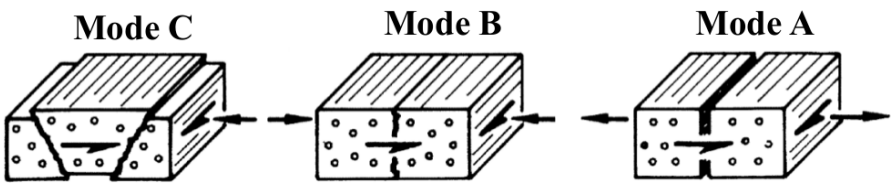

FIGURE 2.4: IFF modes according to Puck [5].

In general, all the IFF modes shown in figure 2.4 can be created from Puck's proposed modes by simply varying the stress ratio between normal and shear stress.
The use of the three modes is also valid for a three-dimensional stress state. Section 2.2.3 provides a detailed insight in Puck's phenomenological failure hypothesis for laminates.

2.1.3 Delamination

Delamination as opposed to the previous failure mechanisms concerns laminates only. Nevertheless, it is discussed within this section since delamination is highly dependent on the IFF.
The interface between the different laminas is, as the matrix material itself, a potentially weak spot. Delamination is considered as the debonding of two or more laminas caused by tension σ_3 in thickness direction of the laminate or inter-laminar shear stress τ_{31} and τ_{32}. Very often delamination is not detectable from outside. Delamination leads to a stiffness loss of the composite. For a composite under compression this can lead to fatal failure of the structure.

For thin-walled laminates without any sharp bends σ_3, τ_{31} and τ_{32} are usually very small and therefore harmless concerning delamination [5]. Based on these findings, Puck and Schürmann [1] proposed three main reasons for the initiation of delamination:

1. As seen in many experiments of stabilizers for trucks made of GFRP, inter fiber failure is always the precursor for delamination. A concentration of inter-laminar shear stress occours arround matrix cracks in the laminate. The stress concentration as shown in figure 2.5 leads to a delamination of the laminae next to the crack tip.

2. Another reason is the anisotropy of the composite. A lamina has different Poisson ratios in transverse as well as in longitudinal direction. At free edges of a laminate this material behavior leads to inter-laminar shear stress and furthermore to the debonding of the laminae. It is obvious that the higher the difference of the Poisson's ratios, the higher is the stress concentration along the free edges. This aspect should be considered in the selection of the material. Figure 2.6 shows the stress concentration at a free surface.

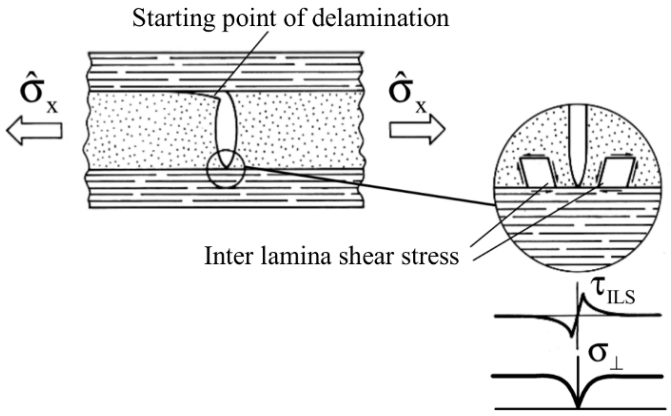

FIGURE 2.5: Stress concentration at the onset of a matrix crack [1].

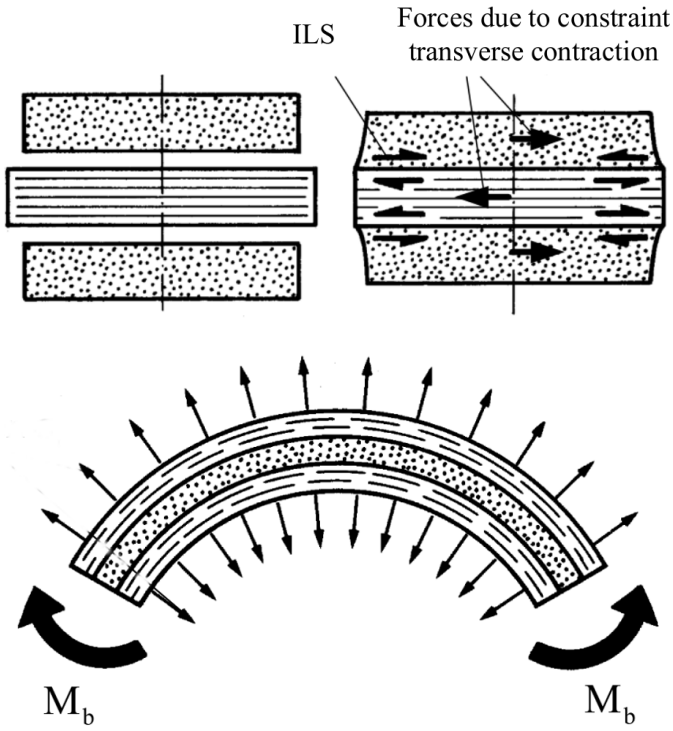

FIGURE 2.6: Stress concentration at free edges (top) and bending of a round (bottom) [1]. The arrows in the bottom figure indicate the moving direction of the top and bottom layers.

3. Furthermore, a common reason for delamination of laminates can be identified in components with rounds. If the round composite part is subjected to an opening moment, a radial tension component is created which tries to debond the layers. The bottom drawing in figure 2.6 depicts a round laminate subjected to a bending moment.

There are many more rather unusual failure mechanisms. Information regarding further failure modes can be found for example in [1] and [21].

2.2 Failure Criteria for a Lamina

No irreversible damage should occur in a composite structure under operational load. In order to design load carrying components, it is necessary to know the initiation of damage. For a simple longitudinal loading of a UD-lamina a comparison with the strength value of the specimen will provide the needed information. Here, the simple maximum stress criterion is enough to reliably determine failure. Usually, more complex stress states are present in a component. Typically, normal and shear stress components are interacting with each other and the simple maximum stress criterion loses its validity.

For metals the von Mises yield criterion is used to transform the three dimensional stress state into a single comparative scalar, which can be used for the assessment against the tensile strength of the material.

However, problems appear upon the assessment of laminates. The anisotropic material behavior can no longer be characterized as a single equivalent value. To resolve this problem, many different failure criteria have been developed by researchers all over the world. In 1986, already 30 different failure criteria exist but only few of them were backed up with sufficient experimental data. Generally speaking, no criteria is universally capable to reliably predict failure. In 1992, the authors of the current failure criteria convened to discuss this drawback. The result was the initiation of the first world-wide failure exercise (WWFE) organized by Hinton et al. [12, 23–29]. In this series of papers the authors of the most commonly used criteria were asked to perform a failure analysis of their own criterion for different laminate types and materials. In total, 14 test cases were carried out during the exercise. The same data were provided for all participants of the WWFE. The results of their analyses were sent back to the organizers who compared the results of their investigations and published them in part A of the WWFE. The comparison in part A revealed a huge difference between the individual criteria. In some cases, the results differed by 570% [24]. This comparison revealed the big uncertainty when dealing with laminates. In part B of the exercise [27], the results of part A were assessed against experimental data which were provided by the organizers. These investigations shed some light on the validity of the individual criteria. Part C of the WWFE [29] gave the participants the opportunity to comment on their results and make corrections if necessary. So far, a second and third WWFE have been carried out in order to evaluate the validity of three dimensional stress states

and the in-situ effect respectively. During the WWFE many new criteria have been developed using the experimental data given in the exercise. The WWFE made a big contribution for the development of laminate analysis theories. It also revealed the truth about the individual theories and to what extent some of the widely used theories are able or unable to predict failure accurately. It indicated once again that further research has to be done in order to improve the assessment quality of laminates.

The results of the WWFE are used in this thesis to determine the best failure criteria for the present stress state in a certain laminate. Puck, as one of the winners of the WWFE was implemented in the FE program ABAQUS. Polar plots have been established which help to find the proper failure criterion for a specific stress state and a certain laminate type. Of course, not all laminate types with all the individual stacking sequences could be covered but the most commonly used sequences are taken into account. These polar plots should help the analysis engineer to predict FPF more accurately.

The chosen theories are described in detail below. Failure criteria can be classified into two different groups:

- Global criteria and
- Failure criteria associated with the failure mode.

A failure criterion mathematically represents a so called "failure surface". The surface indicates the limit of a lamina to carry loads. In other words: Failure occurs if a vector (stress exertion f_E) formed by the plane stress components σ_{11}, σ_{22} and τ_{12} cuts-through the failure surface.

The key value of a fiber composite analysis is the margin of safety (MS) or also called safety margin. The MS is calculated using the stretch factor (f_S) as illustrated in Eqn. 2.1:

$$MS = f_S - 1 \tag{2.1}$$

Obviously, the margin of safety has to be greater than zero. Depending on the risk if failure occurs and the consequences of it, safety margins vary for the different applications. The stretch factor (f_S) is the reciprocal value of the stress exertion f_E. This is only valid as long as residual stresses can be neglected. Otherwise, different calculations as reported in [1] should be used nevertheless.

2.2.1 Global Theories

Global criteria have the advantage of easy use. The criteria are usually second order elliptical equations using the strength values of the lamina to set the boundary conditions of the failure envelope. The big disadvantage of global criteria is the lack of information about the failure mode of the lamina. A single scalar failure index does not provide any indication how the lamina fails. It could be either the rather harmless IFF or the fatal fiber failure. Many researchers criticize this approach but due to their simple application global criteria are widely used.

2.2.1.1 Azzi-Tsai-Hill Criterion

The Azzi-Tsai-Hill theory [30] is very similar to the criterion proposed by Tsai and Hill [31]. The only difference is that the coupling term between σ_{11} and σ_{22} uses the absolute value as can be seen in Eqn. 2.2. Hills theory is an orthotropic version of the von Mises yield criterion. $R_{||}$ and $R_{\perp}$ represent the strength of the material in fiber and perpendicular to the fiber direction respectively. The superscripts c and t stand for compression and tension respectively.

$$\frac{\sigma_{11}^2}{R_{||}^{c,t\,2}} - \frac{\mid \sigma_{11}\sigma_{22} \mid}{R_{||}^{c,t\,2}} + \frac{\sigma_{22}}{R_{\perp}^{c,t}} + \frac{\sigma_{12}}{R_{||\perp}^2} \leq 1 \tag{2.2}$$

2.2.1.2 Tsai-Wu Criterion

One of the most common criterion for a laminae is the theory of Tsai and Wu [32]. It is based on the Hill theory for orthotropic materials. Due to the reasonably good agreement with experimental data, the Tsai-Wu criterion is implemented in almost all programs for the analysis of laminates. The theory assumes a closed failure surface. For a two-dimensional stress state the criterion reduces to the following form:

$$\begin{aligned}(\frac{1}{R_{||}^t} - \frac{1}{R_{||}^c})\sigma_{11} + (\frac{1}{R_{\perp}^t} - \frac{1}{R_{\perp}^c})\sigma_{22} + (\frac{1}{R_{||}^t R_{||}^c})\sigma_{11}^2 + (\frac{1}{R_{\perp}^t R_{\perp}^c})\sigma_{22}^2 \\ - 2\sqrt{\frac{1}{R_{\perp}^t R_{\perp}^c R_{||}^t R_{||}^c}}\sigma_{11}\sigma_{22} + \frac{\sigma_{12}^2}{R_{||\perp}^2} \leq 1\end{aligned} \tag{2.3}$$

The expression $\sqrt{\frac{1}{R^t_\perp R^c_\perp R^t_{||} R^c_{||}}}$ is often given as F_{12} and controls the inclination of the ellipsoid. Due to the linear terms in the equation the ellipsoid is not in the center of the coordinate system. The criterion is depicted in figure 2.7 below.

The Tsai-Wu Criterion is implemented in ABAQUS for post-processing.

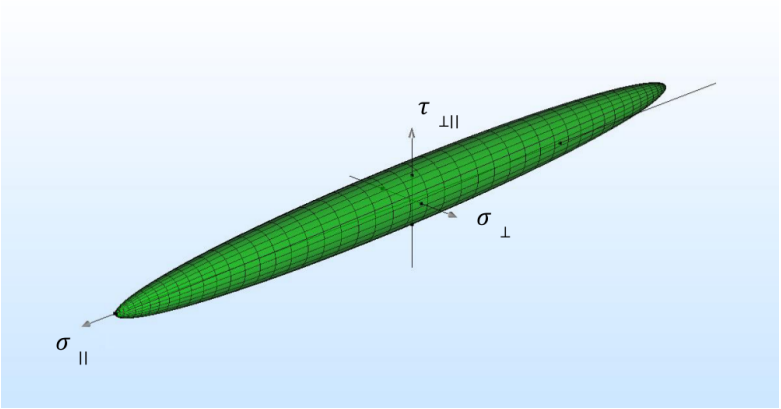

FIGURE 2.7: Failure surface of the Tsai-Wu Criterion.

2.2.2 Failure Criterion associated with the failure mode

Due to the non-homogeneous character of the materials, different failure modes can be observed in a lamina under loading. This group of failure criteria considers this special phenomenon.

2.2.2.1 Hashin Criterion

The Hashin criterion involves two failure modes, one is associated with matrix failure, the other one with fiber failure, respectively. In comparison to the global criteria, the Hashin criterion with its four independent equations is much more complicated in its application. In 1980 Hashin et al. proposed a theory for a three-dimensional stress state. As can be seen in the equations below, the theory accounts for the interaction between shear and normal stress. A second order polynomial approach was chosen to predict matrix failure. For the fiber criterion under tension the parameter α is used to add more weight to the apparent shear stress. The failure mechanisms included in Hashin's theory are as follows:

1. For tensile fiber failure ($\sigma_{11} > 0$):

$$\left(\frac{\sigma_{11}}{R^t_{||}}\right)^2 + \alpha\left(\frac{\sigma_{12}^2 + \sigma_{13}^2}{R^2_{||\perp}}\right) \leq 1 \tag{2.4}$$

2. For compressive fiber failure ($\sigma_{11} < 0$):

$$\left(\frac{\sigma_{11}}{R^c_{||}}\right)^2 \leq 1 \tag{2.5}$$

3. For tensile matrix failure ($\sigma_{22} + \sigma_{33} > 0$):

$$\frac{(\sigma_{22} + \sigma_{33})^2}{{R^t_{\perp\perp}}^2} + \frac{\sigma_{23}^2 - \sigma_{22}\sigma_{33}}{R^2_{||\perp}} + \frac{\sigma_{12}^2 + \sigma_{13}^2}{R^2_{||\perp}} \leq 1 \tag{2.6}$$

4. For compressive fiber failure ($\sigma_{22} + \sigma_{33} < 0$):

$$\left[\left(\frac{R^c_{\perp\perp}}{2R_{||\perp}}\right)^2 - 1\right]\left(\frac{\sigma_{22} + \sigma_{33}}{R^c_{\perp\perp}}\right) + \frac{(\sigma_{22} + \sigma_{33})^2}{4R^2_{||\perp}} + \frac{\sigma_{23}^2 - \sigma_{22}\sigma_{33}}{R^2_{||\perp}} + \frac{\sigma_{12}^2 + \sigma_{13}^2}{R^2_{||\perp}} \leq 1 \tag{2.7}$$

The resultant failure surface is depicted in figure 2.8. It can be observed that the influence of shear is only taken into account for tensile loading.

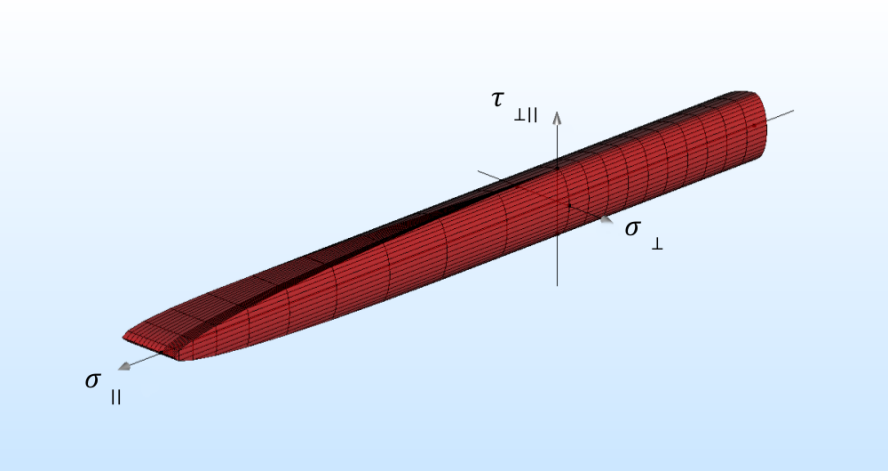

FIGURE 2.8: Failure surface of the Hashin criterion.

2.2.3 Puck Criterion

Puck is one of the winners of the WWFE. The physically based phenomenological failure criterion [33] is in good agreement with the experimental data for a lamina. Furthermore, his approach to describe degradation of laminates is one of the most accurate ones. The theory is based on Hashin's approach. As mentioned above, Puck distinguishes between three different types of matrix failure, cf. figure 2.9. Furthermore, he emphasizes the importance knowing the fracture angle of the fracture plane. Changing from Mode B to Mode C, the fracture plane starts deviating from the load action plane, therefore, it is necessary to determine the fracture angle θ_{fp}. It is obvious that with an increased fracture angle the out of plane stress component increases. Hence, chance of the explosion phenomenon of laminates mentioned above increases.

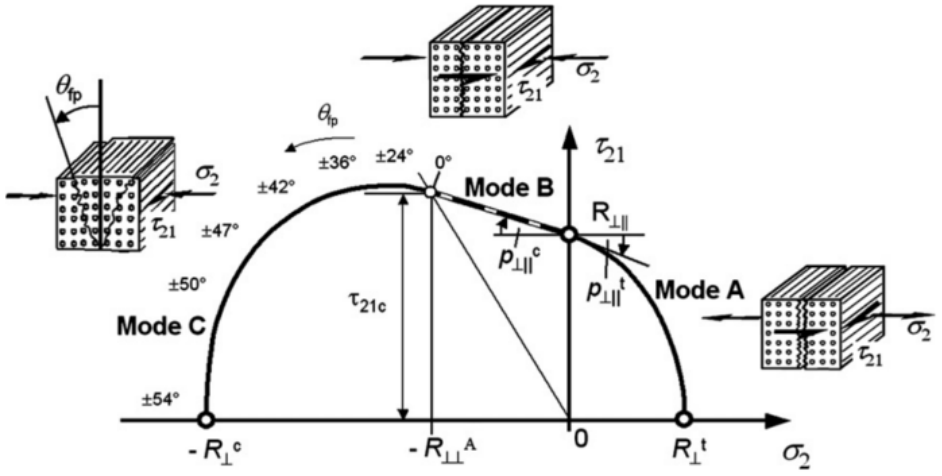

FIGURE 2.9: Inter fiber failure modes according to Puck [6].

Due to the comparatively complex description of matrix failure, the mathematical formulation is complicated. For the two-dimensional state of stress the equations defining the failure limites are listed below:

For mode A ($\sigma_2 \geq 0$):

$$f_E|_{\theta_{fp=0°}} = \frac{1}{R_{\perp||}} \left[\sqrt{\left(\frac{R_{\perp||}}{R^t_{\perp}} - p^t_{\perp||} \right)^2 \sigma_2^2 + \tau_{21}^2} + p^t_{\perp||}\sigma_2 \right] = 1 \tag{2.8}$$

For mode B:

$$f_E|_{\theta_{fp=0°}} = \frac{1}{R_{\perp||}} \left[\sqrt{\tau_{21}^2 + (p^c_{\perp||}\sigma_2)^2} + p^c_{\perp||}\sigma_2 \right] = 1 \tag{2.9}$$

For mode C:

$$f_E|_{\theta_{fp}} = \frac{\tau_{21}^2}{4(R_{\perp||} + p^c_{\perp||} R^A_{\perp\perp})^2} \cdot \frac{(-R^c_\perp)}{\sigma_2} + \frac{\sigma_2}{(-R^c_\perp)} = 1 \tag{2.10}$$

The factors $p^t_{\perp||}$ and $p^c_{\perp||}$ in the equations are curve fitting parameters. The parameters can be chosen individually and without limitations. Nevertheless, in [34] recommendations for the parameters are provided. The failure surface for a two-dimensional stress state is demonstrated in figure 2.10 below. Due to its shape, it is often referred to as "Puck's cigar".

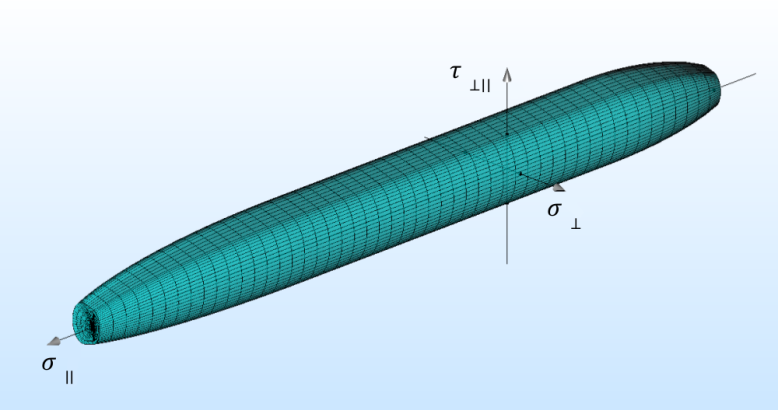

FIGURE 2.10: Failure surface of the Puck criterion.

As can be seen, the matrix strength decreases with an increased longitudinal stress component. Initially, it is assumed that the longitudinal stress in a lamina does not affect the transverse and shear strength. Experiments showed different results in the past. One explanation of this phenomenon can be found in the unusual crack characteristic of laminae. Statistically, many fibers in a lamina fail at a much lower level as the determined longitudinal strength. At the end of a broken fiber a stress concentration is introduced. Thus, this three-dimensional stress state affects the matrix strength. Puck introduced a closed loop description of this phenomenon using an elliptical approach. He describes this weakening of the material properties with two weakening factors, m for transverse and shear direction and s for longitudinal direction of the ellipse. The detailed mathematical formulation can be found in [11].

In a later work, Puck proposed a physically based phenomenological failure criterion for a three dimensional stress state. This theory transforms the current stress state into the fracture plane. With the three new variables σ_n, τ_{n1} and τ_{nt} (see figure 2.11, a master surface can be derived. Out of the master surface, the failure envelope depicted above

in figure 2.9 can be derived following the line depicted in figure 2.11.

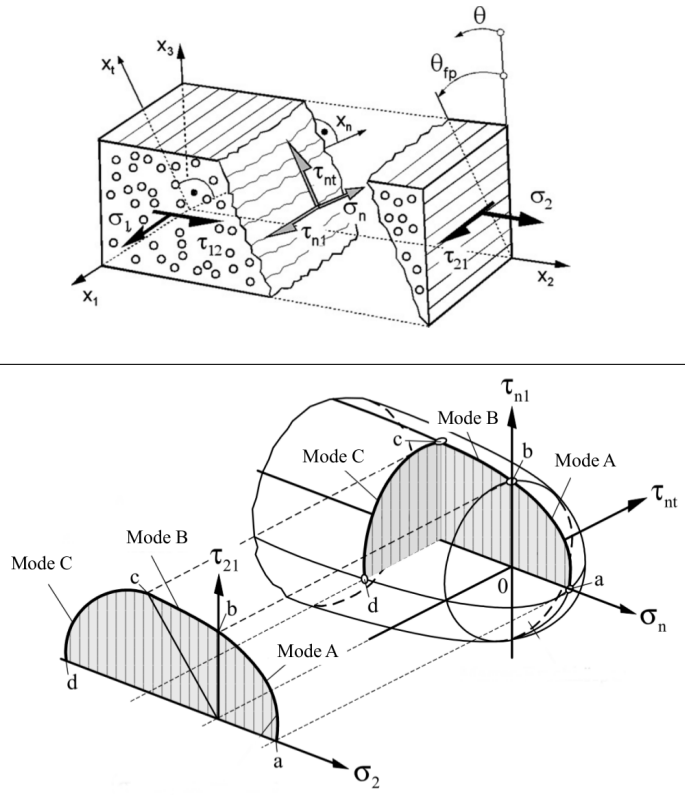

FIGURE 2.11: Stress components in the fracture surface (top) and Puck's master-surface for the components (bottom) [1].

Considering the importance of Puck's physically based approach, the failure criterion was included in the list of criteria under investigation. KluB [1] provides a subroutine for the implementation of Puck's criterion into ABAQUS. The criterion is programmed as a FORTRAN routine which can be used for the post processing of a simulation.

2.2.4 Linde Criterion

Another criterion used in this work is Linde's strain based failure criterion for FRPs. Linde's theory has been developed relatively recently compared to the previous criteria mentioned above. The theory was developed for the simulation of fiber metal laminates at AIRBUS. Linde as well as Hashin and Puck differentiate between fiber and matrix failure. Therefore, two different equations for the stress exertion are necessary as stated

[1] Institute **K**onstruktiver **L**eichtbau **u**nd **B**auweisen of the TU Darmstadt

below:

$$f_f = \sqrt{\frac{\varepsilon_{11}^t}{\varepsilon_{11}^c}(\varepsilon_{11})^2 + \left(\varepsilon_{11}^t - \frac{(\varepsilon_{11}^t)^2}{\varepsilon_{11}^c}\right)\varepsilon_{11}} \tag{2.11}$$

$$f_m = \sqrt{\frac{\varepsilon_{22}^t}{\varepsilon_{22}^c}\varepsilon_{22} + \left(\varepsilon_{22}^t - \frac{(\varepsilon_{22}^t)^2}{\varepsilon_{22}^c}\right)\varepsilon_{22} + \left(\frac{\varepsilon_{22}^t}{\varepsilon_{12}^s}\right)^2 \varepsilon_{12}^2} \tag{2.12}$$

Here, $\varepsilon^t, \varepsilon^c$ and ε^s stand for the failure strain under tension, compression and shear loading. Failure occurs as soon as the threshold value (ε_{11}^t or ε_{22}^t) of either f_f for fibers or f_m for the matrix is exceeded. The failure curve for matrix failure is shown in Fig. 2.12.

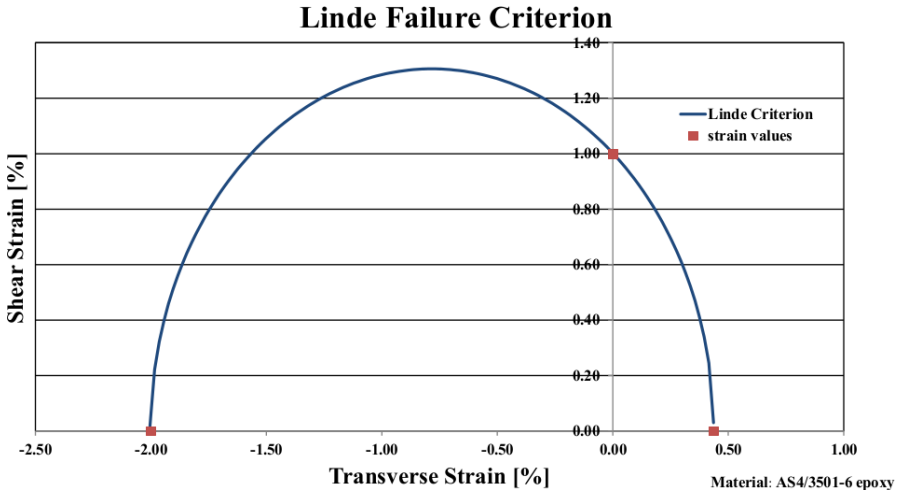

FIGURE 2.12: Failure envelope of Linde's strain-based criterion for matrix fracture.

2.3 Laminate Failure

As mentioned earlier in this work, laminates show some intricate fracture modes. This section provides an overview of the special fracture mechanisms of laminated composites as well as their computational treatment. In particular, the non-linear behavior is discussed.

2.3.1 Nonlinearities of FRPs

Polymer composites show three different types of nonlinearities [35]:

1. Nonlinear bulk behavior of the matrix,
2. nonlinear behavior due to the gradual failure,
3. and nonlinearity caused by the rearrangement of fibers due to IFF.

The material nonlinearity can especially be seen in the stress-strain curves for a lamina under transverse tension $\sigma_\perp$ or longitudinal-transverse shear stress $\tau_{\perp||}$. The main reason for this behavior is micro damage in the matrix and at the interface of fiber and matrix [11]. The material nonlinearity can be taken into account if a secant modulus for $E_\perp$ and $G_{\perp||}$ is used for the analysis instead of a tangent modulus. This requires the knowledge of the stress-strain curve of the material. If the exact stress-strain relation is not known, a standard linear analysis for the calculation of the stresses can be carried out. The fracture analysis will then be shifted towards a more conservative assessment of the laminate. This nonlinear behavior is not considered within the workflow developed in this work. Figure 2.13 represents the material behavior under $\sigma_\perp$ and $\tau_{\perp||}$ stress for CFRP and GFRP. Gradual failure of the individual plies is the reason for the second nonlinearity.

The stiffness decreases continuously according to the present damage state and therefore the slope of the stress-strain curve changes instantaneously, cf. 2.15 (right).

The last nonlinearity from the list above is a rather rare phenomenon, because engineers try to avoid this phenomenon as much as possible. This nonlinearity is triggered by a stress state far beyond the occurrence of first FF. If many cracks have developed within

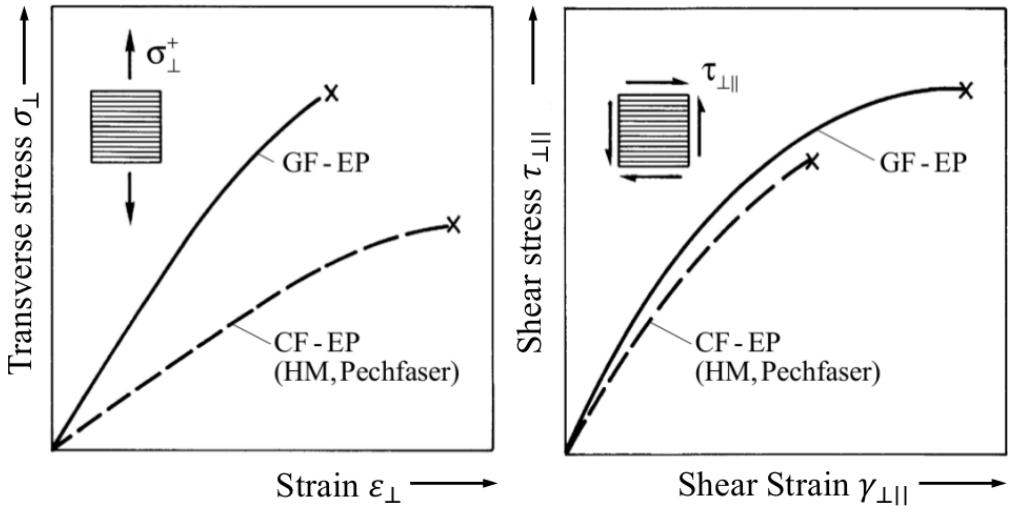

FIGURE 2.13: Representative nonlinear stress-stain curves for transverse and shear stress of carbon and glass reinforced plastics [1].

the laminate, the fibers can realign and change their initial orientation. This leads either to a small increase or a drop of the stiffness. Usually, the fibers tend to rearrange in the loading direction thereby adding stiffness. An example ($\pm 45°$) laminate under uniaxial load showing the effect of fiber realignment is demonstrated in Fig. 2.14.
As can be seen from the chart on the right hand side, a fiber angle change of only 5° leads to a stiffness variation of roughly $\pm 7500 N/mm^2$ for this particular material.

The nonlinear material properties mentioned above are implemented in the freely available CLT tool from KluB. This tool is used for the last ply failure (LPF) analysis in the workflow developed in this work.

2.3.2 Special Effects of Laminates

2.3.2.1 Degradation

With the failure criteria for a lamina, the load responsible for the initial failure can be determined. From this point, the stiffness parameters of the broken ply are reduced adequately. This step is called degradation and leads to a subsequent stress redistribution in the laminate. If the load is increased even more, another ply will fail and thus the stiffness properties decrease again. This procedure can be continued until fracture of the last ply. The stiffness reduction can be observed in the stress-strain curve of the laminate under investigation. Figure 2.15 shows the degradation of a $(0, 90)_s$ cross-ply laminate.

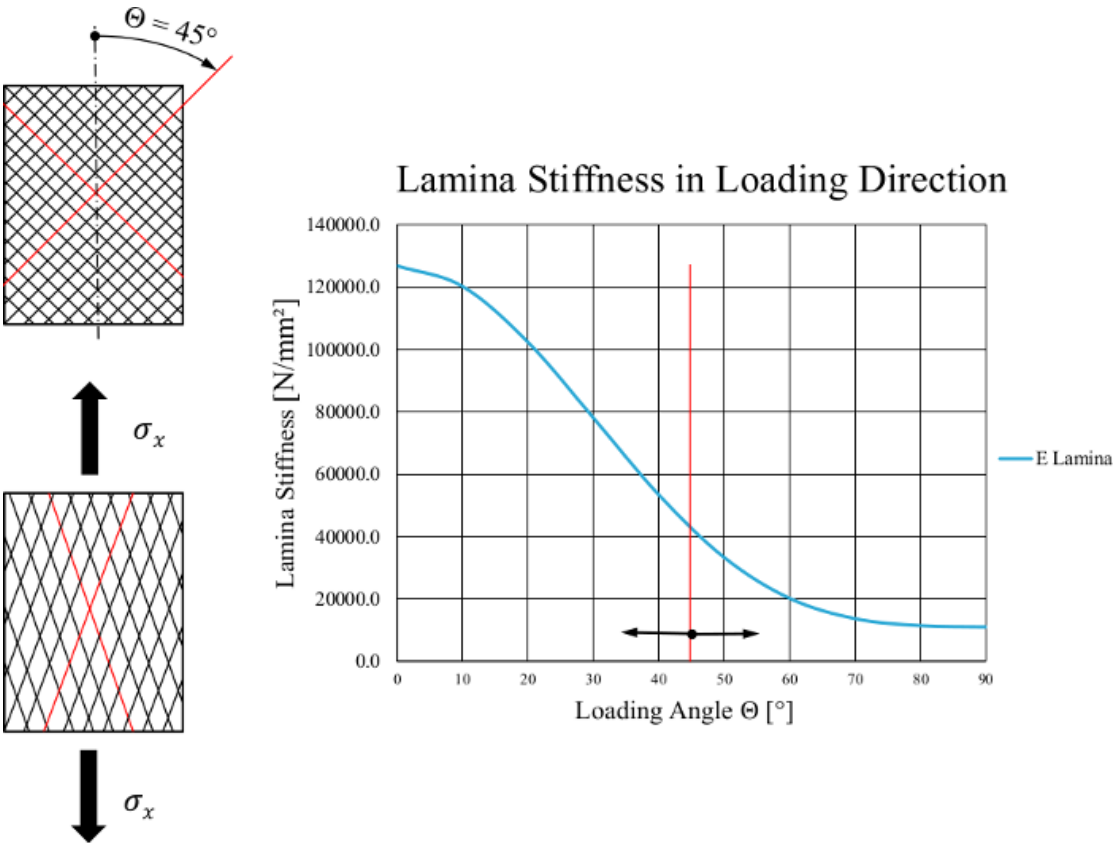

FIGURE 2.14: Geometrical nonlinearity due to fiber realignment. Top left: $(\pm 45°)$ laminate. Bottom left: Changed fiber orientation due to damaged plies. Lamina stiffness change caused by fiber angle variation (right).

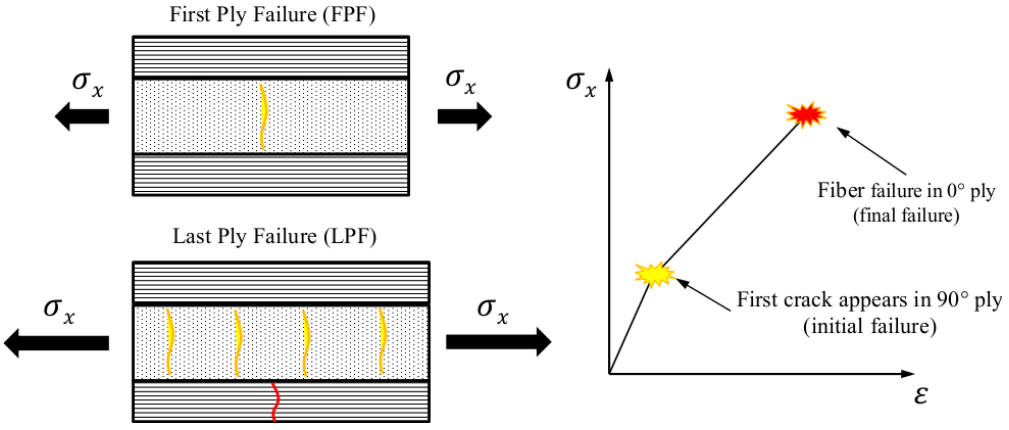

FIGURE 2.15: Characteristic damage state (left) and the stress-strain curve of a $(0, 90)_s$ cross-ply (right).

The bend, shown in the plot, is also called the "knee" of the stress-strain relation. It is an indicator of the FPF. The reduction process of a single layer can be observed as long as the failed ply is able to create more cracks. After a certain amount of cracks has been reached in the damaged ply, the stress strain curve continues linearly until the next ply fails. The procedure starts over again as described above.

Figure 2.15 (left) shows the crack saturation of a $(0, 90)_s$ cross-ply laminate under uniaxial tension. The red line indicates the fiber failure. The yellow lines stand for cracks in the matrix material. As can be seen in the figure, crack saturation means equal distances between the cracks through the lamina. More on this under section 2.3.2.3

2.3.2.2 Delamination

Delamination as one special issue in failed laminates has already been mentioned earlier in this chapter. Its analysis would require a complex and extensive description beyond the scope of this work. Hence, this problem is omitted in here.

2.3.2.3 Characteristic Damage State (CDS) and In-Situ effect

In an isolated lamina, the fracture will lead to separation, i.e. total failure of the material. If the lamina is embedded in a laminate, the adjacent plies will bridge the crack and load the broken lamina again until the next crack appears. In other words, the broken lamina doesn't lose its entire strength after initial failure. The state where no more cracks can be created in a damaged lamina is called crack saturation or characteristic damage state (CDS), cf. figure 2.16. The plies next to the broken layer try to redistribute the load of the damaged by means of inter-laminar shear stresses. If the distance between two cracks is too short, the shear stress cannot fully support the broken layer and hence no more cracks can be initiated. This phenomenon was investigated by Puck [5].

Failure criteria as described earlier are developed for single layers. In reality, the adjacent laminae of a broken ply have a supporting effect (in-situ effect). This means, the actual strength of an embedded ply is higher than that of an individual lamina. Nevertheless, it is assumed that the failure criterion for the lamina is also valid for embedded plies. Further investigations concerning the "in-situ effect" can be found in [36] and in the third part of the WWFE which is in progress at this time. Neglecting the in-situ effect

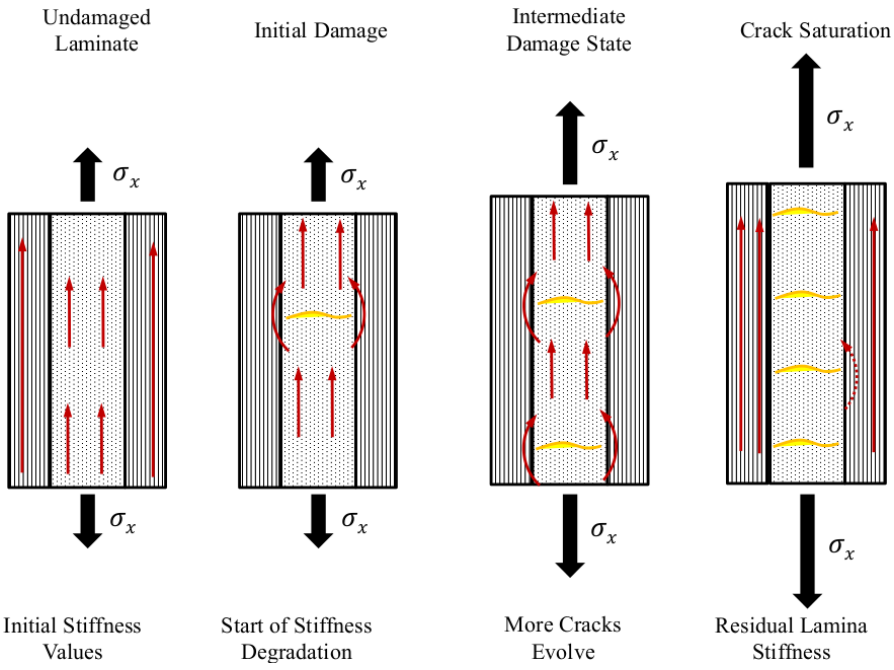

FIGURE 2.16: Crack evolution until crack saturation (CDS) is reached. At CDS, the load in the cracked ply cannot be redistributed again. A residual stiffness of the broken lamina remains.

leads to a more conservative analysis of the laminate.

In addition to these assumptions, it is also assumed that stress concentrations due to a crack within the laminate have no influence on the plies next to the damaged lamina as reported in [11].

2.4 Fracture Analysis

For standard engineering problems the fracture analysis is carried out after the stress analysis. For composites this is true only if a linear analysis is performed. As soon as a nonlinear analysis is carried out, the stress analysis and the fracture analysis are interacting. An iterative process is necessary to find the final load for laminate failure.

The stress analysis of a component is either performed using analytical tools such as the CLT (see chapter 3) or by means of a numerical approximation such as the Finite Element Analysis (FEA) used in this work. A schematic demonstration of the fracture analysis including the iteration can be seen in Fig. 2.17.

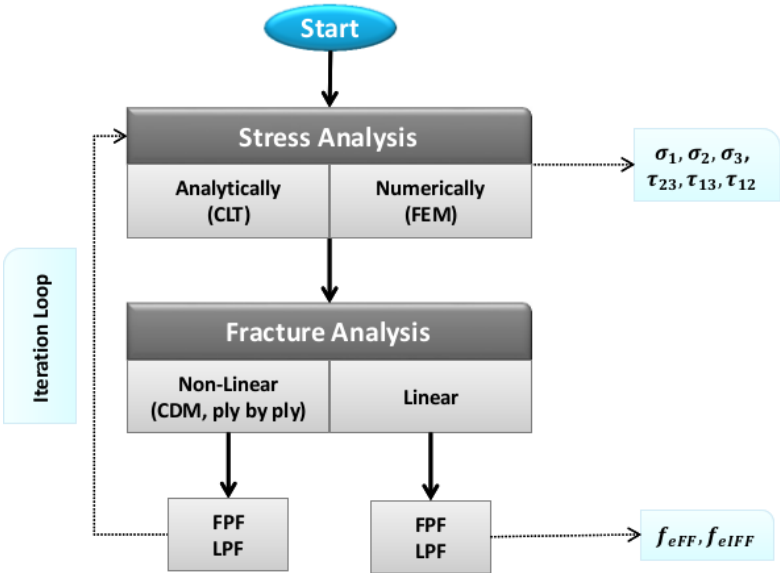

FIGURE 2.17: Flow chart of a fracture analysis for laminates.

2.4.1 FPF vs. LPF Analysis

A first-ply-failure (FPF) analysis largly underestimates the full load carrying capabilities of the layers. In the past, FPF analyses were quite common since the prediction of failure evolution was too complex to understand and furthermore to simulate. Nowadays, engineers want to take advantage of the final capabilities of these advanced materials. Various efforts in the last decades made it possible to predict final failure with acceptable reliability. Still, performing a LPF analysis requires a significant amount of work for the analysis engineer and is computationally highly expensive.
Nowadays, FPF and LPF analyses are used hand in hand. Usually, the FPF analysis is carried out to see whether the component is able to withstand the standard operating loads. In addition to the FPF, the LPF analysis is performed to simulate single time events as for example misuse of the component or crash.

The fracture analysis for laminate composites is carried out in layers. This means for every lamina, the analysis engineer has to apply a proper failure criterion to see whether the layer under investigation will fail or not. Another difficulty lies in the fact that the plies do not break simultaneously. The lamina by lamina fracture analysis allows to account for this successive fracture event.

Lamina by lamina fracture analysis with continuous stiffness reduction beyond FPF leads to a more realistic prediction of laminate failure. It also allows the engineer to observe

if unacceptably large deformations occur. Furthermore, the safety against instability, which reduces with the reduction of the laminate stiffness, can be monitored.

2.4.2 Ply by Ply Discount Method

As described in the previous section, the prediction of final failure is rather complex. One option to track stiffness degradation during laminate failure is the ply by ply discount method. Knops [37] introduced a procedure where the lamina stiffness parameters are reduced according to their stress exertion. The advantage of this approach is that the residual stiffness of a ply is taken into account. Other theories such as the Continuum Damage Mechanics (see section 2.4.3) neglect this factor. The disadvantage of the ply by ply discount method is that it requires many fitting parameters which have to be determined for every single material.

The mathematically degradation is described by the simple reduction of the values $E_{\perp sk}$, $G_{\perp||sk}$ and $\nu_{\perp||sk}$ by the factor η_k as shown below:

$$\begin{aligned} E_{\perp sk} &= \eta_k E^*_{\perp sk} \\ G_{\perp||sk} &= \eta_k G^*_{\perp||sk} \\ \nu_{\perp||sk} &= \eta_k \nu^*_{\perp||sk} \end{aligned} \tag{2.13}$$

The indices s and k stand for secant modulus and the ply number within the stacking sequence. The values marked with an asterisk are the stiffness values shortly before the lamina failure criteria is met. Due to the nonlinear material behavior, the secant modulus and Poisson's ratio are used for the analysis. Puck recommended the following equation for the reduction factor η_k in [5]:

$$\eta_k = \frac{1 - \eta_{Rk}}{1 + a_k(1 - f_{EIFF})^{\xi_k}} + \eta_{Rk} \tag{2.14}$$

with $a_k = 5$ and $\xi_k = 1.3$. The parameter η_R represents the residual stiffness at crack saturation. According to Knops [37], a value of 0.03 for $E_{\perp sk}$ and 0.25 for $G_{\perp||sk}$ and $\nu_{\perp||sk}$ will give accurate results for GFRP's. For CFRP's, these two values are reduced even less ($\eta_R = 0.67$). Note that the stiffness degradation is a hyperbolic function of f_{EIFF} (stress exertion for inter fiber failure). The Figure 2.18 depicts the reduction factor over the calculated stress exertion f_{EIFF}.

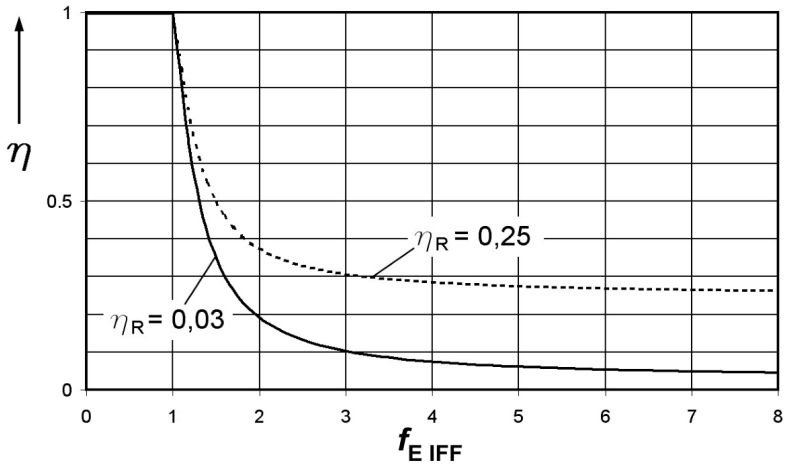

FIGURE 2.18: Reduction factor over stress exertion for IFF.

For a laminate under compression ($\sigma_2 < 0$), $E_{\perp sk}$ and $\nu_{\perp||sk}$ must not be reduced since the normal stress component σ_2 closes the crack and the stiffness will not decrease. Only $G_{\perp||sk}$ is reduced according to Eqn. 2.14. More on this can be found in [5, 11, 37].

In this work, *AlfaLam 2.0*, an analytical analysis tool from KluB, is used to determine LPF. The degradation model of Puck and Knops explained above is implemented in this tool.

2.4.3 Continuum Damage Mechanics CDM

The second approach used in this work for predicting the final failure is continuum damage mechanics. CDM is a rather new but very promising method for commercial use. Here, two different models, the ABAQUS built-in model and Linde's model, are employed. ABAQUS uses the Hashin criterion to predict initial failure and Matzenmiller's approach [38] to model damage. Linde provides an UMAT subroutine which can be executed by ABAQUS. Linde developed his own three-dimensional damage evolution model and uses the strain-based failure criteria as reported earlier (see 2.2.4).
A CDM model introduces damage variables (d) to account for the damage state within a ply. The number of damage variables varies between the CDM theories. The ABAQUS built-in theory employs three damage variables, d_f, d_m, d_s for fiber, matrix and shear failure respectively. Linde only uses d_f and d_m, which simplifies the problem. Below, a rough overview of the mathematical description of the concept is provided. A detailed description of the theory would exceed the scope of this work. An example for a simple

one-dimensional damage variable is the following:

$$d = 1 - \frac{A}{\hat{A}} \quad or \quad d = 1 - \frac{E}{\hat{E}} \tag{2.15}$$

Considering a simple cylindrical truss as depicted in Fig. 2.19, $\hat{A}$ and A are the initial and remaining cross section respectively. Obviously, the range of a damage variable is from 0 to 1. The value $d = 0$ means no crack within the object, hence no stiffness reduction. A value of $d = 1$ corresponds to the total loss of stiffness.

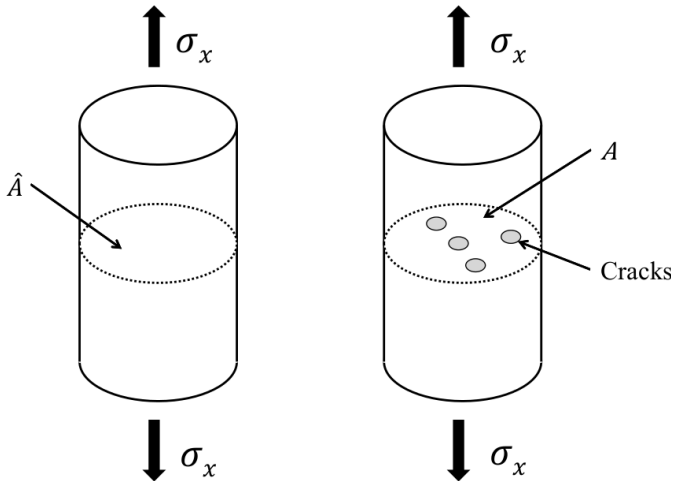

FIGURE 2.19: Undamaged (left) and damaged material (right).

The integration of damage values for a 2D stress state leads to the following stiffness matrix [38]:

$$[C] = \frac{1}{D}\begin{bmatrix} (1-d_f)E_{11} & (1-d_f)(1-d_m)\nu_{21}E_{22} & 0 \\ (1-d_f)(1-d_m)\nu_{12}E_{11} & (1-d_m)E_{22} & 0 \\ 0 & 0 & D(1-d_s)G \end{bmatrix} \tag{2.16}$$

with $D = 1 - (1-d_f)(1-d_m)\nu_{21}\nu_{12}$. The stresses are computed by

$$\{\sigma\} = [C]\{\varepsilon\}. \tag{2.17}$$

The difficulty of these theories is the question of how to degrade the damage values. The built-in model describes a linear stiffness degradation. Linde uses an exponential approach for d_f and d_m as shown below:

$$d_f = 1 - \frac{\varepsilon_{11}^t}{f_f} e^{\left(\frac{-C_{11}\varepsilon_{11}^t(f_f - \varepsilon_{11}^t)}{G_f}\right)} \tag{2.18}$$

$$d_m = 1 - \frac{\varepsilon_{22}^t}{f_m} e^{\left(\frac{-C_{22}\varepsilon_{22}^t(f_m - \varepsilon_{22}^t)}{G_m}\right)} \tag{2.19}$$

with C_{11} and C_{22} from the transverse stiffness matrix of a lamina as in Eqn. 1.8. Remaining factors are defined under section 2.2.4. Note that with the introduction of CDM in the workflow, two additional material constants are necessary for a simulation: G_f and G_m representing the fracture energy of fiber and matrix respectively. A comparison of the two CDM theory used within this work is shown in the figure 2.20.

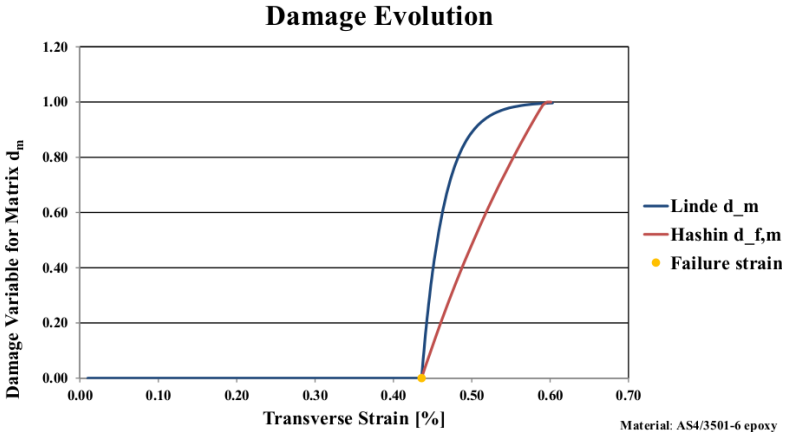

FIGURE 2.20: Comparison of the damage variable for the matrix between Linde and ABAQUS built-in degradation model.

Chapter 3

Analytical Methods for Laminates

3.1 Netting Theory

The netting theory is a rather simple analytical method for the analysis of laminates. The basic assumption of this theory is that the external forces will be transmitted solely through the fiber web. The matrix merely prevents the buckling of the fibers under compression. Under these assumptions in most cases a statically determinate problem formulation is given. The force distribution of the individual layers over the laminate is given by the equilibrium equations.

Due to its simplicity, this theory is a suitable tool for the concept phase during the development of a composite component. The theory will not be discussed here in detail. More information can be found in [11].

3.2 Classical Laminate Theory (CLT)

The CLT is a well-known and widely used method for the analysis of a laminate. The objective of the theory is the calculation of the stresses within each ply of the laminate. In order to find the stresses in each ply, the elastic response of the laminate has to be determined. Therefore, the laminate represents a simple parallelization of the elastic behavior of the individual plies. Using the strains from the global deformation the stresses of the individual plies can be calculated. Before a strength analysis can be carried out, the stress of the ply expressed relative to the global x-y-coordinate system

has to be transformed into the local 1-2-coordinate system. The 1 and 2 direction of the local system represents the longitudinal and transverse direction of the fiber.

The CLT uses the combination of the theories of 2D membrane as well as plate elements. For a single lamina with transversely isotropic material behavior, a uni-axial stress state will not lead to shear stress. Hence, normal stresses do not entail shear strain. However, in a laminate with stacked plies and different orientation of the fibers an interesting phenomenon can be observed. Normal stress in the x-direction of the laminate can bend or even twist it. The mathematical formulation of the combined theory uses a coupling stiffness matrix (B-matrix) to account for these effects. The stiffness matrix for the whole laminate is universally known as the ABD-matrix.

For the classical laminate theory the following assumptions and definitions are made:

- Fibers and matrix carry the load
- Laminae are perfectly bonded together
- The laminate consists of several orthotropic or isotropic layers
- The fiber-matrix compound is considered as a continuum

The four governing equations of the CLT are based on kinematic and constitutive relation, force resultants and equilibrium. The kinematic formulation obeys the constraints for plates:

- The theory is valid only for thin plates ($width > 10 \cdot thickness$)
- Small displacement in transverse direction
- Kirchhoff's assumptions apply:
  - cross sections remain plane
  - the neutral mid-plane and the cross section remain unstreched
  - Normals remain perpendicular to their reference surface

Especially the latter assumptions limit the CLT concerning the analysis of transverse shear. Shear stress inside the layer is not taken into account. In the first order shear

deformation theory (FSDT) the kinematic accounts for shear deformation within the individual plies. If transverse shear deformation can no longer be neglected, the FSDT which takes into account shear deformation has to be employed.

A lamina is considered as a continuum with transversely isotropic material behavior, thus, Hooke's Law can be used describing its constitutive behavior. Using Kirchhoff's strain relations, the stresses in a ply can be calculated using the reduced stiffness matrix as seen in Eqn. 3.8.

Instead of stresses acting on each ply, it is convenient to use equivalent forces and moments acting on the middle surface of the individual layers. The section forces/moments are divided by the width of the laminate and therefore their units are force per unit length and moment per unit length respectively. On a laminate a total of six section forces and moments can be applied. Two normal section forces (n_x, n_y), and a shear force (n_{xy}) can be superimposed with two bending (m_x, m_y) and one twisting moment (m_{xy}). The distribution of forces can be integrateg to form the total section forces acting on the laminate $\{\hat{N}\}$ and $\{\hat{M}\}$. The $(\hat{})$ denotes the total components summed over the section, see figure 3.1.

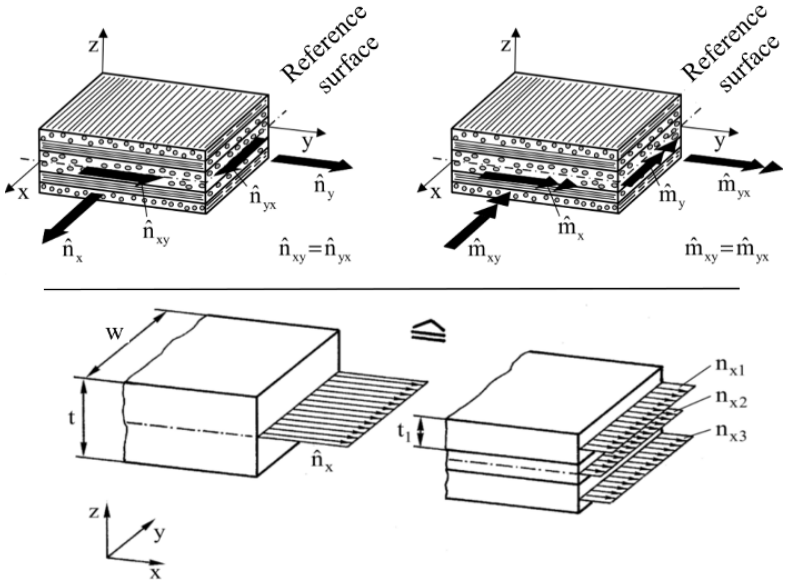

FIGURE 3.1: Forces and moments acting on a laminate (top). Resultant forces in a laminated composite (bottom) [1].

The final cornerstone of the CLT is the equilibrium equation. As usual for elasticity problems, the part and any arbitrary section of the part has to be in equilibrium.

The mathematical procedure of the CLT is carried out in detail below. The resultant forces and moments are defined using the total section forces divided by the span w of the plate:

$$\{\hat{n}\} = \frac{\hat{N}}{w} \tag{3.1}$$

$$\{\hat{m}\} = \frac{\hat{M}}{w} \tag{3.2}$$

The reaction force and moment of the k-th ply are defined as:

$$\{\hat{n}\} = \sum_{k=1}^{n} \int_{z_{k-1}}^{z_k} \{\sigma\}_k \, dz \tag{3.3}$$

$$\{\hat{m}\} = \sum_{k=1}^{n} \int_{z_{k-1}}^{z_k} \{\sigma\}_k z \, dz \tag{3.4}$$

As mentioned above, before the stiffness matrix of the whole laminate can be calculated, the elasticity matrices Q for the plies have to be determined, starting with Hooke's Law:

$$\{\varepsilon\}_k = [S]_k \{\sigma\}_k \tag{3.5}$$

for a plane stress state the compliance matrix for a lamina reduces to

$$[S]_k = \begin{bmatrix} S_{11} & S_{12} & 0 \\ S_{21} & S_{22} & 0 \\ 0 & 0 & S_{66} \end{bmatrix}_k = \begin{bmatrix} \frac{1}{E_1} & \frac{-\nu_{21}}{E_2} & 0 \\ \frac{-\nu_{12}}{E_1} & \frac{1}{E_2} & 0 \\ 0 & 0 & \frac{1}{G_{12}} \end{bmatrix}_k \tag{3.6}$$

The elasticity matrix $[Q]_k$ is obtained by inverting the compliance matrix for the lamina.

$$[Q]_k = [S]_k^{-1} \tag{3.7}$$

Then, the two dimensional stress vector is calculated as following

$$\begin{Bmatrix} \sigma_1 \\ \sigma_2 \\ \tau_{12} \end{Bmatrix}_k = \begin{bmatrix} Q_{11} & Q_{12} & 0 \\ Q_{21} & Q_{22} & 0 \\ 0 & 0 & Q_{66} \end{bmatrix}_k \begin{Bmatrix} \varepsilon_1 \\ \varepsilon_2 \\ \gamma_{12} \end{Bmatrix}_k \tag{3.8}$$

using

$$\begin{array}{rcccl} Q_{11} & = & \frac{S_{22}}{S_{11}S_{22}-S_{12}^2} & = & \frac{E_1}{1-\nu_{12}\nu_{21}} \\ Q_{12} & = & \frac{\nu_{12}E_2}{1-\nu_{12}\nu_{21}} & = & \frac{\nu_{21}E_1}{1-\nu_{12}\nu_{21}} \\ Q_{22} & = & \frac{S_{11}}{S_{11}S_{22}-S_{12}^2} & = & \frac{E_2}{1-\nu_{12}\nu_{21}} \\ Q_{66} & = & \frac{1}{S_{66}} & = & G_{12} \end{array} \tag{3.9}$$

as the matrix entries. The elasticity matrix of the lamina has to be transformed into the global coordinate system utilizing the transformation matrix $[T]_k$. The Index k denotes an expression which can be formed for every ply.

$$[T]_k = \begin{bmatrix} \cos(\theta)^2 & \sin(\theta)^2 & 2\cos(\theta)\sin(\theta) \\ \sin(\theta)^2 & \cos(\theta)^2 & 2\cos(\theta)\sin(\theta) \\ \cos(\theta)\sin(\theta) & -\cos(\theta)\sin(\theta) & \cos(\theta)^2 - \sin(\theta)^2 \end{bmatrix}_k \tag{3.10}$$

The stress and strain vector can be transformed according to:

$$\begin{Bmatrix} \varepsilon_x \\ \varepsilon_y \\ \gamma_{xy} \end{Bmatrix}_k = [T]_k^{-T} \begin{Bmatrix} \varepsilon_1 \\ \varepsilon_2 \\ \varepsilon_6 \end{Bmatrix}_k \tag{3.11}$$

$$\begin{Bmatrix} \sigma_x \\ \sigma_y \\ \tau_{xy} \end{Bmatrix}_k = [T]_k^{-T} \begin{Bmatrix} \sigma_1 \\ \sigma_2 \\ \tau_{12} \end{Bmatrix}_k = [T]_k^{-1}[Q]_k[T]_k^{-T} \begin{Bmatrix} \varepsilon_x \\ \varepsilon_y \\ \gamma_{xy} \end{Bmatrix}_k . \tag{3.12}$$

The inverse and the transposed inverse of the transformation matrix can be used to form the stiffness matrix of a lamina in the global coordinate system.

$$[\bar{Q}] = [T]_k^{-1}[Q]_k[T]_k^{-T} \tag{3.13}$$

The stress-strain-relation can therefore be written as

$$\begin{Bmatrix} \sigma_x \\ \sigma_y \\ \tau_{xy} \end{Bmatrix}_k = [\bar{Q}]_k \begin{Bmatrix} \varepsilon_x \\ \varepsilon_y \\ \gamma_{xy} \end{Bmatrix}_k \tag{3.14}$$

3.2.1 ABD-Matrix

The ABD-matrix denotes the stiffness matrix of the laminate. It relates the global strain of the laminate to the line loads acting on it. It consists of three distinct quadrants. The A-quadrant which is the membrane quadrant, the D-quadrant, representing the plate theory, and the B-quadrant, coupling those two matrices.

$$\left\{\begin{array}{c} n_x \\ n_y \\ n_{xy} \\ \hline m_x \\ m_y \\ m_{xy} \end{array}\right\} = \left[\begin{array}{ccc|ccc} A_{11} & A_{12} & A_{13} & B_{11} & B_{12} & B_{13} \\ A_{21} & A_{22} & A_{23} & B_{21} & B_{22} & B_{23} \\ A_{31} & A_{32} & A_{33} & B_{31} & B_{32} & B_{33} \\ \hline B_{11} & B_{12} & B_{13} & D_{11} & D_{12} & D_{13} \\ B_{21} & B_{22} & B_{23} & D_{21} & D_{22} & D_{23} \\ B_{31} & B_{32} & B_{33} & D_{31} & D_{32} & D_{33} \end{array}\right] \left\{\begin{array}{c} \varepsilon_x^0 \\ \varepsilon_y^0 \\ \varepsilon_{xy}^0 \\ \hline \kappa_x \\ \kappa_y \\ \kappa_{xy} \end{array}\right\} \tag{3.15}$$

In short notation, the equation simplifies to

$$\left\{\begin{array}{c} \{n\} \\ \{m\} \end{array}\right\} = \begin{bmatrix} [A] & [B] \\ [B] & [D] \end{bmatrix} \left\{\begin{array}{c} \{\varepsilon^0\} \\ \{\kappa\} \end{array}\right\} \tag{3.16}$$

The individual quadrants also called sub-matrices, can be calculated using the stiffness matrices of the plies. Weighting them with the distance to the mid-surface and adding them up leads to the following expressions.

$$\begin{array}{rcll} [A] & = & \sum[\bar{Q}]_k(z_k - z_{k-1}) & \text{Extensional Stiffness} \\ [B] & = & 1/2 \ \sum[\bar{Q}]_k(z_k^2 - z_{k-1}^2) & \text{Coupling Stiffness} \\ [D] & = & 1/3 \ \sum[\bar{Q}]_k(z_k^3 - z_{k-1}^3) & \text{Bending Stiffness} \end{array} \tag{3.17}$$

The strains of the laminate are determined by simply inverting 3.16.

$$\left\{\begin{array}{c} \{\varepsilon^0\} \\ \{\kappa\} \end{array}\right\} = \begin{bmatrix} [A] & [B] \\ [B] & [D] \end{bmatrix}^{-1} \left\{\begin{array}{c} \{n\} \\ \{m\} \end{array}\right\} \tag{3.18}$$

In some cases the contribution of transverse shear has to be taken into account. Then, the FSDT has to be enforced. The theory introduces the H-matrix which represents the transverse shear stiffness of a plate. Similar to the normal forces and moments in Eqn.

3.15, the transverse forces $\hat{V}$ or $\hat{v}$ can be written as:

$$\begin{Bmatrix} v_y \\ v_x \end{Bmatrix} = \begin{bmatrix} H_{44} & H_{45} \\ H_{54} & H_{55} \end{bmatrix} \begin{Bmatrix} \gamma_{yz} \\ \gamma_{xz} \end{Bmatrix} \tag{3.19}$$

The components of the H matrix can be obtained similar to Eqn. 3.17 by the following expression:

$$H_{ij} = \frac{5}{4} \sum [\bar{Q}_{ij}]_k (t_k - \frac{4}{t^2}(t_k z_k^2 + \frac{t_k^3}{12}); i, j = 4, 5 \tag{3.20}$$

These stiffness values have to be defined for a simulation in ABAQUS if thick shell elements are used and transverse shear is calculated. How the values can be set in ABAQUS is described in section 4.3.2.

Before the stresses and strains of the individual laminae can be calculated in terms of the local coordinate system, the stresses of the UD-lamina have to be determined in the global coordinate system.

The stresses and strains inside the individual plies are calculated starting with global strains and curvatures of the laminate. Once these values are known, the global strains of the individual plies can be calculated.

$$\begin{Bmatrix} \varepsilon_x \\ \varepsilon_y \\ \gamma_{xy} \end{Bmatrix}_k = \begin{Bmatrix} \varepsilon_x + \kappa_x z_k \\ \varepsilon_y + \kappa_y z_k \\ \gamma_{xy} + \kappa_{xy} z_k \end{Bmatrix} \tag{3.21}$$

With the elasticity matrix of the k-th UD-ply in the global coordinate system (see Eqn. 3.14), the stresses can be obtained using these strains.

$$\begin{Bmatrix} \sigma_x \\ \sigma_y \\ \tau_{xy} \end{Bmatrix}_k = [\bar{Q}]_k \begin{Bmatrix} \varepsilon_x \\ \varepsilon_y \\ \gamma_{xy} \end{Bmatrix}_k \tag{3.22}$$

The last step of this procedure is to transform the global stresses of each ply back into the local 1,2-coordinate system. This can easily be done using the transformation matrix in Eqn. 3.10.

$$\begin{Bmatrix} \sigma_1 \\ \sigma_2 \\ \tau_{12} \end{Bmatrix}_k = [T]_k \begin{Bmatrix} \sigma_x \\ \sigma_y \\ \tau_{xy} \end{Bmatrix}_k \tag{3.23}$$

The strains in the main direction of a lamina are determined using the compliance matrix of Eqn. 3.6

$$\begin{Bmatrix} \varepsilon_1 \\ \varepsilon_2 \\ \gamma_{12} \end{Bmatrix}_k = [Q]^{-1} \begin{Bmatrix} \sigma_1 \\ \sigma_2 \\ \tau_{12} \end{Bmatrix}_k \tag{3.24}$$

With the stresses in the fiber direction, a stress analysis can be carried out using one of the failure criteria as described in Chapter 2. As mentioned above, the classical laminate software tool *AlfaLam 2.0* provided by KluB will be used in the workflow developed in this work.

Chapter 4

Modeling Techniques for Composites in ABAQUS

The preprocessing of a finite element analysis is a very important step. It determines the quality of the simulation and hence the accuracy of the results. The preparation of the model is a very time consuming procedure. Besides the mesh generation, loads and constraints have to be applied, the geometry has to be prepared and the desired output is set within this process. The following chapter gives a detailed insight into special modeling techniques for laminates.

4.1 Model Description

Before one can start thinking about different modeling techniques, a detailed description of the real part is necessary. A list of compulsory information is shown below:

- Manufacturing method
- Detailed knowledge of the constituents material properties
- Plybook

Without the knowledge of the above mentioned issues, a productive analysis is not possible. The manufacturing method predetermines the orientation of the fibers. Even though the design engineer defines the fiber orientation, the orientation in a real part will

always deviate. The more complex the geometry is, the more deviation from the defined orientation can be observed. For the best possible results of the simulation, a draping simulation should be carried out before the structural analysis is executed. Here, the fiber rearrangement during the manufacturing process is simulated. One example is the preforming of woven fabrics before the Resin Transfer Molding (RTM) process. Listing all the available manufacturing processes is not part of this work. More information is reported in [15]

In comparison to metallic materials, the strength values of different specimens vary much more. There are many parameters which influence the ultimate strength of a ply, for example the strength values of the constituents, the manufacturing method or the bonding between fiber and matrix. A very important factor is the fiber volume fraction V_f or ϕ. In practice, fiber volume fractures between 0.3 and 0.65 are produced. For the determination of the material properties it is recommended to always measure the full stress strain curve of the constituents. The values required for a composite analysis in ABAQUS are reported in section 4.3.1

The plybook represents the stacking sequence of the laminate. Every layer with its orientation angle, its corresponding thickness, and the material defined is reported in the book. If the composite part is not fully developed, the analysis engineer can optimize the stacking sequence according to the simulation. Therefore, results contribute to a refined version of the plybook.

4.2 3D vs. 2D Modeling

The treatment of the imported geometry is a very important step concerning time consumption of the analysis. Before the simulation engineer starts preparing the geometry, he needs to be aware of the future effects of different preparation strategies. Initially, it has to be decided if the problem will be meshed as a solid part or a shell part. This decision leads to completely different options in the further modeling process.
One is well advised to perform major geometry changes in cooperation with the design engineer. Many simplifications on the model can easily be done using the native CAD program. ABAQUS provides some features which can be used for geometry changes.

However, these features are not easy to use and often lead to a corrupt geometry which gives difficulties in meshing.

Three-dimensional models are recommended when loads are applied in the out-of-plane direction. The model preparation is rather easy since the imported geometry is usually three-dimensional.

More problems evolve if the imported 3D-geometry has to be transformed into a 2D-geometry. For this task, ABAQUS provides some tools to treat surfaces and regions. Under *Tools* ⇒ *Geometry Edit* a list of certain edge, face and part treatment features can be obtained.

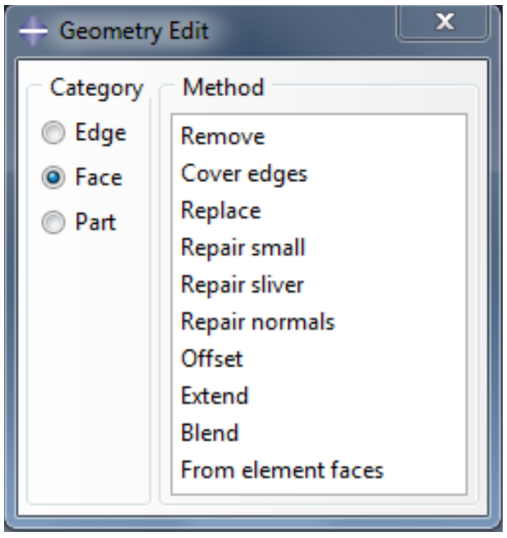

FIGURE 4.1: Options to modify the imported geometry in ABAQUS 6.13.

To convert the 3D-geometry into a 2D-geometry, the following steps have to be executed carefully:

- *Assign Midsurface Region:* This step will transform the volume geometry into a transparent phantom geometry.
- *Offset Faces:* With the option Offset Faces, the faces which will be used for the analysis can be chosen.

For the offset of the faces ABAQUS 6.13 gives the engineer some options of how to set the distance. It can either be defined manually or automatically by the program. By experience, the latter option works well only for simple geometries and should not be chosen for more complex components. It is also recommended to use either the top or

the bottom surface of the component since ABAQUS doesn't have to compute a mid-surface. The mid-surface extraction often leads to corrupt surfaces due to small entities which might vanish due to the extraction process. The logical consequence is to take the top or bottom surface and set the reference surface in the *Property Module* to the corresponding face. More on this is documented in section 4.3.2.

A very powerful feature which has to be mentioned here is the *Replace Faces* option. The feature allows the user to exclude entities as for example holes, ribs or rounds. The use of the Replace Faces is not recommended unconditionally though. By simply replacing the faces, redundant edges and vertices will remain in the model. These features will disturb the mesh and a rework of the geometry will be necessary later on. The use of the *Virtual Topology* is the better choice to get rid of small and unnecessary faces and edges.

Figure 4.2 shows the transformation process from a 3D-geometry to a 2D-geometry. Note that unnecessary entities as chamfers or holes have been removed from the converted model.

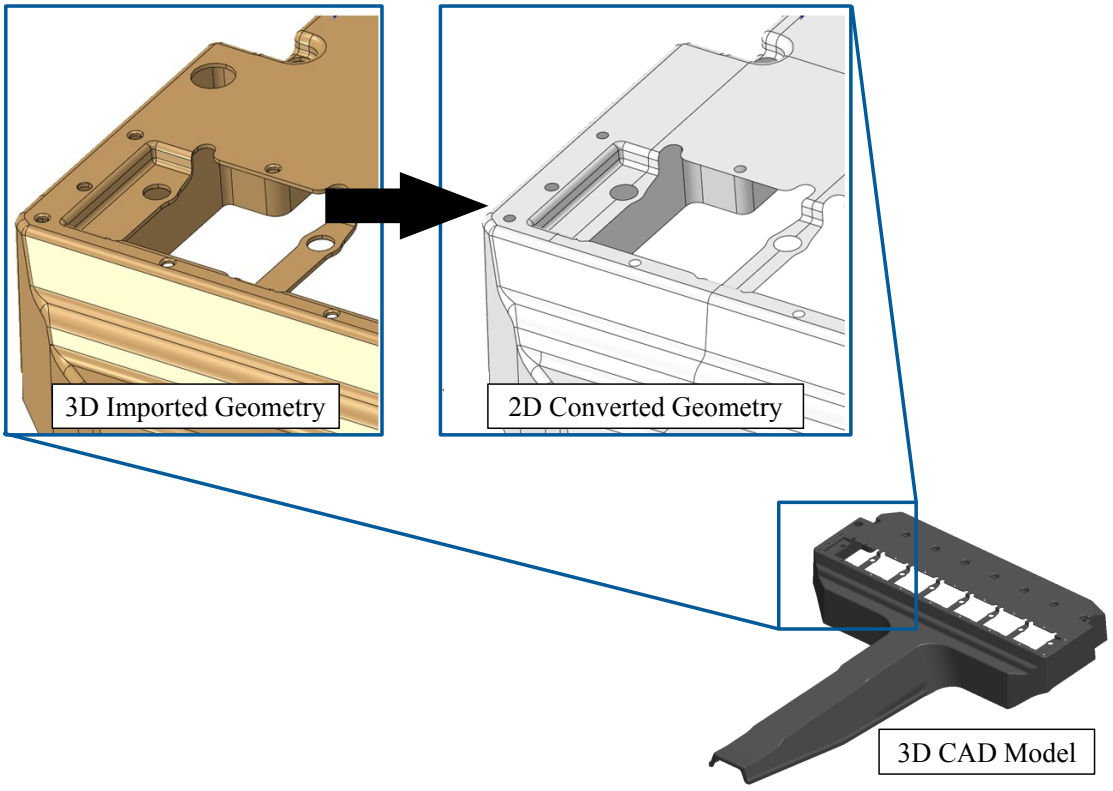

FIGURE 4.2: Convert a 3D imported geometry into a 2D model by means of the features shown in 4.1.

4.3 Material Definition

In section 4.1 the importance of model and material description was pointed out. The information of this step will be used in the following sections to define the material model in ABAQUS. The software provides some features for this process which will be described in detail in the following.

4.3.1 Material Model

In the *Property Module* in ABAQUS the user has some options to define the material behavior of a fiber laminate. The mechanical behavior is either *Elastic*, in case of FPF, or *Damage for Fiber-Reinfored Composites* if LPF is simulated using the damage model implemented in ABAQUS. For the *Elastic* type, the user can basically choose between the two types: Lamina and Engineering Constants

Lamina can be chosen if only UD laminas are modeled. In total, five constants are necessary to define the material. Other constants are calculated by the program. The modeling of woven fabric requires the definition of further constants. Therefore, the *Engineering Constants* option will be the best.
Due to the fact that experimentally evaluated material properties usually deviate from the calculated ones, it is recommended to use the *Engineering Constants* method also for UD laminas. This way, the constants for all directions can be defined individually.
For the use of the failure criteria, the strength values have to be defined in the *Fail Stress* suboption. A list of constants necessary for the FPF analysis material definition is plotted in table 4.1.

Elastic Type	**Required Material Properties**
Lamina	$E_{11}, E_{22}, \nu_{12}, G_{12}, G_{13}, G_{23}$
Engineering Constants	$E_1, E_2, E_3, \nu_{12}, \nu_{13}, \nu_{23}, G_{12}, G_{13}, G_{23}$

TABLE 4.1: Mechanical properties for laminates.

Suboption	**Required Material Properties**
Fail Stress	$R^t_{\|\|}, R^c_{\|\|}, R^t_{\perp}, R^c_{\perp}, R_{\perp\|\|}$

TABLE 4.2: Necessary material parameters for the failure criteria implemented in ABAQUS.

For the integration of Puck's theory, the UVARM subroutine provided by KLuB[1] has to be used. Therefore, a total of nine *User Output Variables* have to be set under the *General* tag. The subroutine takes its input variables from the material name. Therefore, the material name needs to have a specific order. The strength values, weakening factors and fitting parameters needed for Puck's theory have to be included in the name. Since ABAQUS doesn't allow the user to define a name with more than 38 characters, the material name has to be modified after the input file has been created. An example for a name definition in an analysis is shown below:

GG800T/DT120_807_46_706_539_92_35_3_275_275_5_5

GG800T/DT120 is the current name of the material. The values separated with the underscore represent the values as listed in table 4.3. Note that the last six values are originally decimal numbers (0.35, 0.3, 0.275, 0.275, 0.5, 0.5).

In order to obtain the results of the subroutine, the *UVARM* box in the *Field Output Request* has to be checked. Table 4.3 provides a list with the parameters necessary for the Puck integration. A detailed description of the subroutine and its application is provided in [39].

Subroutine	**Number of UVARM Parameters**	**Required Material Properties**
KLuB-VDI2014 v2.0	9	$R^t_{\|\|}, R^c_{\|\|}, R^t_{\perp}, R^c_{\perp}, R_{\perp\|\|}, p^t_{\perp\|\|}, p^c_{\perp\|\|}, p^t_{\perp\perp}, p^c_{\perp\perp}, s, m$

TABLE 4.3: Input parameters for the *KLuB-VDI2014 v2.0* subroutine.

Performing a LPF in ABAQUS is possible using either the built-in damage model or a user subroutine. As mentioned earlier in this work, for the use of the built-in damage model, the parameters under the *Damage for Fiber-Reinforced Composites* have to be defined. In addition to the FPF analysis, the fracture toughness for damage evolution and damping parameters for the iteration process are required.

As described in section 2.4.3, the subroutine used in this work follows the procedure of Linde's continuum damage model. The UMAT subroutine calculates the stiffness values at each integration point for every single time increment. For this process, the routine

[1] Institute **K**onstruktiver **L**eichtbau **u**nd **B**auweisen of the TU Darmstadt

requires the definition of ten *Solution Dependent State Variables* (SDVs). The SDVs as well as the 14 parameters for the *User Material* can be set under the *General* tag. Again, for the visualization of the results, the *SDV* box in the *Field Output Request* has to be checked. A list of necessary parameters for the LPF analyses is provided in table 4.4.

Damage Model	**Number of SDV**	**Required Parameters**
Built-in (Hashin)	-	Elastic: see table 4.1 Strenght: $R_{\|\|}^{t,c}, R_{\perp}^{t,c}, R_{\perp\|\|}, R_{\|\|\perp}$ Evolution: $G_{Ic\|\|}^{t,c}, G_{Ic\perp}^{t,c}, \eta_{v\|\|}^{t,c}, \eta_{v\perp}^{t,c}$
Linde	10	Elastic: $E_{11}, E_{22}, G_{12}, G_{23}, \nu_{12}, \nu_{23}$ Strenght: $R_{11}^{t,c}, R_{22}^{t,c}, S_{12}$ Evolution: G_{Icf}, G_{Icm}, η_v

TABLE 4.4: Input parameters for damage models.

Both models require the input of a *Damage Stabilization*. For the built-in model the user can set four different viscosity values for tension and compression as well as for longitudinal and transverse direction respectively. The viscosity coefficients (usually small in comparison to the time increment) improve the convergence behavior of the increment. In the ABAQUS Documentation [31], for η_v a value of 0.001 is recommended for each direction and loading. Linde uses only one damping coefficient. The effect of the viscosity coefficient on the simulation has to be studied in detail in future work. An example of how to define the Linde's damage model in ABAQUS is given in appendix A.

4.3.2 Composite Layup Tool vs. Section Assignment

After the material definition is complete, the material has to be assigned to the geometry according to the model description carried out beforehand. This can also be done within the *Property Module*. ABAQUS basically provides two distinct options to assign a material to a predefined region:

- Section Definition/Assignment (SD/SA)
- Composite Layup (CL)

During the material assignment, the stacking sequence has to be defined according to the plybook. The user has to decide which method will be more suitable for the analysis. Usually, the Composite Layup tool is the more convenient one to use.
The first option requires the definition of the section, the section assignment and the material orientation to be carried out separately. The CL combines these steps into one single feature. The settings for the analysis remain the same for both:

Ply name, thickness, material, region, ply orientation, number of integration points and the element orientation.

These properties can be specified in either the *Basic* category using the SD method or under the *Plies* registry using CL, respectively. The *Advanced/Shell Parameter* registry enables the user to specify the transverse shear stiffness and transverse modulus. If transverse shear is taken into account during the analysis (always for Linde), these values have to be defined as well. The H_{ij} values can be calculated as reported in Eqn. 3.19.

The thickness specification requires the knowledge of the meshing method. If the model is three dimensional, the total thickness of the laminate is predefined by the imported geometry, therefore, the thickness of each ply has to be set as a relative value. This can be confusing since the thickness of a standard prepreg (0.06 - 1.2mm) is of the same magnitude as the relative thickness value of a ply in a commonly used airplane laminate (0.125). For a 2D geometry absolute values are used.
In addition, the reference surface has to be set according to the model preparation (compare section 4.2). This is possible under the *Offset* tab using CL and during the section assignment using SD.

Another setting worth mentioning here is the definition of the element orientation. Figure 4.3 below shows the different approaches to define the element orientation in a simulation.

The element orientation should be set according to the main fiber orientation of the composite part. It is recommended to use the *Discrete* method especially for curved components. As demonstrated in figure 4.4, the element definition follows the contour of the part. Therefore, a normal and primary axis direction have to be defined as indicated in the figure.

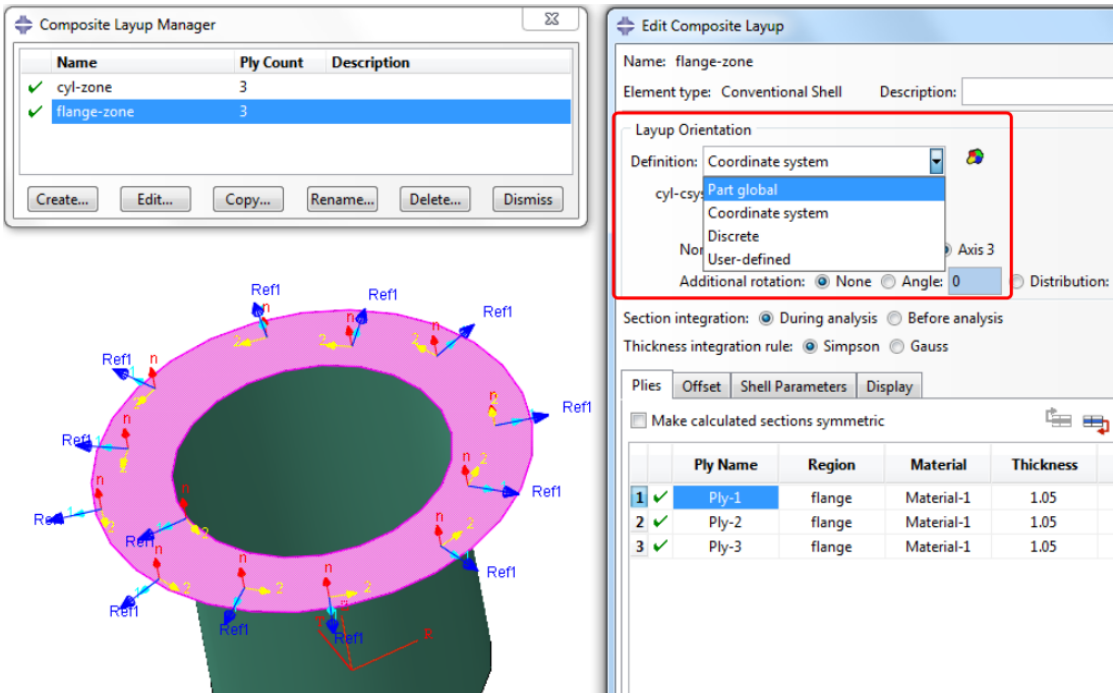

FIGURE 4.3: Different options to define the element orientation of a region.

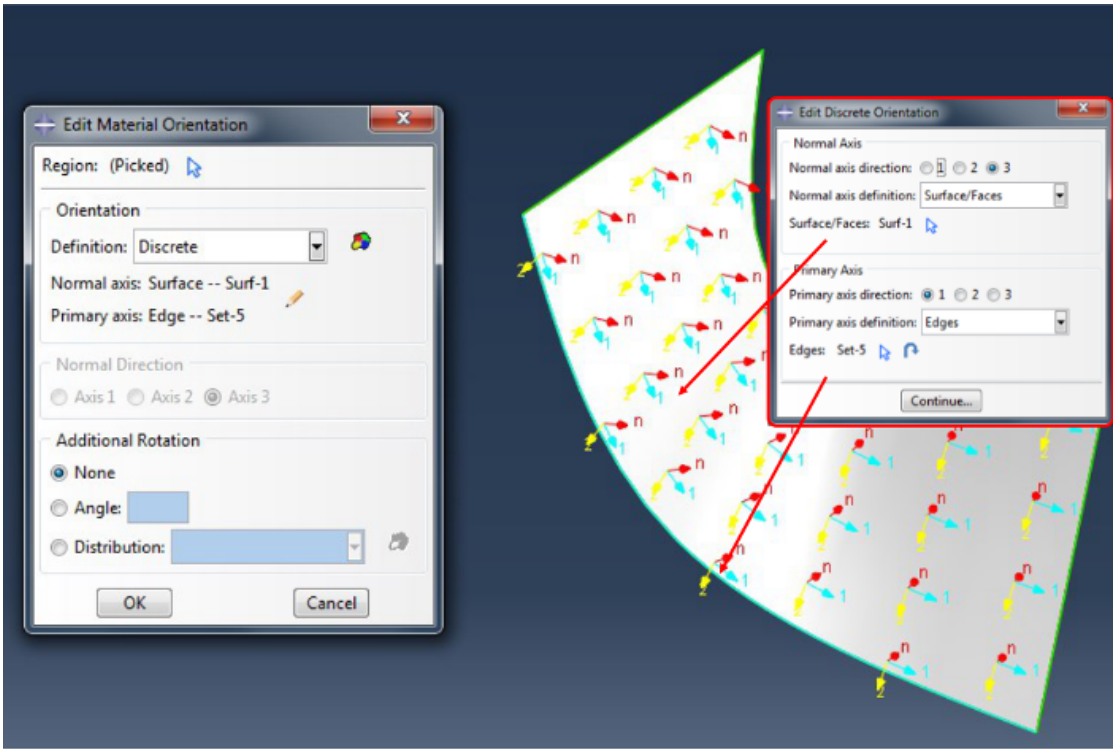

FIGURE 4.4: *Discrete* method for the element definition of a curved component.

Obviously, the *Section Assignment* method requires more work for the analysis engineer than the CL. Still, SA offers some advantages over Composite Layup. Since the definition is similar to metallic materials, the composite analysis can easily be changed to a metal analysis. This can be very helpful during the concept phase of a project. A comparison between a conventional design and a composite design can be carried out easily.

During the definition of the composite layup, ABAQUS highlights the orientation of the current ply under modification in the viewport. For large models this can cause stuttering movements of the model even for high level workstations. Within the *Display* tab under the *Edit Composite Layup* window, the display options can be set in order to provide a fluent operation of the computer. By default, ABAQUS shows the orientation vector of every surface of the model in the viewport. This can be reduced by unchecking the directions not of interest under the *Display* tab and disabling the ply region highlighting.

Particular attention has to be paid if *continuum shell* elements are used for the simulation. Since CS elements are much smaller in one dimension than in the others, one may assume that the thickness direction of the element is equal to the stacking direction of the laminate. This is not always the case. ABAQUS randomly assigns the stacking direction, therefore, the user has to check whether the stacking direction of the elements matches the layup direction of the material. This can be done using *Mesh Controls* ⇒ *Assign Stacking Direction* option. Figure 4.5 shows an example of a laminated plate with correct and incorrectly assigned stacking orientation.

4.3.3 Checking the Material Definition

As described above, the material definition is an essential step for the simulation. In comparison to standard engineering simulation tasks, the material definition and assignment is rather complex and tricky. Due to the various material parameters necessary for a composite material and the different material definition methods for FPF and LPF mistakes may happen easily. To avoid inaccurate results and costly rework, it is recommended to check the material definition of the model during pre- and post-processing. The following approach can serve as a guideline through the simulation process:

- Preprocessing:

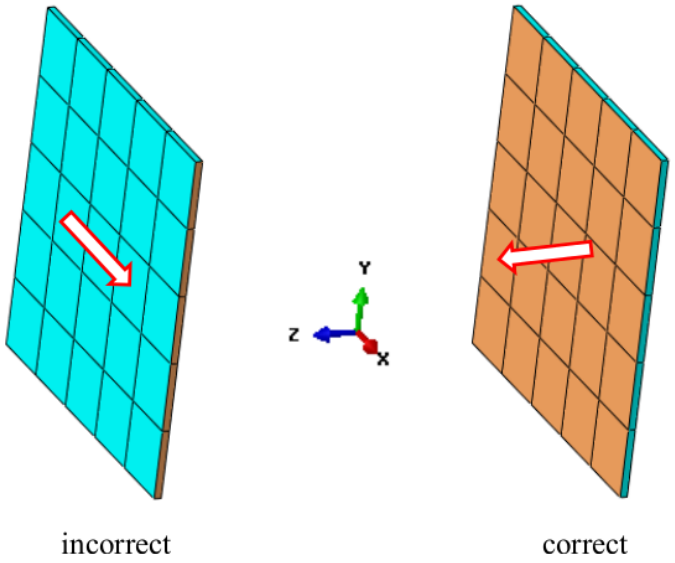

FIGURE 4.5: Example of an incorrectly and correctly assigned stacking orientation for continuum shell elements. The red arrow indicates the stacking of the material from bottom to top. The brown face represents the top surface of the laminate.

1. Check if the model description is complete
2. Review the material parameters and their definition
3. Make sure that the partitioning of the model is accurate and the region definition is correct
4. Check if the sections are defined according to the plybook
   (a) First the outward normal and
   (b) then the 1-direction.
5. For CS elements review the stacking direction

- Postprocessing:

  1. Use the *Plot Material Orientation* in the *Visualization Module* to monitor the material definition of every single element. This is especially important in draped areas and highly loaded areas of the model.

Another very helpful tool to review the stacking definition of the different regions is the *Ply Stack Plot*. This tool can be requested under the *Property Module* ⇒ *Query* ⇒ *Ply Stack Plot* ⇒ *click on region of interest*. Within this very convenient tool, the stacking sequence, the thickness of each ply, its material definition and the fiber orientation as well as integration points can be plotted. One example of a laminated symmetric airplane laminate is shown in figure 4.6.

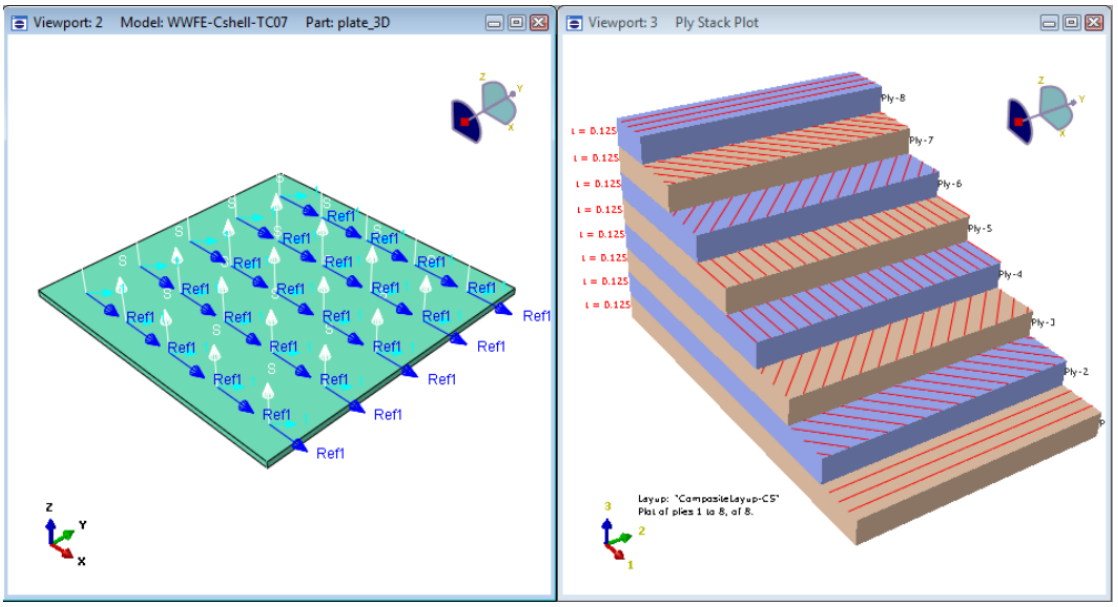

FIGURE 4.6: Ply stack plot for an airplane laminate. Here, only the thickness and the ply name are plotted. Other parameters can be added as desired.

4.3.4 Meshing the Model

The mesh of a FE model determines the overall quality of the final result of an analysis. Over the last decades, more than 100 different element types have been developed. Starting from 1D, 2D and 3D elements using different integration methods, commercial FE programs offer a huge variety. This subsection provides an overview of the most commonly used elements for composite application. More details of different element types are documented in [31].

4.3.4.1 Shell vs. Continuum Elements

Basically there are two types of elements available for the computation of FRPs: 2D (shell) and 3D (continuum or solid) elements cf. figure 4.7. The question which suits the analysis better is nontrivial. One important factor for the element selection is the stress state within the component. If a two dimensional stress state cannot be assumed, the use of continuum elements is inevitable. Stresses in the out of plane direction ($\sigma_3, \tau_{23}, \tau_{13}$) can only be captured accurately using solid elements [10].

Another general rule is reported in [11]. If the slenderness of a composite is greater than 5 to 7 (ratio between *length* and *thickness* of the part), a discretization using

solid elements is not necessary. Due to the increased number of nodes using continuum

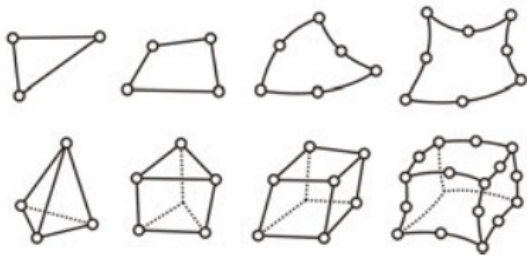

FIGURE 4.7: Top row: 2D elements, bottom row: 3D elements. Quadratic elements contain an additional node in every edge of the element [7].

elements, the simulation will be more accurate as the 2D approach, obviously it will be computationally more expensive. Therefore, the analysis engineer has to find the optimum between computation time and number of nodes on one hand and accuracy and costs on the other hand.

Generally, three-dimensional stress states can be found in load application areas. If these areas are highly loaded, a 3D approach is required. One way of keeping costs in the budget frame and still produce accurate results is to run a global analysis using the two-dimensional approach and afterwards running several smaller submodels on regions of interest using solid elements. This, of course, is only productive if the geometry is large enough so that the time saved by the 2D model is considerable.

A guideline for the element selection based on the properties of the different elements is provided in the following chapter.

4.3.4.2 Shell Elements

Basically, there are two groups of shell elements available in ABAQUS:

- *Conventional Shell* and
- *Continuum Shell* elements.

Conventional shell elements require a 2D geometry in the three-dimensional space. Conventional shell elements include thin and thick shell elements as for example S8R5 and S8R respectively. These elements contain 5 degrees of freedom (DOF) per node for thin and 6 DOF per node for thick shell elements. Thin shell elements enforce the Kirchhoff

constraints as reported in chapter 3. Therefore, the transverse shear deformations γ_{13} and γ_{23} are set to zero. Thick shell elements as opposed to thin elements enforce the FSDT for better prediction of the transverse deformation. This requires input values for the transverse shear stiffness values H_{44} to H_{55} as documented in chapter 3.

Continuum shell (CS) elements (SC6R and SC8R) are actually solid elements and therefore require a 3D geometry. These elements contain more nodes to represent the thickness of the shell. Each node has only 3 DOF (translation) which enables the element to be stacked and connected to standard solid elements. CS elements enforce the FSDT and therefore maintain a constant thickness of the element. Their main advantage compared to solid elements is that CS elements have no aspect ratio problems. As mentioned earlier, continuum shell elements can be stacked, and with an increased number of stacked elements the prediction of transverse shear approaches the exact analytical solution [10].

Due to the relatively low in-plane shear modulus of composites, they should be modeled as thick shells using either conventional shells such as S3R, S3RS, S4R, S4RS, S4RSW, S8R or continuum shell elements such as SC6R and SC8R if better prediction of transverse shear deformation is required.

4.3.4.3 Solid Elements

Continuum elements can reproduce orthotropic material behavior. Similar to continuum shell elements, solid elements have three translational DOFs for each node. Linear elements with 8 and 6 nodes depending on the shape (rectangular or triangle) are available. Quadratic elements contain 20 and 9 nodes per element.

Compared to shell elements solid elements are able to predict transverse compression or tension. Thus, if transverse loading is present in the model as for example in load application areas, the use of solid elements is inevitable.

Note that the change of transverse shear over the thickness can be predicted more accurately using shell elements. Due to the extrapolation errors solid elements calculate a non-zero value for the shear at the surfaces (compare with [31] Benchmark Manual 1.1.3).

For higher accuracy, the solid elements have to be stacked, therefore a finer mesh is required and computational costs increase.

4.4 Special Problems of Composite Modeling

Developing fiber composite parts requires different design approaches than standard engineering applications. To account for these particularities, certain design tools have been developed for composites. This section provides a detailed insight into these special problems.

4.4.1 Sandwich Composites

Sandwich components are used to increase the thickness of the part without adding too much weight. With an increased thickness, the stiffness and in particular the bending stiffness of the part is enhanced. A sandwich component consists of two thin face plates (e.g. CFRP, GFRP,...) which are supposed to carry all the in-plane stresses and a relatively thick core (e.g. honey comb, foam, wood,...). The core is meant to carry the transverse load. An example of a sandwich panel is shown in figure 4.8.

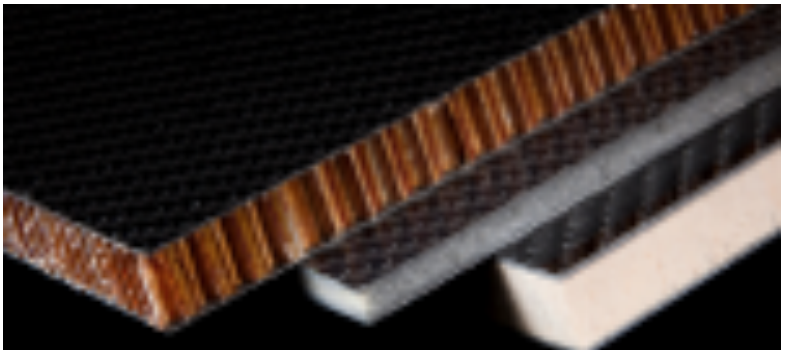

FIGURE 4.8: Sandwich composites with different core material [8].

According to [10], there are four different options to model sandwich elements:

1. Conventional shell elements,
2. one single continuum shell element representing the entire thickness,
3. several continuum shell elements stacked over the entire thickness,
4. and a continuum shell element representing the core while conventional shell elements serve as the face plates.

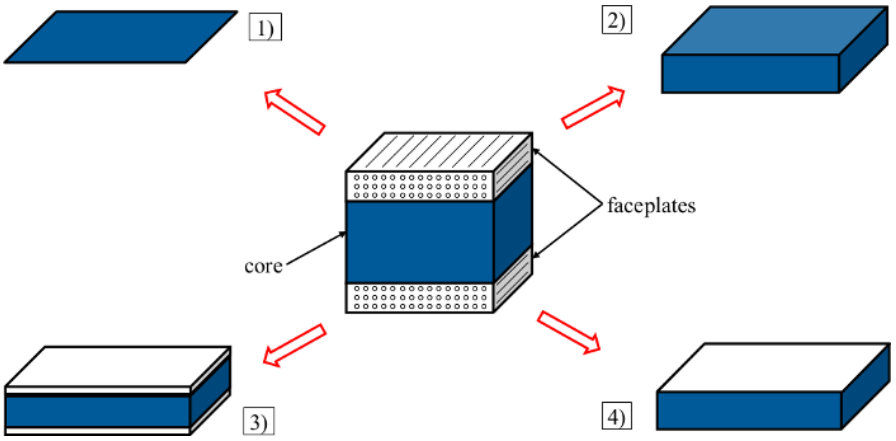

FIGURE 4.9: Concepts of different modeling techniques for sandwich composites.

The different concepts are depicted in Figure 4.9. Method 1 is the easiest modeling approach. The whole sandwich definition basically takes place in the *Composite Layup* tool. The drawback of this technique is that transverse shear cannot be simulated. Option 2 accounts for shear in transverse direction since *Continuum Shell* elements are used. One will get the most accurate prediction by stacking multiple continuum shell elements on top of each other (3). Since CS elements enforce the FSDT, transverse shear will be predicted most accurately.

Within the *Property Module*, ABAQUS provides the *Create Skin* feature. This tool allows the user to take the skin of a volume element and to assign a shell element to it. The results for option 4 are on the same level as for option 3. It is also considered computationally less expensive than the previous method. Attention has to be paid when defining the offset of the conventional shell element attached to the CS element. For the top and the bottom elements, different reference surface definitions (*Top* or *Bottom*) have to be applied.

It has to be mentioned that all of the above mentioned methods are still approximations of the real material behavior. If a detailed analysis of the sandwich section has to be carried out, different approaches as described in [19] have to be used.

4.4.2 Ply Drop-Off

One important parameter to determine the stiffness of the composite component is its thickness. Developing lightweight parts requires the variation of thickness according to the desired stiffness properties over the surface. The thickness reduction is accomplished by a so called "ply drop-off" or simply "ply drop". Figure 4.10 shows a standard ply

drop for laminates. A certain ratio between the ply thickness and the stagger distance has to be observed in order to limit the risk of delamination. A rule of thumb is to keep the drop off between a ratio of 1:16 to 1:20. Due to the ply drop, a resin pocket will be created at the triangle between two plies. This pocket leads to stress concentration, hence, these regions should be placed far from highly loaded areas.

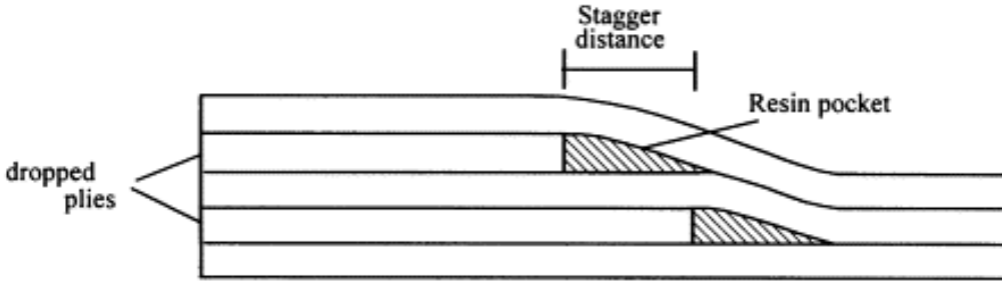

FIGURE 4.10: Concept of a ply drop [9].

Barbero [10] described a very simple way of modeling a ply drop in ABAQUS. Each cross section with a different number of plies should be modeled as an individual section within ABAQUS. The sections are subsequently assigned to the specific regions. This usually requires some preparation of the geometry. The regions can be easily defined using the various *Partion Face* features.

In order to connect the individual sections correctly, it is necessary to set the reference surface under the *Edit Section Assignment* to *Bottom Surface*.

Figure 4.11 depicts the concept of Barbero's approach.

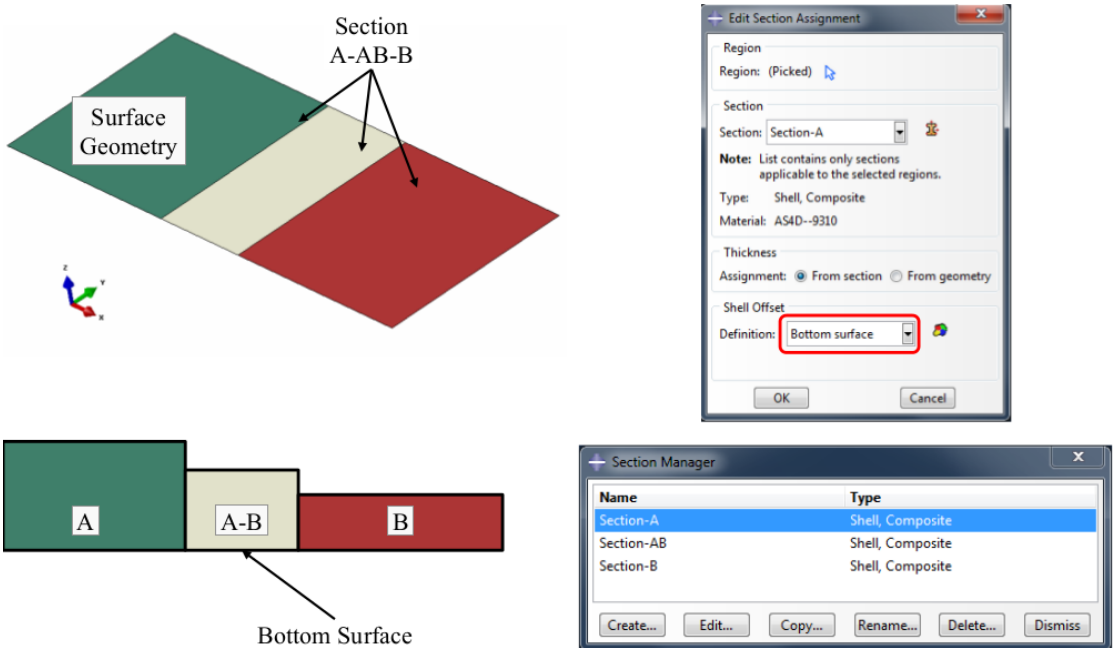

FIGURE 4.11: Settings for a ply drop analysis in ABAQUS using shell elements.

This method is suitable for shell element modeling only. If a more precise analysis of ply drops has to be carried out, a three-dimensional simulation is recommended. Every ply has to be modeled using solid elements as for example continuum shell elements. A detailed description of this process would exceed the scope of this work. More information on the modeling of ply drops is documented in [9, 40].

4.4.3 Inserts

Inserts are used to connect different components (composites and other) parts with each other. Due to the variety of inserts for laminates, the modeling approach strongly depends on the insert used for the design. Again, for an analysis where accurate results in the area of the insert is claimed, the use of 3D elements is indispensable.

A special case occurs if three-dimensional inserts have to be connected to two-dimensionally modeled laminates. The analysis engineer can choose between two options to connect the constituents with each other.
The *Tie* constraint is easy to apply and therefore user-friendly. The second option is to use the *Shell to Solid Coupling* tool provided in ABAQUS. Here, a distance between the solid and the shell elements is necessary. It has to be decided for the particular case which modeling technique is more suitable. *Shell to Solid Coupling* shows a dependence of the distance which is necessary for the application of these couplings.

In general, the application of *tie* constraints seems to be the more convenient method. An example is depicted in figure 4.12. The cut shows a metal insert integrated in a carbon composite part. The contact between the constituents is shown as red circular line. The translucent region demonstrates the thickness of the composite. Due to the transformation process from 3D to 2D, only the reference surface is displayed opaque. The thickness representation can be turned off for convenience by toggling off the *Reference Representation* in ABAQUS.

With the method described above, a detailed modeling of inserts is not possible. As mentioned earlier, a 3D modeling approach is necessary to capture this problem in detail. More detailed research is necessary for the modeling of inserts especially due to the huge amount of different inserts available.

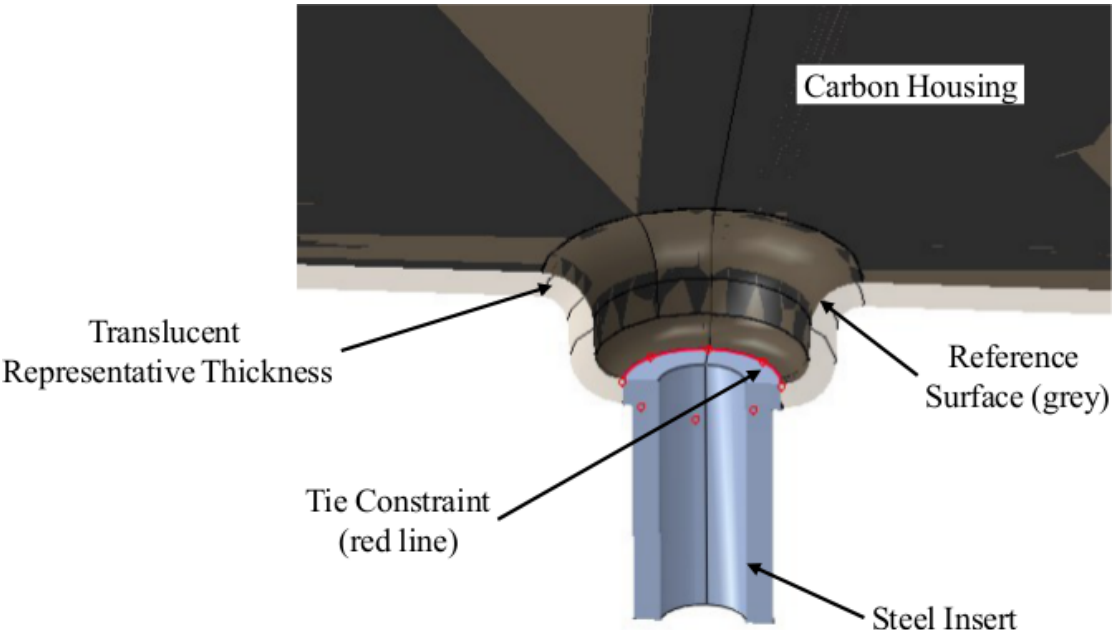

FIGURE 4.12: Tie constraint used to connect a shell structure with a solid insert.

Chapter 5

Analysis Procedure for Fiber Composite Laminates

Keeping in mind the difficulties and limitations of composite analysis, this chapter utilizes the information of the foregoing chapters to establish a guideline for the analysis procedure of composites. Furthermore, example problems to verify the accuracy of the simulation are carried out. For the demonstration of the workflow developed in this work, two examples from the industry are chosen.

5.1 Development of the Workflow

Based on best practice and the state of the art in composite modeling, a workflow was developed for the FEA of Laminates. The goal was to set up a workflow every analysis engineer is able to follow, even with only basic knowledge of fiber composites.
Similar to the standard FEA procedure (Pre-Processing, Processing and Post-processing), the workflow is divided into 4 main processes:

- Model Description,
- Modeling (Pre-Processing),
- Simulation (Processing) and
- Assessment (Post-Processing).

As mentioned in section 4.1, a detailed model description is necessary for a serious analysis. To emphasis its importance, an additional process is introduced. The processes Modeling, Simulation, and Assessment correspond in large parts to Pre-Processing, Processing and Post-Processing, respectively. The overall workflow is depicted in figure 5.1. The black dotted lines show optimization loops in case of a weak component design. The engineer can choose between three distinct options:

- Option 1: Create a submodel of the critical zone.
- Option 2: Redefine the Composite Layup if possible (ply thickness t, Orientation θ, material,...).
- Option 3: Profound design change through design engineer.

Creating a submodel is a standard procedure for an analysis in ABAQUS. It enables the user to refine the mesh, and within reasonable limits, the geometry, in order to obtain better results. This might lead to a changed stress state and therefore changes the result of the fracture analysis (see figure 2.17).

Option 2 is a very convenient method to apply minor to moderate changes to the model. By simply varying some material and layup parameters, the stresses can be shifted from layer to layer and thus the stress exertion will be different. Of course, one has to keep in mind the design limitations during the variation of the parameters.

The last option is the most undesirable solution in a development process. Profound design changes are time consuming and therefore rather expensive.

Another loop illustrated on the right hand side of the main process concerns the prediction of transverse shear. As mentioned earlier in this work, in load application zones three dimensional stress states can arise. If these zones are in highly loaded areas, a more detailed modeling has to be carried out to allow for the prediction of transverse stress and shear stress, respectively.

Due to the complexity of some steps in the workflow, sub-workflows have been developed. Two of these workflows are intended to support the user during the modeling phase. One is to clarify the input options for the material definition, another one for the meshing technique and geometry preparation. The meshing and the preparation step strongly

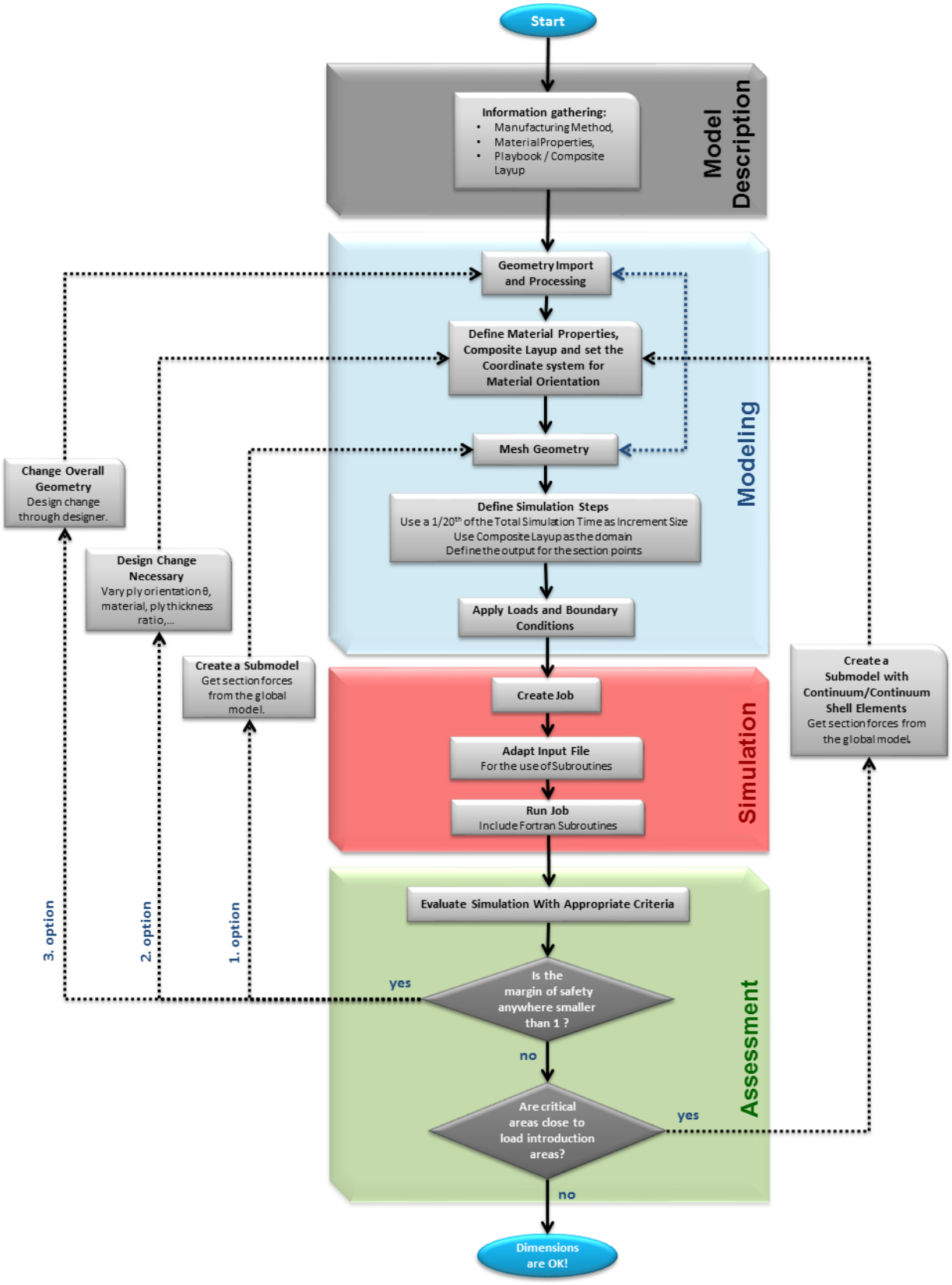

FIGURE 5.1: Overall simulation workflow for the analysis of composites in ABAQUS.

interact with each other. The model preparation predetermines the meshing technique and vice versa. Thus, a workflow to combine these processes has been developed. The blue dotted line in Figure 5.1 illustrates the interaction between meshing and geometry preparation. Figure 5.2 depicts the meshing sub-workflow.

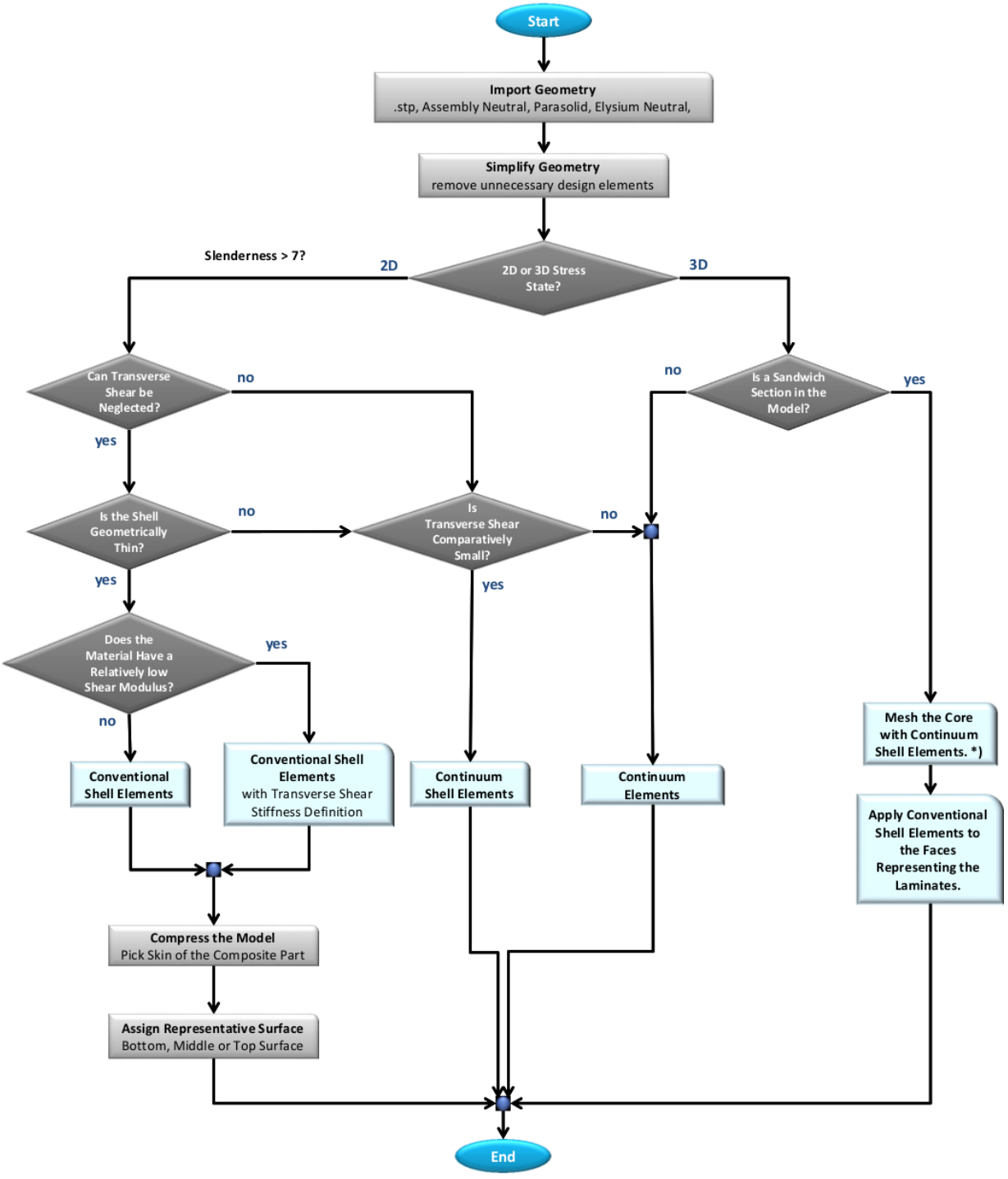

FIGURE 5.2: Guideline for the element selection process and geometry preparation of a model. *)according to [10] in Chapter 3.

The second sub-workflow in the modeling process deals with the material definition. It provides a detailed guideline for the definition of the necessary input values for the user subroutines as well as a description of the modeling technique of the various lamina types. The material definition sub-workflow is illustrated in Fig. 5.3.

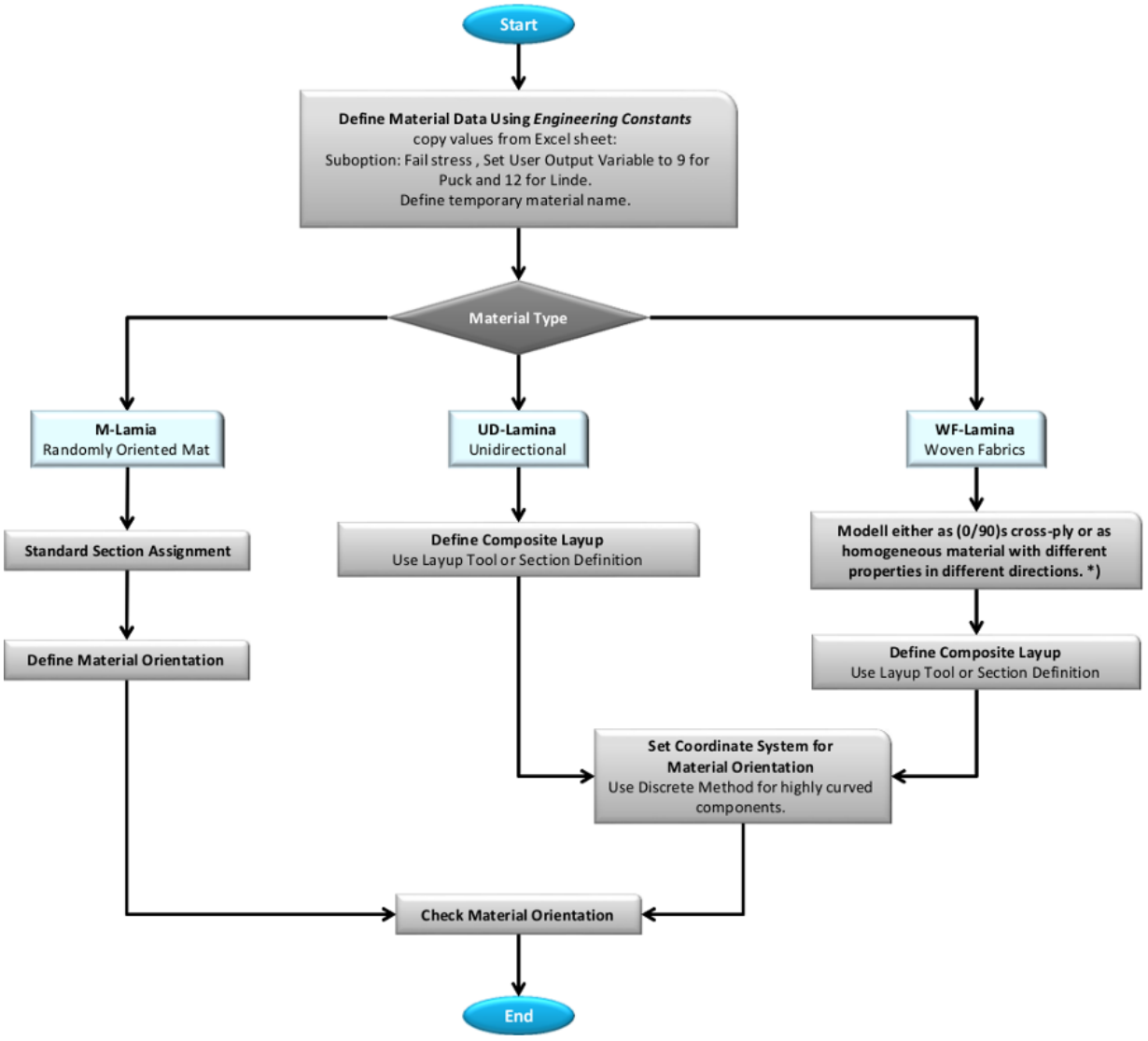

FIGURE 5.3: Process structure for the material definition of composites using ABAQUS. *) according to [11] under section 4.5.

A third workflow was generated to guide the analysis engineer through the very important assessment process. The sub-workflow splits into different branches according to the material under investigation (M-lamina or fabrics) and the analysis type (linear or non-linear) carried out. Another distinction was made between the analysis theories of the nonlinear simulation. The nonlinear analysis using ABAQUS is based on the theory of continuum damage mechanics. To back up these results, the ply by ply degradation method by Puck and Knops [37] is used. The theory is integrated in a CLT tool provided

by KLuB. If the theories agree, the results are considered to be trustworthy. If not, the theory which fits best should be used as explained in section 5.2.2 below.

For the linear FPF analysis the failure criterion selection plots as described in section 5.2.1 should be used for best results.

The key value for the fracture analysis is the margin of safety (MS) as described under section 2.3. Recommendations for the MS are not given in the literature. Obviously the safety margin has to be greater than zero. Accompanying material and component tests will provide the needed experience. Depending on the application, the safety margins have to be chosen adequately. The assessment workflow is depicted in figure 5.4.

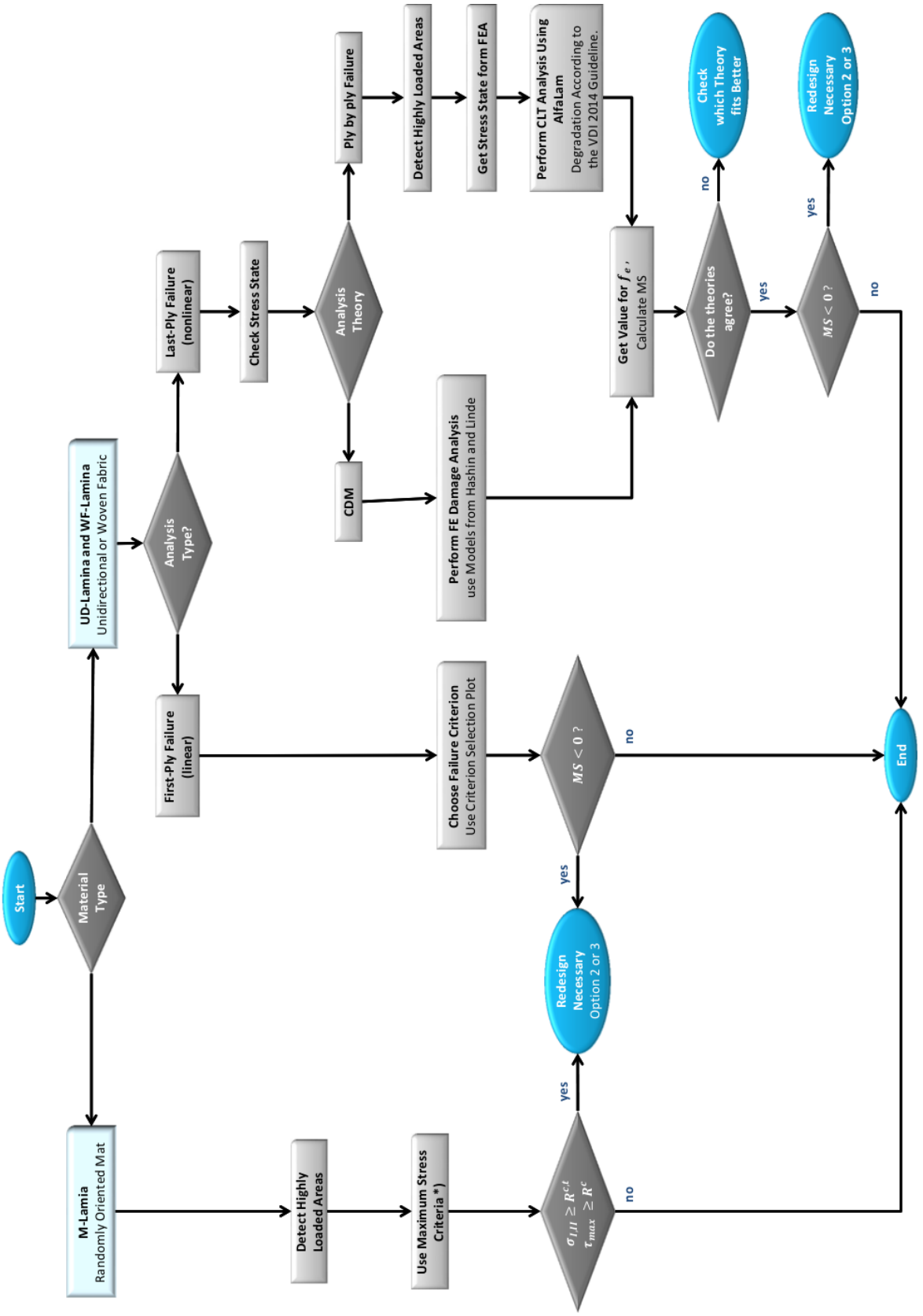

FIGURE 5.4: Sub-workflow for the assessment of FRPs.

5.2 Verification of the Workflow

Verifying the accuracy, the strength and weakness of a simulation is an essential point while developing a standard workflow. As mentioned earlier in this work, the results from the WWFE provide the data to validate the simulation.

In the WWFE Part I, 14 test cases were carried out to compare failure theories against each other. Nine out of the 14 test cases were chosen for the verification, three for the FPF analysis and six for the nonlinear simulation. The test cases are depicted in figure 5.5. In addition to different loading conditions and stacking sequences, two different materials were under investigation, namely glass fiber epoxy and carbon fiber epoxy laminates.

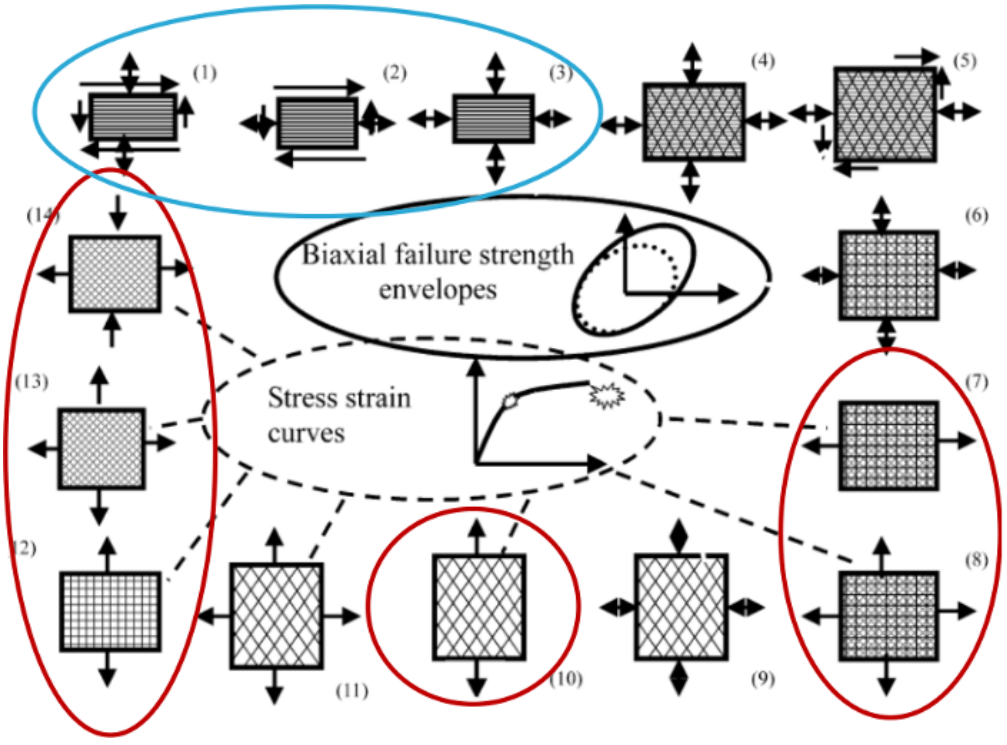

FIGURE 5.5: Selected Test cases from the WWFE [12]. The test cases highlighted in blue provide the basis for the failure plots as under section 5.2.1. The cases highlighted in red are used for the nonlinear verification under section 5.2.2.

5.2.1 Failure Criteria Selection Plots for the FPF Analysis

As mentioned earlier, finding the proper failure criterion is a rather difficult task. Most of the time, engineers are tempted use the failure criterion implemented in their commercial analysis software. Knowing from the WWFE that these criteria often deviate

significantly from experimental data, this assessment approach might not be state of the art. Software developers started adding more and more of the widely used criteria. In ABAQUS, six commonly used failure criteria are implemented (Tsai-Wu, Tsai-Hill, Azzi-Tsai-Hill, Hashin, Max-Stress and Max-Strain). In addition to that, the freely available subroutine for Puck's criterion can be used. As Puck is one of the winners of the WWFE, an improved prediction of failure is now possible.

Still, the user has to decide which of the failure criteria would be the best choice. To simplify this task, failure criteria selection plots were generated based on the results for test cases 1 to 3 of the WWFE. The above mentioned criteria are compared against each other and the experimental results, cf. figure 5.6. Depending on the stress state, one or two criteria are selected to form a polar plot covering the whole range of two-dimensional lamina loading.

Representative for the first test case, the comparison of the theories and the polar plot are depicted in figure 5.6 and 5.7. The additional results and plots of further test cases are documented in appendix B.

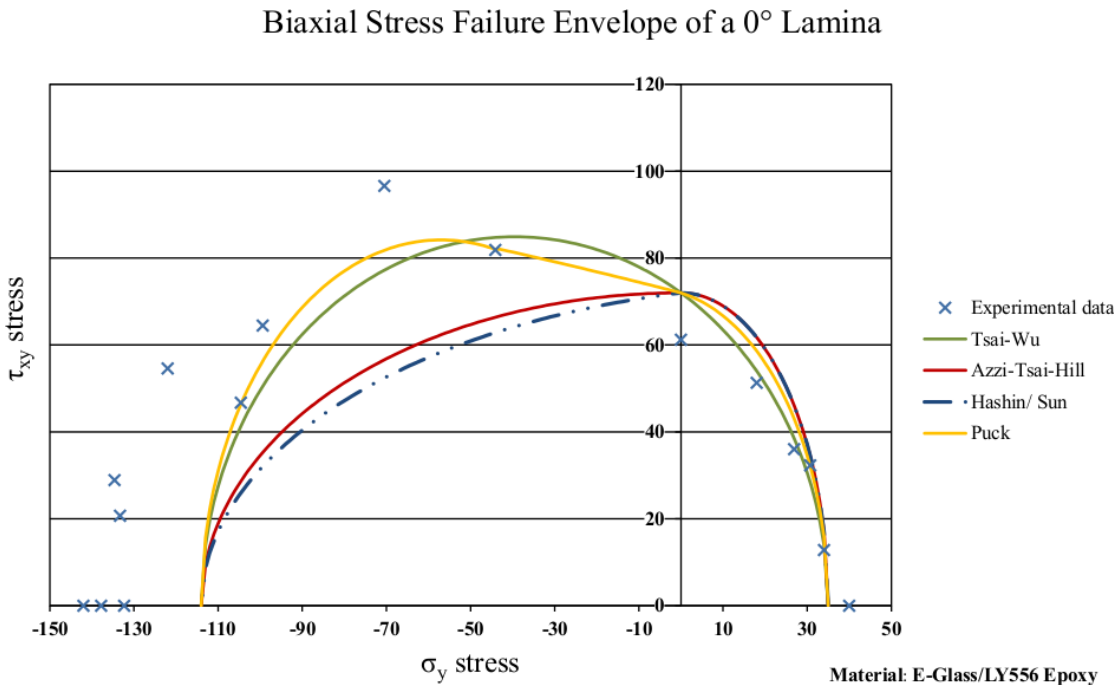

FIGURE 5.6: Comparison of the failure criteria against each other. Test case 1 of the WWFE.

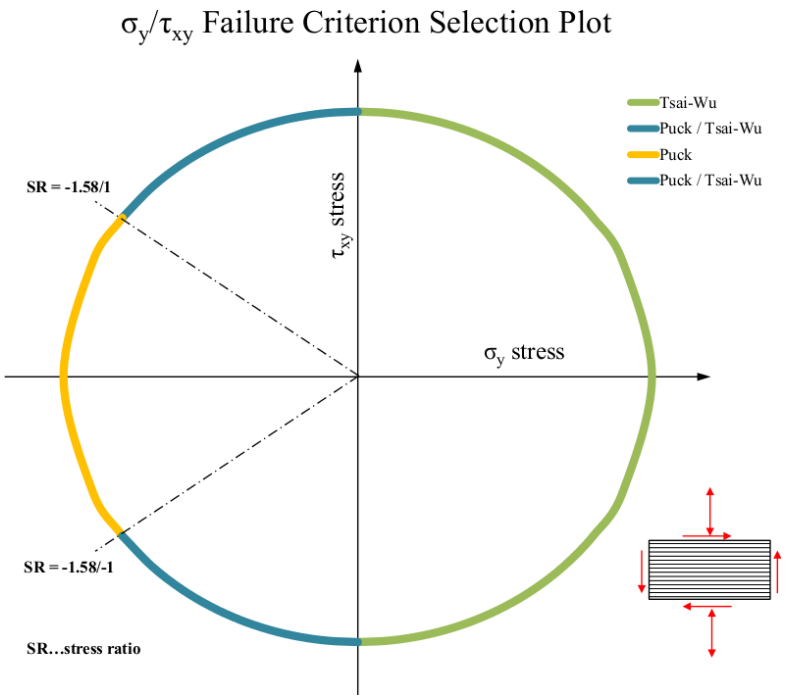

FIGURE 5.7: Failure criterion selection plot for an in-plane stress state (σ_2, τ_{12}).

5.2.2 Comparison of Nonlinear Theories

For the nonlinear analysis stress-strain curves of different layups and materials have been compared. The built-in CDM theory in ABAQUS utilizes Hashin's failure criterion to predict initial failure and furthermore decreases the stiffness linearly beyond this point. The steering parameter for the linear degradation is the fracture toughness of the lamina.

The second continuum damage mechanics approach also integrates the fracture toughness into the degradation model. As opposed to the built-in model, Linde uses the fracture toughness of the matrix and the fiber material individually in two exponential approaches, cf. figure 2.20. Failure initiation is predicted using Linde's strain-based failure criterion (compare with chapter 2).
Both theories obtain their stresses from a FE analysis.

The third nonlinear approach *AlfaLam* utilizes the CLT for the stress computation. Initial failure is predicted using Puck's phenomenological criterion. Knops developed a ply-by-ply discount method to account for degradation as described under section 2.4.2. A hyperbolic function is used to degrade the lamina stiffness according to the stress exertion cf. figure 2.18. Unfortunately, only section forces can be applied to a cut-out of

the component by means of the CLT as opposed to the FE analysis where the boundary forces and constraints can be applied to the whole model.

5.2.2.1 Results

Six test cases were chosen to compare these completely different approaches against experimental data. Qualitative as well as quantitative measures were observed. For every test case the overall curve prediction, the prediction of initial failure, the prediction of final failure stress and the capability to predict final strain were the subject of this investigation. Table 5.1 explains the meaning of the different measures.

TABLE 5.1: Explanation of qualitative and quantitative measures

measure	qualitative	quantitative error to experimental data
+ +	very good prediction	$< 12.5\%$
+	good prediction	$> 12.5 - 25.0\%$
∘	acceptable prediction	$> 25.0 - 37.5\%$
-	bad prediction	$> 37.5 - 50.0\%$
- -	very bad prediction	$> 50\%$

The results for a $(0, \pm 45, 90)_s$ laminate under uniaxial stress (test case 7 of the WWFE) is shown in figure 5.8. As can be seen in the chart, all of the analysis approaches predict the overall curve fit well. The Puck/Knops theory is best in predicting failure. Linde and Hashin (ABAQUS built-in model) over-predict the effect of initial failure as can be seen as a kink of the curves. The failure stress is predicted well by all theories, compare table 5.2. Minor weaknesses can be observed in Linde's and Hashin's approach considering the prediction of transverse failure strain. Overall, the theories are capable of predicting LPF of these laminate types with similar stress states.

TABLE 5.2: Comparison of the simulation results for TC07.

		Built-in	Linde	Puck (*AlfaLam*)
Overall Curve Match		+	+	+ +
Prediction of Initial Failure		+	+	+ +
Prediction of Final Failure Stress	σ_y	+ +	+	+ +
Prediction of Final Strain	ε_x	-	∘	+ +
	ε_y	+ +	+ +	+ +

A second test case (TC) discussed here in detail is TC 10 of the WWFE. The test specimen is a simple (± 55) laminate under uniaxial transverse tension, as can be seen

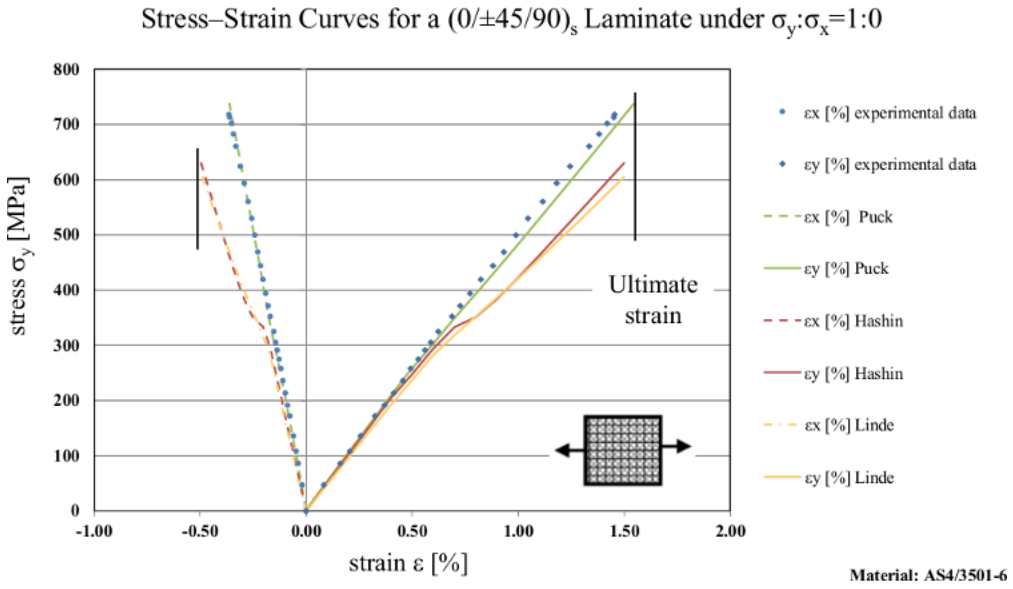

FIGURE 5.8: Comparison of stress-strain curves of TC07.

in figure 5.9, all theories fail to predict the stress-strain curve qualitatively as well as quantitatively. Failure stress and strains deviate from the experimental value by more than 50%. The reason for this is the stress state in the plies. Under these conditions, shear stress dominates. Recalling the nonlinearities from section 2.3.1 it is clear that material nonlinearity and fiber realignment are dominant. None of the theories account for material nonlinearity and only Puck/Knops take fiber realignment into account. Hence, the theories are not able to capture the behavior of this kind of laminates under the given stress state.

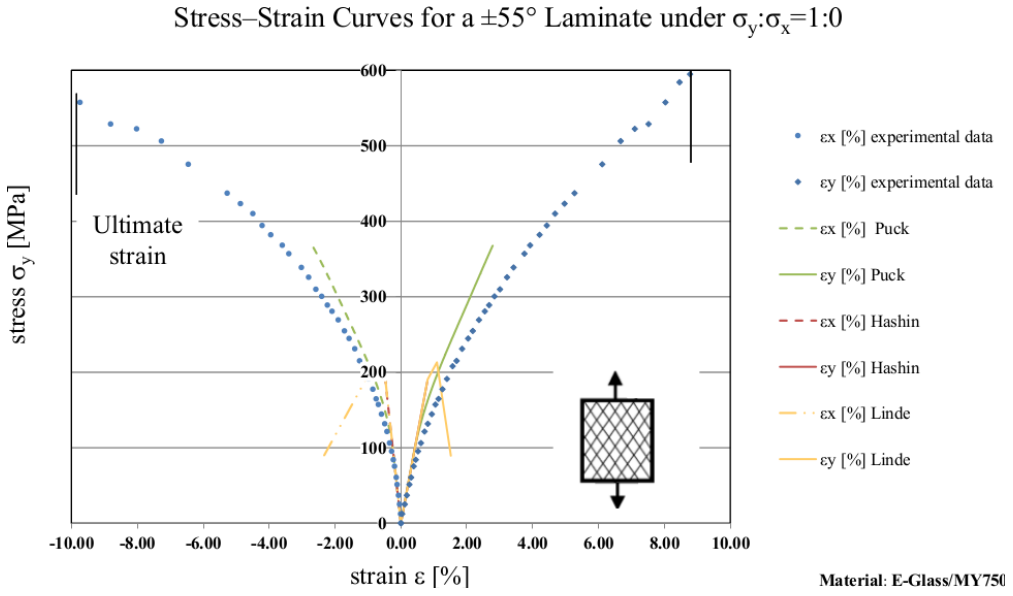

FIGURE 5.9: Comparison of stress-strain curves of TC10.

TABLE 5.3: Comparison of the simulation results for TC10.

		Built-in	Linde	Puck (AlfaLam)
Overall Curve Match		- -	- -	-
Prediction of Initial Failure		- -	- -	-
Prediction of Final Failure Stress		- -	- -	-
Prediction of Final Failure Strain	ε_x	- -	- -	- -
	ε_y	- -	- -	- -

More results expressed in terms of stress strain curves are given in appendix B.
The results from this investigation can be summed up as follows:

- If normal stress components dominate in a ply, the theories are able to predict final failure well. In general, as long as the load transfer within a laminate is statically determined (at least three plies in a laminate carry the load), the final failure can be predicted.
- If only two plies form a laminate or remain undamaged and shear is the dominant stress state, the theories are not able to predict failure adequately.

This is the reason why engineering designers try to avoid statically undetermined laminates and the $(0, \pm 45, 90)_s$ airplane laminate is commonly used.
The FPF analysis hand in hand with the nonlinear simulation form a very strong tool for the assessment of laminates.

5.3 Demonstration of the Workflow

To demonstrate the application of the workflow, two fiber composite components from industrial projects are demonstrated.

5.3.1 Pressure Plate

The first demonstrator for the workflow is the pressure plate of a power generator for a hydro power plant. The pressure plate compresses the lamination stack of the generator. Therefore, bolt loads are applied to the plates. One plate is on top, the counter plate is located at the bottom of the lamination stack. Figure 5.10 illustrates a 16^{th} of the circumferential section of the entire generator.

Any type of failure has to be prevented, therefore a standard analysis has to be carried out. Under operation, the mean temperature in the generator housing is $80°C$. The effects of temperature change on the stresses in the laminate cannot be detected by means of the workflow. However, the increased bolt load due to the enhanced temperature was captured in the analysis.

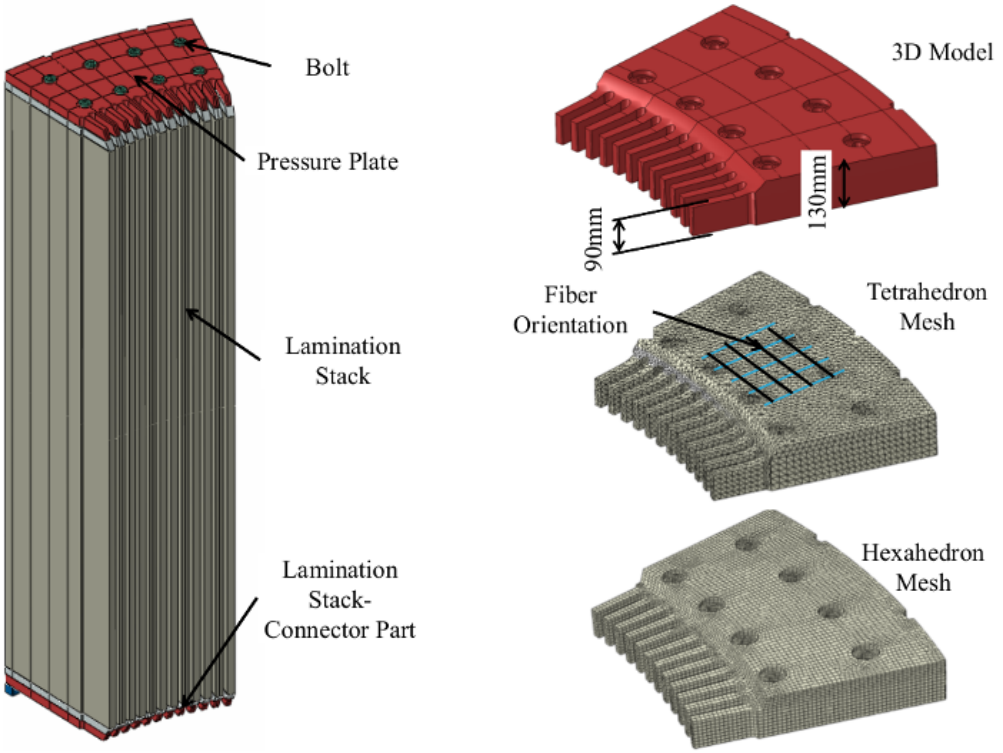

FIGURE 5.10: Model of the power generator (left) and pressure plate with different meshing methods (right).

5.3.1.1 Model Description

The composite pressure plate is a laminated plate made of GFRP with a thickness of 130mm. The properties of the glass fiber epoxy material (Gatex GX 11.3309 GWS) can be reviewed in the data sheet provided by the manufacturer (see [41] and Appendix C). The thickness of a lamina is 0.46mm, hence, 283 layers are necessary to add up the total thickness of the plate. The layers are woven fabrics with equal mechanical properties in longitudinal and transversal direction.

The geometry of the composite is comparatively simple. As depicted in figure 5.10, the pressure plate is a simple flat plate with machined cutouts.

5.3.1.2 Modeling

The bolts are perpendicular to the pressure plate and therefore the loads are applied in the out-of-plane direction (3D stress state). This requires the model to be meshed with solid elements as recommended in the modeling workflow. Two different types of elements can be used: tetrahedron and hexahedron elements. Here, both methods are used to compare the results of the different approaches.

The geometry is provided as 3D models, hence, no further geometry treatment is necessary. To enable hexahedron meshing, minor geometry modifications are applied to the pressure plate as depicted in 5.11. The changes will not affect final results in the highly loaded areas as demonstrated in figure 5.13. These modifications also allow the user to model the plates in layers. Due to the expected stress state, a modeling in layers is not necessary and actually cumbersome for this case. The plate is modeled as a single continuum with orthotropic material properties. The mechanical properties and strengths are listed in table 5.4.

TABLE 5.4: Stiffness values for the Gatex GFRP material.

	E_1	E_2	E_3	ν_{12} [-]	ν_{13} [-]	ν_{23} [-]	G_{12}	G_{13}	G_{23}
Gatex 11.3309GWS [GPa]	24.4	24.4	9	0.079	0.375	0.375	3.04	2.86	2.86

Four load steps are considered: a dummy load case for establishing the surface to surface contacts, another one representing the bolt preload, one accounts for gravity, and a final case simulates the temperature rise during operation, respectively. The bolt loads are

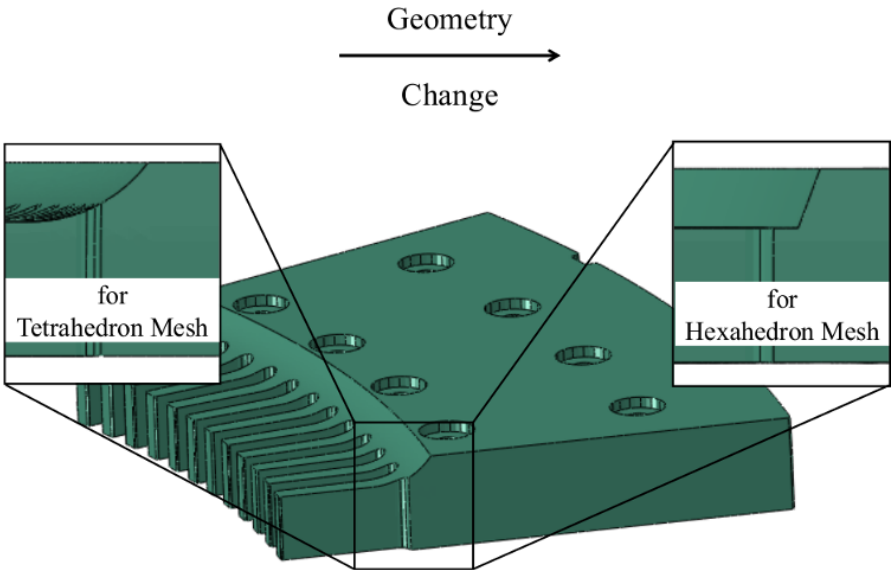

FIGURE 5.11: Geometry change to enable hexaeder meshing.

115kN for each bolt. The temperature changes from $20°C$ initially to the operating temperature of $80°C$. Table 5.5 lists the load cases for the simulation. The boundary

TABLE 5.5: Load step description of the pressure plate analysis.

	Description	Value
Step 1: Dummy Step	Apply Displacement to Bolts	$2mm$
Step 2: Bolt Preload	Apply Specific Preload	$115kN$
Step 3: Gravity	Apply Gravity	$9.81m/s^2$
Step 4: Temperature	Increase Temperature	$20 \rightarrow 80°C$

conditions are shown in figure 5.12. Respective symmetry constraints are applied to the bounding planes of the generator model. The generator section is supported in z-direction via a ledge. The bolt heads are tied to the pressure plate for simplicity. In order to obtain a realistic result for the pressure distribution under the pressure plate, the lamination stack - connector part and the pressure plate are connected using a contact formulation in ABAQUS. More details about the simulation are reported in [42].

Comparing with the material definition workflow under section 5.1, the right most branch is chosen to define the material properties. Recalling the meshing workflow, the element selection is straight forward using continuum elements (*3D stress state* $\rightarrow$ *no sandwich*)

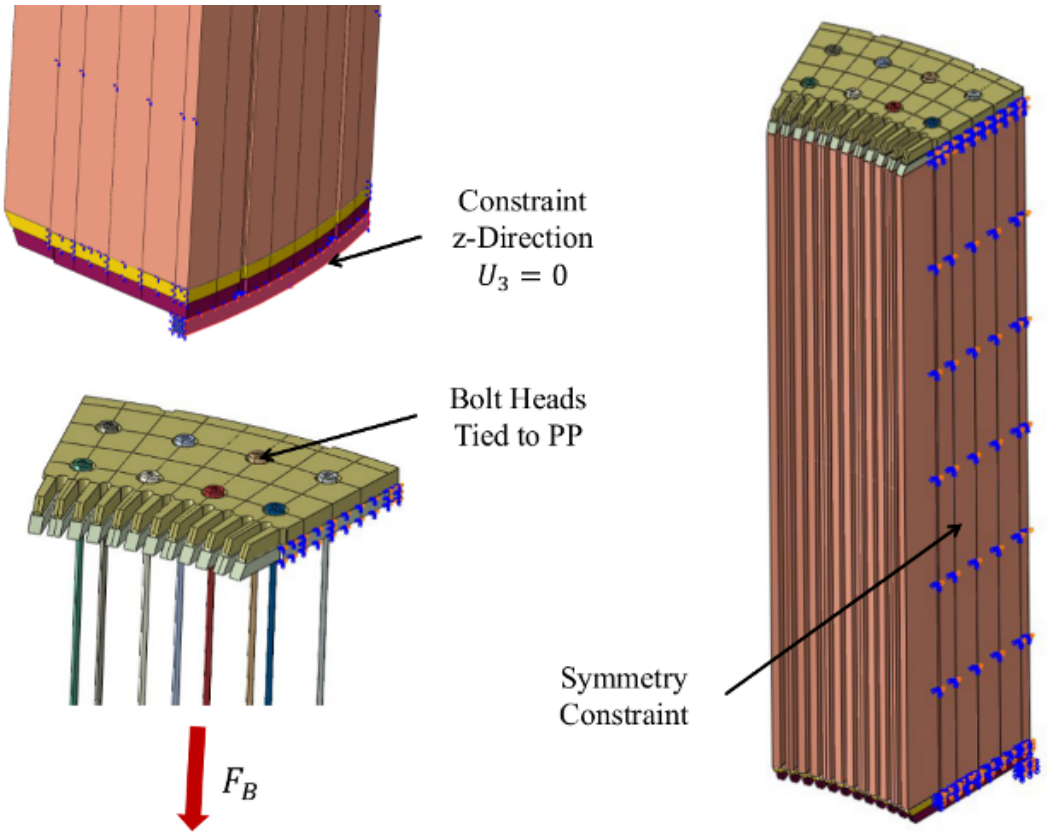

FIGURE 5.12: Boundary conditions applied to the pressure plate model

5.3.1.3 Simulation

The simulation requires no special treatment or parameters. Since a standard stress analysis is carried out, no subroutine had to be executed.

5.3.1.4 Assessment

Due to the fact that the component is loaded almost exclusively in the out-of-plane direction, the assessment process is different compared to that of standard composite parts. Therefore, the assessment workflow can not be used for this particular problem and the component can be treated as a standard plastic part according to [43]. Thus the assessment process is similar to problems involving standard plastics. For plastic components the von Mises yield criterion is applied, as opposed to composite parts where stress exertions and safety margins are employed. Therefore, the equivalent stress σ_v has to be smaller than the design stress σ_d. The design stress is calculated using the

relation below:

$$\sigma_{vmax} \leq \sigma_d = \frac{K}{S \cdot A} \tag{5.1}$$

Here, K is the strength value provided by the manufacturer, S is a safety factor and A is the cumulative reduction factor. Erhard [43] recommends a safety factor against fracture of $S = 2$. The reduction factor A aims at covering all unknown effects on the strength of the material. It is proposed as:

$$A = A_T \cdot A_{st} \cdot A_{dyn} \cdot A_A \cdot A_W \cdot \ldots \tag{5.2}$$

The individual factors stand for temperature influence, static and dynamic loading, aging and moisture absorption (water), respectively. Other authors include several more factors depending on the application.
For this particular problem, the influence of aging and dynamic loading can be neglected. The factor for thermal influence (A_T) can also be neglected since the strength values are already given for increased temperatures ($120°C$). Erhard [43] recommends a factor for long-time static loading of $A_{st} = 2$. Assuming a moisture absorption of 1% in weight, a reduction factor of $A_W = 1.282$ can be calculated using the following equation:

$$A_W = \frac{1}{1 - 0.22 \cdot f} \tag{5.3}$$

with $f = 1$ corresponding to an assumed moisture absorption of one percent. This leads to a total reduction factor of 2.56. The design stress is therefore:

$$\sigma_d = \frac{K}{S \cdot A} = \frac{400 N/mm^2}{2 \cdot 2.56} = 78 N/mm^2 \tag{5.4}$$

The eqivalent stresses are provided by the FE computation. The hexahedron model is used for the assessment.

The maximum stress can be found under the bolt heads as depicted in figure 5.14. The maximum von Mises value is $45 N/mm^2$ which is low compared to the design stress.
However, for this particular problem the contact pressure is the critical measure. As depicted in figure 5.14, the stress values are much higher. In order to predict the stress distribution under the bolt head more accurately, a submodel, as recommended in the workflow, is analyzed. Due to numerical edge effects the stresses at the edge of the contact show some unrealistically high values ($539 N/mm^2$). These values are not valid

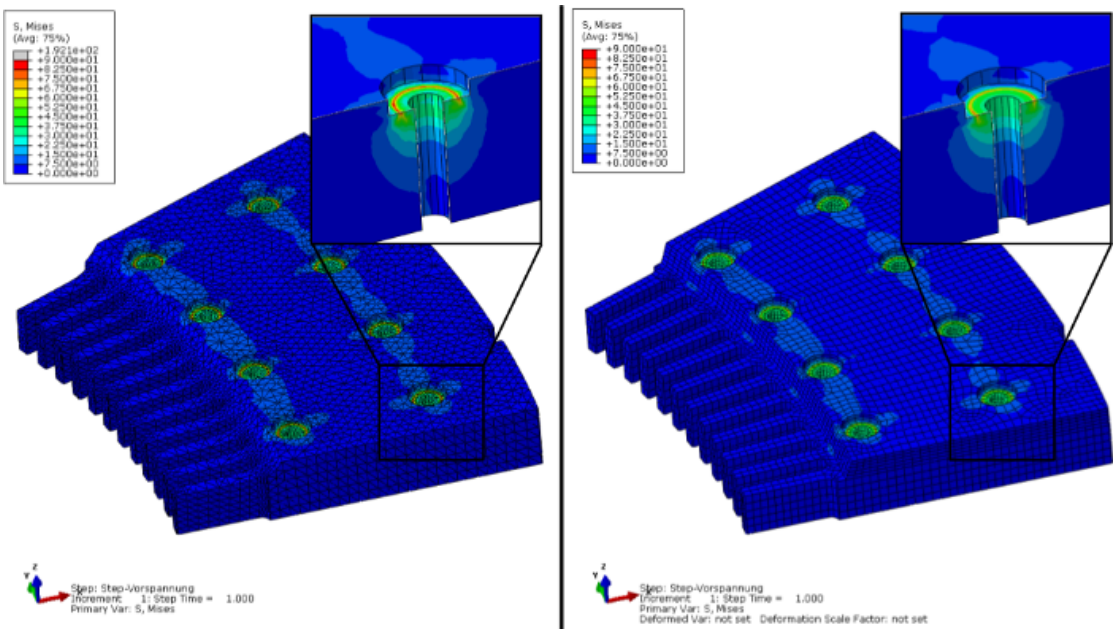

FIGURE 5.13: Comparison of FE results with tetrahedron (left) and hexahedron mesh (right)

for the assessment. Further stress values of the contact area are between $78N/mm^2$ and $92N/mm^2$ and therefore exceed the design stress. There is certain risk, that cracks would appear under the bolt heads after years of operation due to aging of the material. Since cracks are not allowed for this problem, a fracture mechanics analysis which provide information if the crack would grow is therefore not considered.
Design changes are recommended in order to guarantee a safe life for the composite plate.

Due to the fact that the problem shifted from a composite analysis in the classical sense to a standard plastic analysis, the assessment workflow is not applied for this analysis. Erhard's [43] analysis approach was chosen to assess the plate. In his book, some of the reduction factors are valid for fiber composites which supports the assumption made in this work.

5.3.1.5 Final Comments

In general, Erhard's approach is rather conservative. Some of the reduction values can be neglected if experimentally evaluated material properties are available. Unfortunately, at the end of this work these material values were not available. Furthermore, the

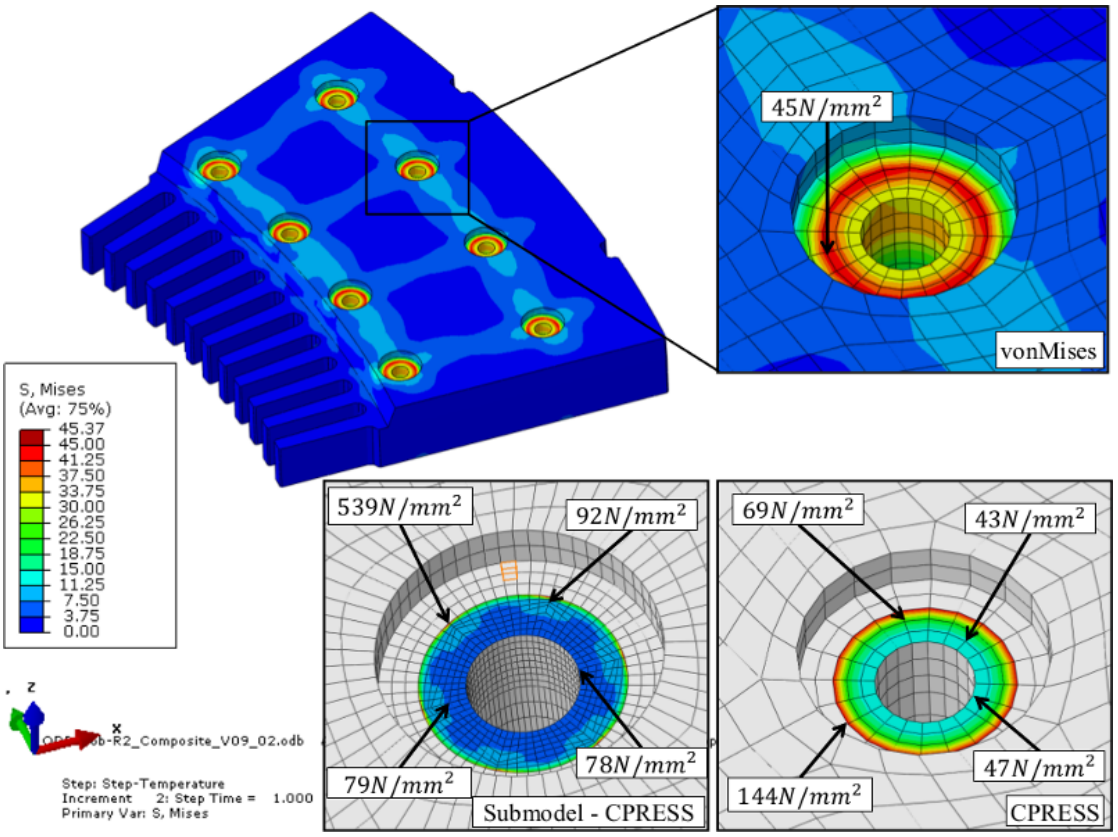

FIGURE 5.14: Equivalent stress for the composite pressure plate.

moisture absorption has to be determined. A more detailed assessment can be carried out after these values are available.

5.3.2 Battery Pack

As a second demonstrator for the workflow, the cover for a battery pack of a hybrid vehicle was chosen. The composite cover has no intended structural function and primarily serves as protection against environmental influences only. However, it is loaded through the several contained masses in rough road conditions. The entire battery pack is depicted in figure 5.15.

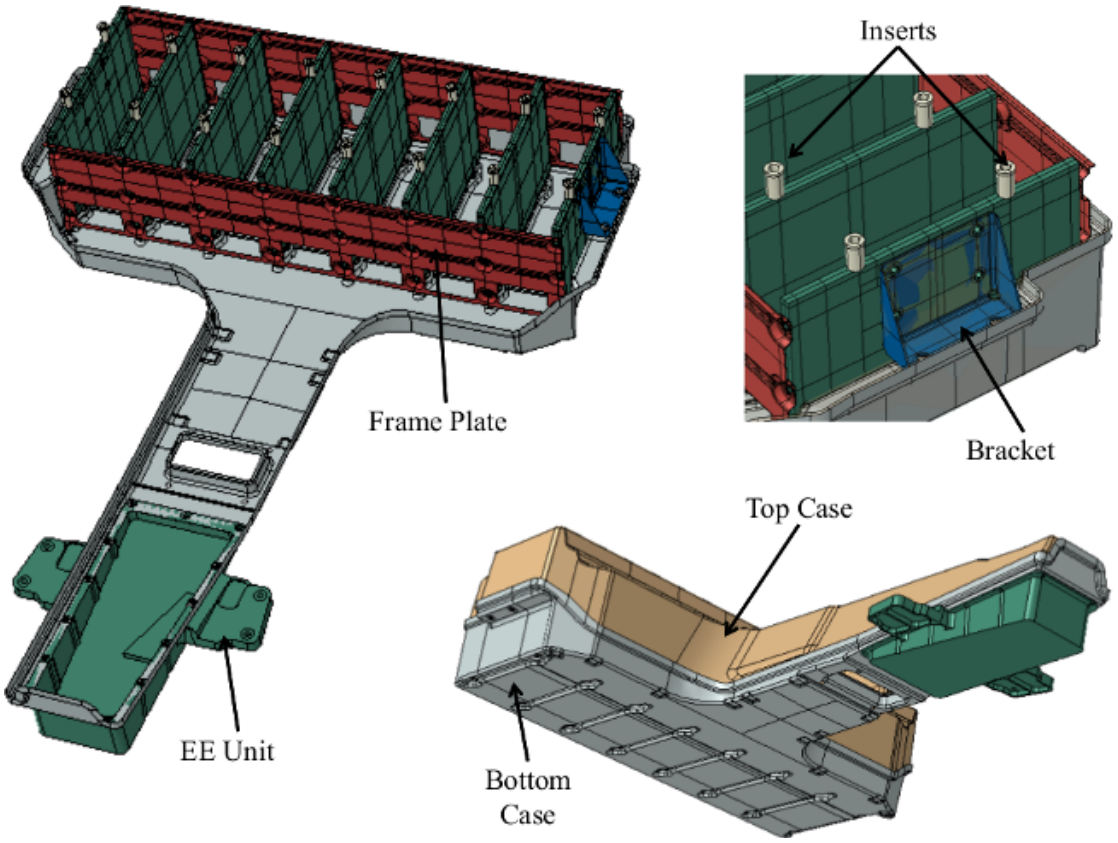

FIGURE 5.15: Components of the battery pack.

5.3.2.1 Model Description

The cover is hand laminated using DELTAtech prepregs (GG800T-D120-38 see [13]). Three layers of prepregs are stacked on top of each other. The lamina stacking sequence is (0,90,0). The prepreg weaving style is a Twill 2x2 with supposedly equal properties in the 1 and 2 directions. The experimental data (see Appendix C) show different values as reported in the data sheet of the manufacturer [13].

Unfortunately, the detailed draping and cutting during manufacturing is not documented. Therefore, assumptions are made considering fiber alignment. Further assumptions are made concerning material properties. Poisson ratios ν_{12}, ν_{23}, transversal stiffness E_3 and fracture toughness K_{IC} are chosen according to similar materials and weaving types.

5.3.2.2 Modeling

One dimension (thickness) is much smaller than the remaining dimensions (slenderness of 326 (width/thickness)). Therefore, a two dimensional stress state is expected. The CAD geometry is three-dimensional. In order to mesh the model utilizing shell elements, the 3D geometry has to be converted into a 2D geometry (see figure 4.2).
Thin S4R shell elements are chosen as element type and the element size is set to 12mm. The stacking sequence can be seen in figure 5.16. The material properties are shown in tables 5.6 and 5.7.

TABLE 5.6: Mechanical properties of the DELTAtech carbon material [13].

	E_1	E_2	E_3	ν_{12} [-]	ν_{13} [-]	ν_{23} [-]	G_{12}	G_{13}	G_{23}
GG800T-DT120-38 [GPa]	54.9	54.7	18.2	0.28	0.28	0.4	3.74	3.2	3.2

TABLE 5.7: Strength values of the DELTAtech carbon material.

	$R^t_{\|\|}$	$R^c_{\|\|}$	$R^t_{\perp}$	$R^c_{\perp}$	$R_{\|\|\perp}$
GG800T-DT120-38 [MPa]	807	546	706	539	92

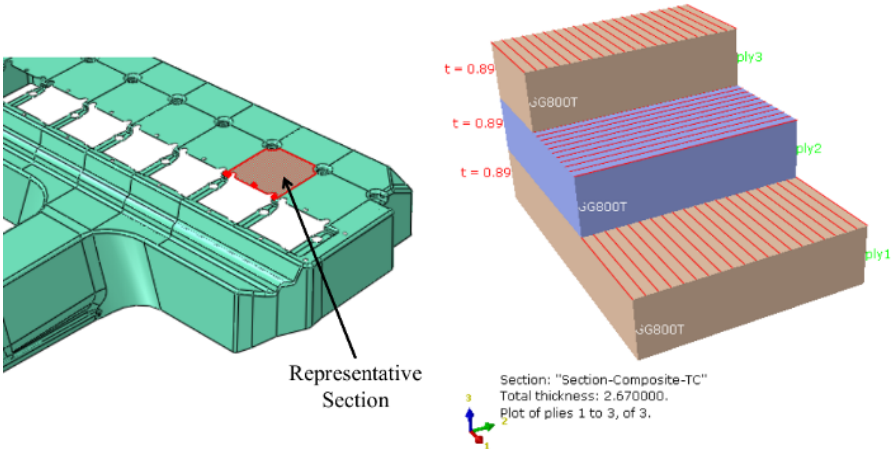

FIGURE 5.16: Illustration of the stacking sequence (right) for a representative section (left) of the model.

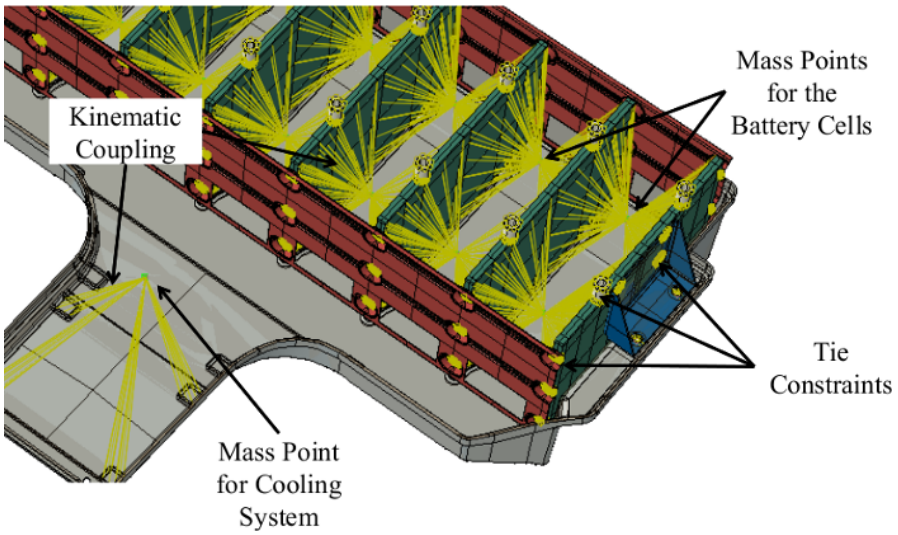

FIGURE 5.17: Constraints applied during the modeling phase.

Unfortunately, no load spectrum is available for this example problem. Representative loads are assumed to demonstrate the simulation procedure and the assessment. Three load sets were created representing typical loads under rough road conditions. Acceleration values of 6g in all three directions and gravity are assumed as static loads acting on the battery case (see table 5.8). Pinned constraints are applied at the contact surfaces between battery pack and the frame of the car (the frame is not depicted in the figure). The boundary conditions are illustrated in figure 5.18.

TABLE 5.8: Load cases for the simulation of the battery pack.

	Load Direction	a_x	a_y	a_z
Load Case 1	vertical upward	0	0	+7g (+7g+1g)
Load Case 2	longitudinal backward	+6g	0	-g
Load Case 3	horizontal right	0	+6g	-g

The battery cells, represented by mass points, are connected to the clamping plates using kinematic couplings. The steel inserts are tied to the top and bottom case. Similarly, the brackets and the EE Unit are tied to the connection surfaces of the laminate as depicted in figure 5.17.

5.3.2.3 Simulation

Since Puck's theory will be used for the analysis, the subroutine provided by KLuB has to be included. In order to communicate with the subroutines, additional field output

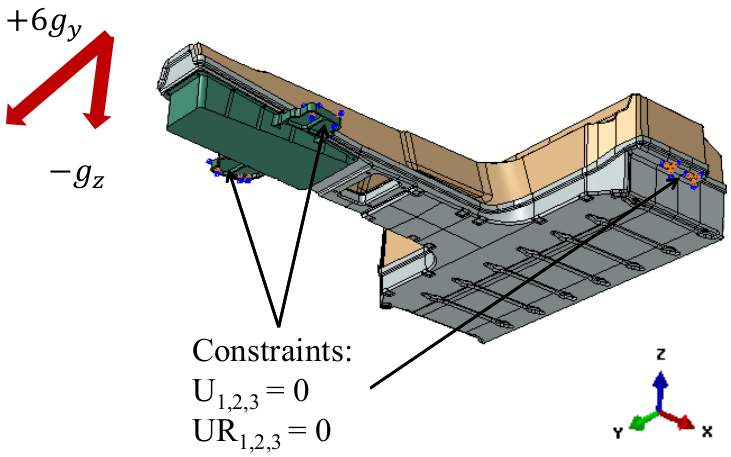

FIGURE 5.18: Boundary conditions applied to the model. The loads shown in the figure correspond with load case 3.

data are required. A list of recommended field output variables for the analysis of composites is provided below in table 5.9: In addition to the field output, the name of

TABLE 5.9: Required field output variables for the analysis.

Field Output Variables	Abbreviation
Stress Components	S
Total Strain Components	E
Translations and Rotations	U
Nodal Forces	NFORCE
Failure Measure Components	CFAILURE
Damage Initiation Criteria	DMICRT
Nodal Temperature	NT
Solution Dependent State Variable	SDV
User-defined Output Variable	UVARM

the material has to be changed in the input file as described under section 4.3.1.

5.3.2.4 Assessment

After running the analysis, the results have been visualized. Here, the highly loaded zones can be detected and the stress state at the critical nodes are identified. Due to the fact that the composite parts are not used as structural elements, the stresses in these parts are rather small and therefore noncritical. Nevertheless, a failure assessment is demonstrated here:

As mentioned earlier under section 4.3.3, the first thing during the post-processing is to check the material orientation. Figure 5.19 shows the material orientation for every

element at the critical area. As can be seen, the normal direction (red line) was defined correctly. Due to the missing information of the resulting fiber orientation, a detailed review is impossible for this case. It is shown that the 1 direction (blue lines) remains unchanged passing the corner of the top case. This might be true but it doesn't necessary have to. This allows for a significant uncertainty concerning the assessment.

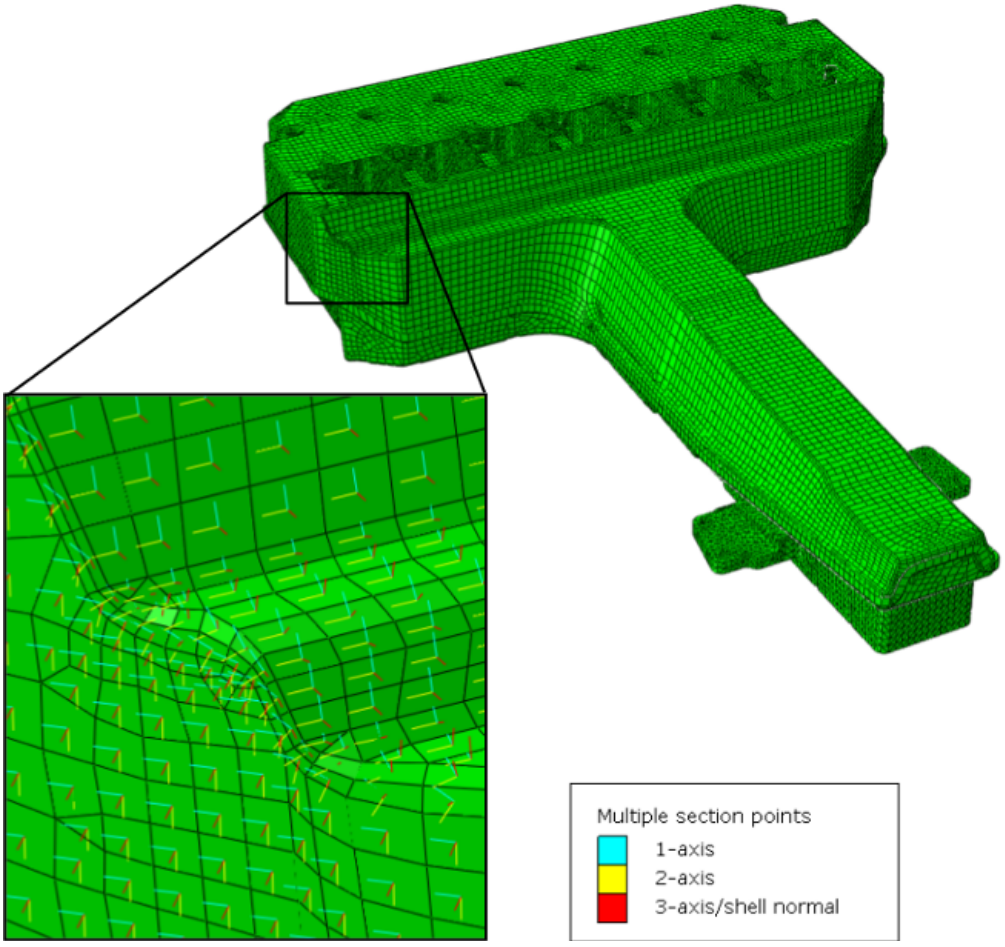

FIGURE 5.19: Checking the material orientation of the battery pack.

Load case 1 yields the highest stresses. The critical area is shown in figure 5.20. The stresses for the node under investigation are listed in table 5.10. Note that the critical area is not merely defined as a location on the geometry, but also by a specific layer. The critical layer is indicated in the legend as highlighted in the figure.

TABLE 5.10: Nodal stresses for the critical ply

Stress Component	Value $[N/mm^2]$
S_{11}	-51
S_{22}	-77
S_{12}	0

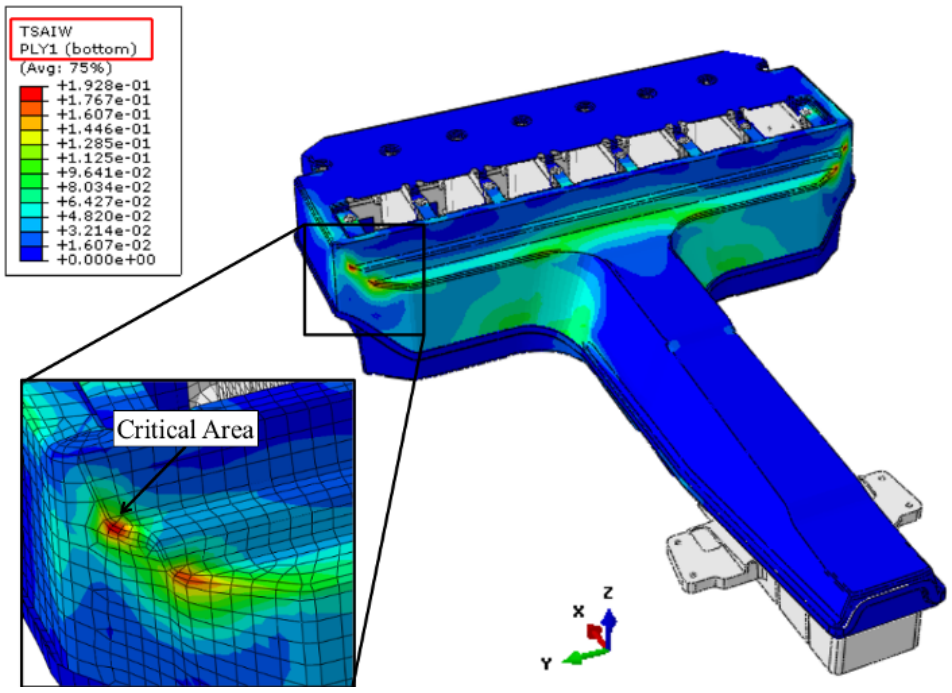

FIGURE 5.20: Critical area at the top case of the battery pack.

According to the stresses in table 5.10, the stress ratio is 0.66/1 (S_{11}/S_{22}) corresponding to the third quarter of the selection plot in figure B.4. Therefore, Puck and Hashin yield the most trustworthy values. The margin of safety for this zone is 5.66 using Puck.

TABLE 5.11: Different stress exertions evaluated for the critical ply.

Criterion	f_e	$f_{e,IFF}$	$f_{e,FF}$
Tsai-Wu	0.193		
Tsai-Hill	0.138		
Azzi-Tsai-Hill	0.138		
Max-Stress	0.145		
Puck		0.150	0.0936

5.3.2.5 Final Comments

A final conclusion concerning the structural capability can not be made at this point after this simulation.

Nevertheless, most of the steps of the workflow are demonstrated.

Chapter 6

Conclusion

The goal of this thesis was the development of a universal simulation workflow for fiber composites using commercial finite element software packages, in particular SIMULIA/ABAQUS. Due to the complex failure behavior of composites, this work provides a detailed description of the various failure mechanisms and the corresponding failure criteria to capture the most common failure modes.

Besides the numerical simulation of composites in ABAQUS, the analytical treatment of laminates is shown in detail. Furthermore, the analytical method was compared with simulation results as well as with experimental data.

In order to yield best simulation results, the modeling of a structure has to be as accurate as possible. Therefore, various modeling techniques in ABAQUS were reported in this work. Especially the geometry preparation and special problems of composite modeling were carried out in detail.
Strongly related with the geometry preparation is the meshing of the model. The meshing technique predetermines the required geometry and vice versa. The required mesh depends on the desired resolution of the results, i.e. in particular on the stress state in the model. To account for all these factors, sub-workflows for the modeling phase pertaining to the overall workflow were developed.

In addition to the modeling part of the analysis, a workflow was developed for the assessment of fiber composites. Depending on the analysis type (FPF or LPF) and the material (UD, M and WF lamina), different steps are necessary to arrive at a final conclusion whether the design of the components are adequate or not. The assessment

workflow provides an overview and guides the engineer through this complex process. As part of the workflow, failure criterion selection plots were created. These charts help the user to choose the best failure criteria for the prevalent stress state.

To investigate the LPF analysis, degradation models are necessary to describe the non-linear behavior. Three different degradation theories were compared and introduced in the workflow. The comparison helps to develop an overall understanding of the failure behavior of laminates as well as it allows an insight in the capabilities of the underlying theories.

Finally, the analysis workflow was tested on two diverse demonstrators. The application of the workflow on the demonstrators highlighted some weaknesses of such an analysis. Especially the first step of the workflow, the model description, is an essential point within the process. To obtain best results, a draping simulation or detailed reports of the layup and manufacturing processes are recommended. Furthermore, the material parameters should be evaluated before an analysis is carried out.

The workflow provides a good basis for further investigations concerning the analysis of composites in ABAQUS. The test cases for stress-strain curves showed good agreement with the experimental data. Especially the failure criterion selection plots simplify the work for the analysis engineer and help predicting failure more accurately, and reliably.

Appendix A

Examples

An example definition for the use of Linde's theory is shown below. Note that the order of the entries have to remain unchanged. In addition to the *User Material*, the SDVs under the *Depvar* category have to be set to a value of 10. Figure A.1 represents the AS4/3501-6 material. The data are from Soden's [23] and Linde's [44] work.

Entry	Parameter
1	Young's Modulus in 1 direction E_1
2	Young's Modulus in 2 direction E_2
3	Shear Modulus in 12 plane G_{12}
4	Shear Modulus in 23 plane G_{23}
5	Poison's ratio ν_{12}
6	Poison's ratio ν_{23}
7	Failure stress in tension $R^t_{\|\|}$
8	Failure stress in compression $R^c_{\|\|}$
9	Failure stress in tension $R^t_{\perp}$
10	Failure stress in compression $R^c_{\perp}$
11	Failure stress in shear $S_{\perp\|\|}$
12	Fracture Energy in matrix G_m
13	Fracture Energy in fiber G_f
14	Viscosity for regularization η

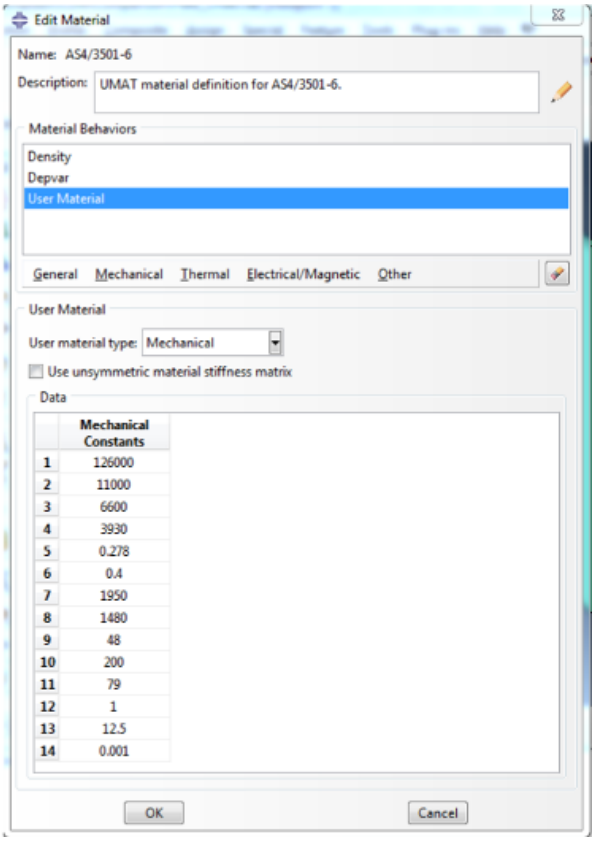

FIGURE A.1: Material parameters for the use of Linde's Model in ABAQUS (left) and an example (right).

Appendix B

Additional Verification Results

In addition to the results shown in chapter 5, more results from the study of the WWFEE are reported below:

B.1 Comparison of Failure Envelopes

The results of the comparison of the failure criterion implemented in ABAQUS are as following:

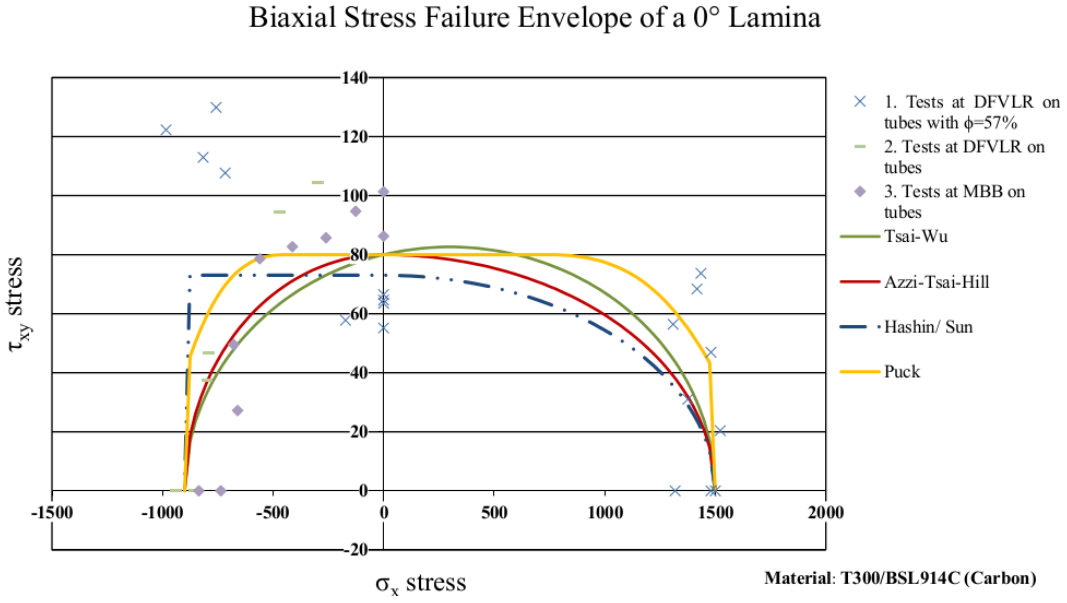

FIGURE B.1: Comparison of the failure criteria implemented in ABAQUS. Test case 2 of the WWFE.

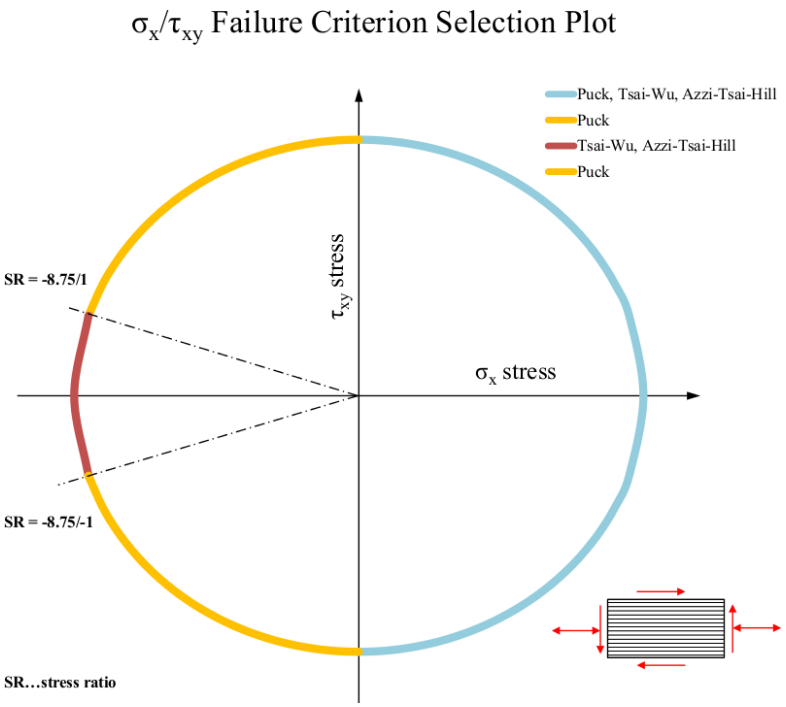

FIGURE B.2: Failure criteria selection plot for an in-plane stress state (σ_1, τ_{12}).

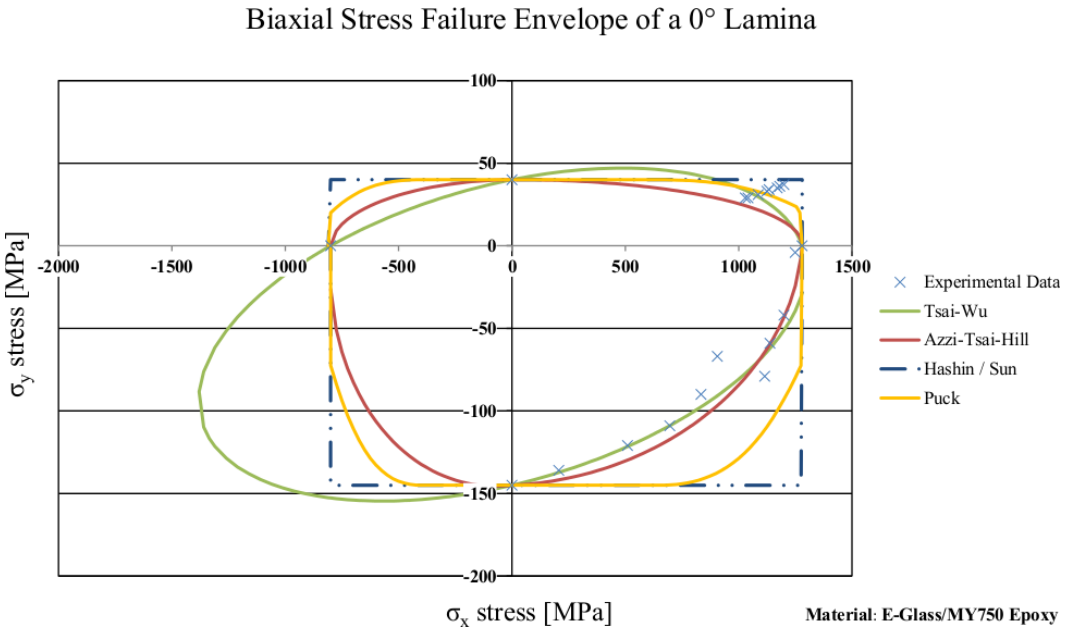

FIGURE B.3: Comparison of the failure criteria against each other. Test case 3 of the WWFE.

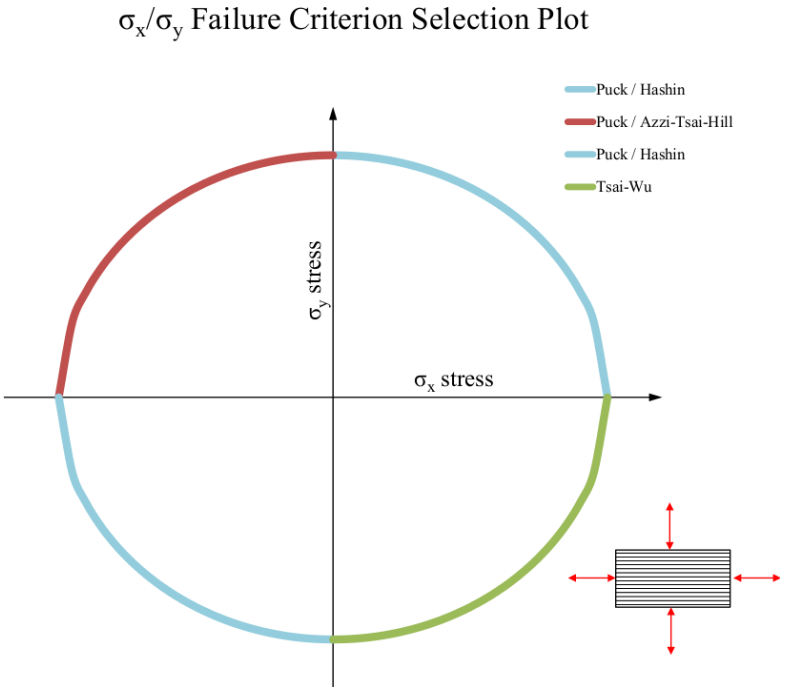

FIGURE B.4: Failure criteria selection plot for an in-plane stress state (σ_1, σ_2).

B.2 Results from the Comparison of Stress-Strain Curves

Additional verification results as under section 5.2.2 are reported below. Test Case 8:

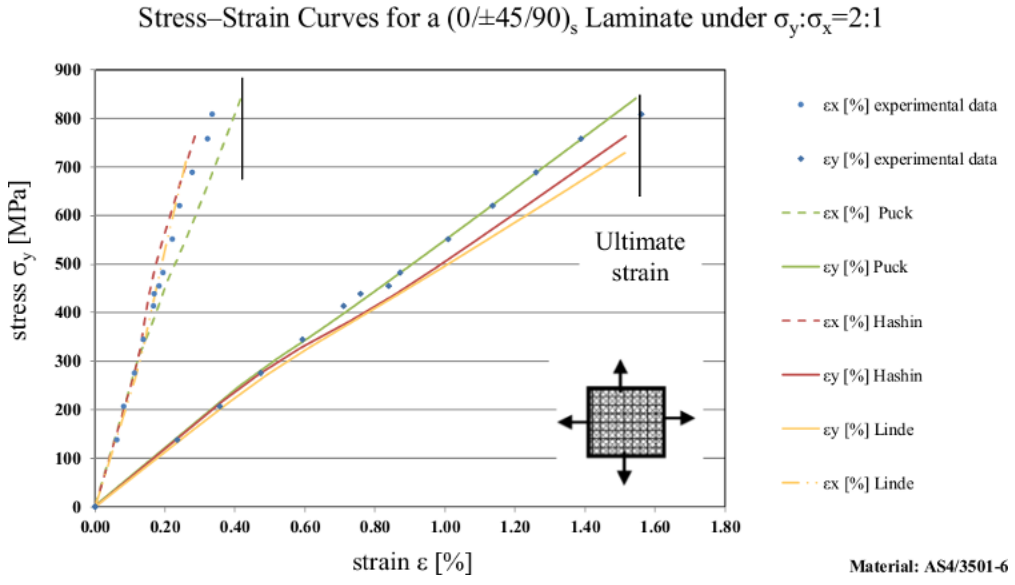

FIGURE B.5: Comparison of stress-strain curves of TC08.

TABLE B.1: Comparison of the simulation results for TC08

		Built-in	Linde	Puck (AlfaLam)
Overall Curve Match		+	+	+
Prediction of Initial Failure		+	+	+
Prediction of Final Failure Stress		+ +	+ +	+ +
Prediction of Final Failure Strain	ε_x	+ +	+ +	+ +
	ε_y	+	+ +	+

Test Case 12:

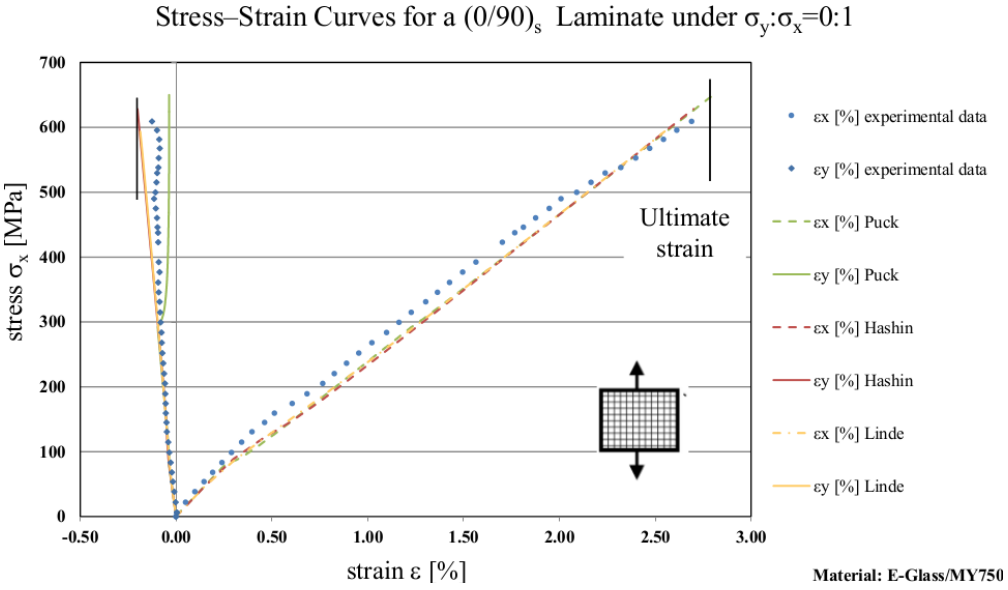

FIGURE B.6: Comparison of stress-strain curves of TC12.

TABLE B.2: Comparison of the simulation results for TC12

		Built-in	Linde	Puck (AlfaLam)
Overall Curve Match		+ +	+ +	+ +
Prediction of Initial Failure		+	+	+
Prediction of Final Failure Stress		+ +	+	+ +
Prediction of Final Failure Strain	ε_x	+ +	- -	+ +
	ε_y	- -	-	- -

Test Case 13:

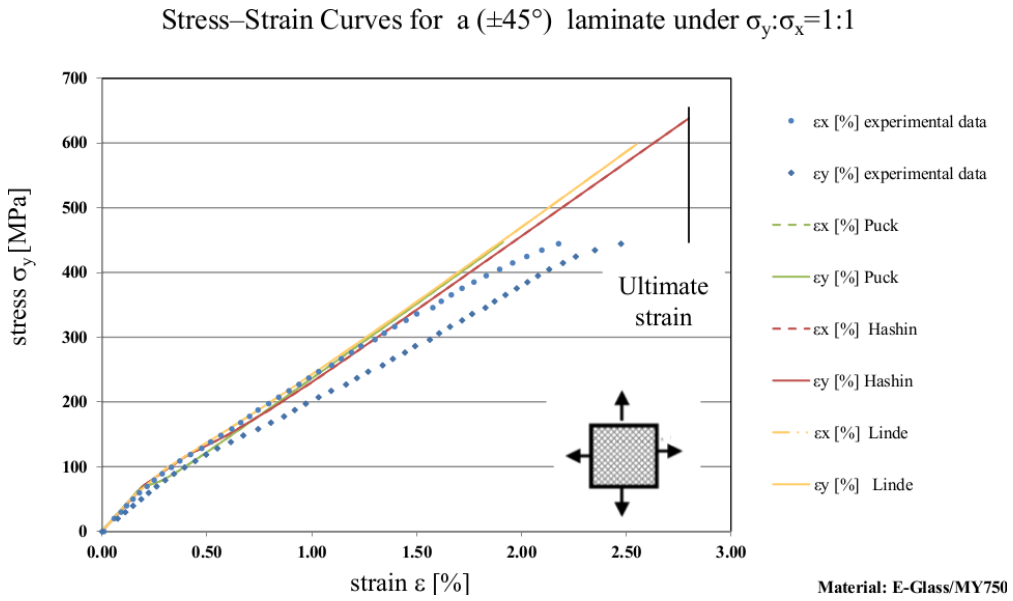

FIGURE B.7: Comparison of stress-strain curves of TC13.

TABLE B.3: Comparison of the simulation results for TC13

		Built-in	Linde	Puck (AlfaLam)
Overall Curve Match		+	+	+
Prediction of Initial Failure		+ +	+ +	+ +
Prediction of Final Failure Stress		-	○	+ +
Prediction of Final Failure Strain	ε_x	+	+	+ +
	ε_y	○	+ +	+

Test Case 14:

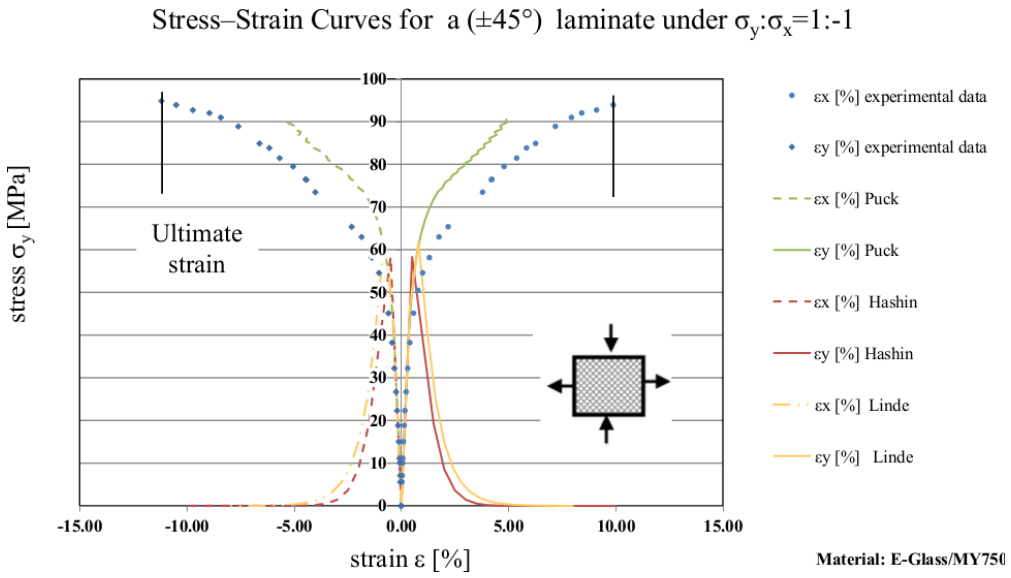

FIGURE B.8: Comparison of stress-strain curves of TC14.

TABLE B.4: Comparison of the simulation results for TC14

		Built-in	Linde	Puck (AlfaLam)
Overall Curve Match		-	-	○
Prediction of Initial Failure		- -	- -	○
Prediction of Final Failure Stress		-	○	+ +
Prediction of Final Failure Strain	ε_x	- -	- -	- -
	ε_y	- -	- -	- -

Appendix C

Data Sheets

Eigenschaften	Norm	Einheit	Wert
Dichte	ISO 1183/A	g/cm³	ca. 2,0
Biegefestigkeit bei 23°C parallel	ISO 178	MPa	min. 600
Biegefestigkeit bei 23°C senkrecht	ISO 178	MPa	min. 600
Elastizitätsmodul aus dem Biegeversuch	ISO 178	GPa	ca. 25
Kerbschlagzähigkeit (Charpy) parallel zur Schichtrichtung in Längsrichtung	ISO 179/3C	kJ/m²	min. 300
Kerbschlagzähigkeit (Charpy) parallel zur Schichtrichtung in Querrichtung	ISO 179/3C	kJ/m²	min. 250
Kerbschlagzähigkeit (Charpy) senkrecht zur Schichtrichtung in Längsrichtung	ISO 179/3C	kJ/m²	min. 200
Kerbschlagzähigkeit (Charpy) senkrecht zur Schichtrichtung in Querrichtung	ISO 179/3C	kJ/m²	min. 200
Schlagzähigkeit (Charpy) parallel zum Laminat	ISO 179/3C	kJ/m²	min. 350
Schlagzähigkeit (Charpy) senkrecht zum Laminat	ISO 179/3C	kJ/m²	min. 350
Zugfestigkeit in Längs- / und Querrichtung	ISO 527	MPa	min. 400/400
Druckfestigkeit senkrecht zu den Schichten bei 23°C	ISO 604	MPa	min. 400
Isolationswiderstand nach Eintauchen in Wasser	IEC 167	Ohm	min. 10^9
Durschlagspannung bei 90°C in Öl parallel zur Schichtrichtung	IEC 60893/IEC243	kV	min. 40
Permitivität bei 1MHz	ASTM D150/ ASTM D229	-	max. 5,5
Dielektrischer Verlustfaktor 1MHz	ASTM D150/ ASTM D229	-	max. 0,04
Thermisches Langzeitverhalten	IEC 60216	T.I.	180
Wasseraufnahme (Dicke 4 mm)	ISO 62 / 1	mg	max. 20

FIGURE C.1: Excerpt from the data sheet of the Gatex material.

MECHANICAL PROPERTIES

Product Denomination	GG800T-DT120-38 (H 100 cm)			
Weaving Style	Twill 2x2			
Yarn Type	STS40 F13 24K			
F.A.W. (g/m^2)	800			
Fiber Volume Fraction	53%			
Resin/Matrix System	DT120			
Resin Content (By Weight)	38%			
Cure Conditions vs. Mechanical Data	Autoclave 130°C / 90 min / 6 bar			
Average Density of Cured Sample (g/cm^3)	1.50			
Test Conditions	18-20°C Dry			
TEST ID	CM12-09			
TENSILE 0°	ASTM 3039			
Average Thickness Specimen (mm)	3,49			
Tensile modulus (GPa)	54,90			
Tensile strength (MPa)	807,40			
Elongation at break (%)	1,43			
Tensile Poisson ratio (-)				
TENSILE 90°	ASTM 3039			
Average Thickness Specimen (mm)	3,49			
Tensile modulus (GPa)	54,70			
Tensile strength (MPa)	706,60			
Elongation at break (%)	1,26			
Tensile Poisson ratio (-)				
COMPRESSION 0°	ASTM 6641			
Average Thickness Specimen (mm)	3,53			
Compression modulus (GPa)	61,80			
Compression strength (MPa)	546,40			
Elongation at break (%)	0,98			
Compression Poisson ratio (-)				
COMPRESSION 90°	ASTM 6641			
Average Thickness Specimen (mm)	3,49			
Compression modulus (GPa)	62,35			
Compression strength (MPa)	538,80			
Elongation at break (%)	0,96			
Compression Poisson ratio (-)				
IN-PLAIN SHEAR	EN 6031			
Shear modulus (GPa)	3,74			
Shear strength (MPa)	91,9			

Preliminary data of reference, to be intended provisional, pending further investigation and completion

FIGURE C.2: Data sheet for the material of the battery case

Bibliography

[1] Helmut Schürmann. *Konstruieren mit Faser-Kunststoff-Verbunden*. VDI-Buch. Springer Berlin Heidelberg, 2007. ISBN 978-3-540-72189-5. doi: 10.1007/978-3-540-72190-1_3. URL http://dx.doi.org/10.1007/978-3-540-72190-1_3.

[2] Chokri Cherif. *Textile Werkstoffe für den Leichtbau*. Springer Berlin Heidelberg, 2011. ISBN 978-3-642-17991-4. doi: 10.1007/978-3-642-17992-1_3. URL http://dx.doi.org/10.1007/978-3-642-17992-1_3.

[3] R&G Faserverbundwerkstoffe GmbH. *Handbuch Faserverbundwerkstoffe*. R&G Faserverbundwerkstoffe GmbH, 2003. URL http://www.r-g.de.

[4] Jenny+CoAG. Verstärkungsmaterialien, June 2014. URL http://www.jenny.ch/Brosch%C3%BCren_Flyer_2012/Deutsch/Verst%C3%A4rkungsmaterialien_2011_D.pdf.

[5] Alfred Puck. *Festigkeitsanalyse von Faser-Matrix-Laminaten: Modelle für die Praxis*. hanser Verlag, 1996. ISBN 3-446-18194-6. URL http://www.klub.tu-darmstadt.de/forschungsbericht/downloads_3/downloads_3.de.jsp.

[6] A. Puck and M. Mannigel. Physically based non-linear stress–strain relations for the inter-fibre fracture analysis of {FRP} laminates. *Composites Science and Technology*, 67(9):1955 – 1964, 2007. ISSN 0266-3538. doi: http://dx.doi.org/10.1016/j.compscitech.2006.10.008. URL http://www.sciencedirect.com/science/article/pii/S0266353806003952.

[7] Lutz Nasdala. *FEM – Formelsammlung Statik und Dynamik*. Springer Vieweg, 2012. ISBN 978-3-8348-2260-4. doi: DOI10.1007/978-3-8348-2260-4. URL http://www.springer.com/springer+vieweg/bauwesen/konstruktion/book/978-3-8348-1841-6.

[8] Protech Composites. Carbon fiber sandwich panels, September 2014. URL http://www.thomasnet.com/profile/30192759/protech-composites.html.

[9] A Mukherjee and B Varughese. Design guidelines for ply drop-off in laminated composite structures. *Composites Part B: Engineering*, 32(2):153 – 164, 2001. ISSN 1359-8368. doi: http://dx.doi.org/10.1016/S1359-8368(00)00038-X. URL http://www.sciencedirect.com/science/article/pii/S135983680000038X.

[10] Ever J. Barbero. *Finite Element Analysis of Composite Materials using Abaqus^{TM}*. CRC Press, 2013. ISBN 978-1-466-51661-8. URL http://www.crcpress.com/product/isbn/9781466516618.

[11] VDI-Fachbereich Kunststofftechnik. *VDI2014 Blatt 3: Entwicklung von Bauteilen aus Faser-Kunststoff-Verbund - Berechnungen*. beuth Verlag, 2006. URL http://www.klub.tu-darmstadt.de/forschungsbericht/downloads_3/downloads_3.de.jsp.

[12] M.J. Hinton, A.S. Kaddour, and P.D. Soden. Evaluation of failure prediction in composite laminates: background to 'part b' of the exercise. *Composites Science and Technology*, 62(12–13):1481 – 1488, 2002. ISSN 0266-3538. doi: http://dx.doi.org/10.1016/S0266-3538(02)00094-5. URL http://www.sciencedirect.com/science/article/pii/S0266353802000945.

[13] N.N. Deltatech product information, March 2011.

[14] World Economic Forum. Carbon composites one of top 10 emerging technologies 2014. *Reinforced Plastics*, 58(3):8 –, 2014. ISSN 0034-3617. doi: http://dx.doi.org/10.1016/S0034-3617(14)70120-1. URL http://www.sciencedirect.com/science/article/pii/S0034361714701201.

[15] AVK – Industrievereinigung Verstärkte Kunststoffe e. V. *Handbuch Faserverbundkunststoffe/Composites*. Springer Fachmedien Wiesbaden, 2013. ISBN 978-3-658-02754-4. doi: 10.1007/978-3-658-02755-1_3. URL http://dx.doi.org/10.1007/978-3-658-02755-1_3.

[16] Roman Teschner. *Glasfasern*. Springer Berlin Heidelberg, 2013. ISBN 978-3-642-38328-1. doi: 10.1007/978-3-642-38329-8_10. URL http://dx.doi.org/10.1007/978-3-642-38329-8_10.

[17] Peter Morgan. *Carbon Fibers and Their Composites*. VDI-Buch. CRC Press, 2005. ISBN 978-0-8247-0983-9. doi: 10.1201/9781420028744.fmatt. URL http://dx.doi.org/10.1201/9781420028744.fmatt.

[18] Salil K. Roy Manas Chanda. *Plastics Technology Handbook*. CRC Press, 2006. ISBN 978-0-8493-7039-7. doi: doi:10.1201/9781420006360.ch2. URL http://dx.doi.org/10.1007/978-3-658-02755-1_3.

[19] Kevin Anthony Brown. *Finite Element loading of static and dynamic impact behavior of thermoplastic composite sandwich structures*. PhD thesis, University of Nottingham, 2007.

[20] George E. Mase G. Thomas Mase, Ronald E. Smelser. *Continuum Mechanics for Engineers, Third Edition*. CRC Press, 2010. ISBN 978-1-4200-8538-9. URL http://www.crcpress.com/product/isbn/9781420085389.

[21] Talreja Ramesh and Chandra Veer Singh. *Damage and Failure of Composite Materials*. Oxford University Press, 2012. ISBN 978-1-139-41530-9. URL http://www.cambridge.org/us/academic/subjects/engineering/materials-science/damage-and-failure-composite-materials.

[22] Richard M. Christensen. *Damage and Failure of Composite Materials*. Oxford University Press, 2013.

[23] P.D. Soden, M.J. Hinton, and A.S. Kaddour. Biaxial test results for strength and deformation of a range of e-glass and carbon fibre reinforced composite laminates: failure exercise benchmark data. *Composites Science and Technology*, 62(12–13):1489 – 1514, 2002. ISSN 0266-3538. doi: http://dx.doi.org/10.1016/S0266-3538(02)00093-3. URL http://www.sciencedirect.com/science/article/pii/S0266353802000933.

[24] P.D. Soden, M.J. Hinton, and A.S. Kaddour. A comparison of the predictive capabilities of current failure theories for composite laminates. *Composites Science and Technology*, 58(7):1225 – 1254, 1998. ISSN 0266-3538. doi: http://dx.doi.org/10.1016/S0266-3538(98)00077-3. URL http://www.sciencedirect.com/science/article/pii/S0266353898000773.

[25] P.D. Soden, M.J. Hinton, and A.S. Kaddour. Lamina properties, lay-up configurations and loading conditions for a range of fibre-reinforced composite laminates. *Composites Science and Technology*, 58(7):1011 – 1022, 1998. ISSN 0266-3538. doi: http://dx.doi.org/10.1016/S0266-3538(98)00078-5. URL http://www.sciencedirect.com/science/article/pii/S0266353898000785.

[26] M.J Hinton and P.D Soden. Predicting failure in composite laminates: the background to the exercise. *Composites Science and Technology*, 58(7):1001 – 1010, 1998. ISSN 0266-3538. doi: http://dx.doi.org/10.1016/S0266-3538(98)00074-8. URL http://www.sciencedirect.com/science/article/pii/S0266353898000748.

[27] M.J Hinton, A.S Kaddour, and P.D Soden. A comparison of the predictive capabilities of current failure theories for composite laminates, judged against experimental evidence. *Composites Science and Technology*, 62(12–13):1725 – 1797, 2002. ISSN 0266-3538. doi: http://dx.doi.org/10.1016/S0266-3538(02)00125-2. URL http://www.sciencedirect.com/science/article/pii/S0266353802001252.

[28] M.J. Hinton, A.S. Kaddour, and P.D. Soden. Evaluation of failure prediction in composite laminates: background to 'part c' of the exercise. *Composites Science and Technology*, 64(3–4):321 – 327, 2004. ISSN 0266-3538. doi: http://dx.doi.org/10.1016/S0266-3538(03)00216-1. URL http://www.sciencedirect.com/science/article/pii/S0266353803002161. Failure criteria in fibre reinforced polymer composites Part C: Additional theories conclusions and recommendations.

[29] M.J Hinton, A.S Kaddour, and P.D Soden. A further assessment of the predictive capabilities of current failure theories for composite laminates: comparison with experimental evidence. *Composites Science and Technology*, 64(3–4):549 – 588, 2004. ISSN 0266-3538. doi: http://dx.doi.org/10.1016/S0266-3538(03)00227-6. URL http://www.sciencedirect.com/science/article/pii/S0266353803002276. Failure criteria in fibre reinforced polymer composites Part C: Additional theories conclusions and recommendations.

[30] V.D. Azzi and S.W. Tsai. Anisotropic strength of composites. *Experimental Mechanics*, 5(9):283–288, 1965. ISSN 0014-4851. doi: 10.1007/BF02326292. URL http://dx.doi.org/10.1007/BF02326292.

[31] Dassault Systèmes. *ABAQUS 6.13 Documentation*. Dassault Systèmes Simulia Corp., Providence, RI, 2013.

[32] Stephen W. Tsai and Edward M. Wu. A general theory of strength for anisotropic materials. *Journal of Composite Materials*, 5(1):58–80, 1971. doi: 10.1177/002199837100500106. URL http://jcm.sagepub.com/content/5/1/58.abstract.

[33] A. Puck and H. Schürmann. Failure analysis of {FRP} laminates by means of physically based phenomenological models. *Composites Science and Technology*, 62(12–13):1633 – 1662, 2002. ISSN 0266-3538. doi: http://dx.doi.org/10.1016/S0266-3538(01)00208-1. URL http://www.sciencedirect.com/science/article/pii/S0266353801002081.

[34] A. Puck, J. Kopp, and M. Knops. Guidelines for the determination of the parameters in puck's action plane strength criterion. *Composites Science and Technology*, 62(3):371 – 378, 2002. ISSN 0266-3538. doi: http://dx.doi.org/10.1016/S0266-3538(01)00202-0. URL http://www.sciencedirect.com/science/article/pii/S0266353801002020.

[35] Jianxin Tao C. T. Sun. Prediction of failure envelopes and stress/strain behaviour of composite laminates. *Composites Science and Technology*, 58(9):1125–1136, 1998.

[36] Pedro P. Camanho, Carlos G. Dávila, Silvestre T. Pinho, Lorenzo Iannucci, and Paul Robinson. Prediction of in situ strengths and matrix cracking in composites under transverse tension and in-plane shear. *Composites Part A: Applied Science and Manufacturing*, 37(2):165 – 176, 2006. ISSN 1359-835X. doi: http://dx.doi.org/10.1016/j.compositesa.2005.04.023. URL http://www.sciencedirect.com/science/article/pii/S1359835X05002526. CompTest 2004.

[37] M. Knops and C. Bögle. Gradual failure in fibre/polymer laminates. *Composites Science and Technology*, 66(5):616 – 625, 2006. ISSN 0266-3538. doi: http://dx.doi.org/10.1016/j.compscitech.2005.07.044. URL http://www.sciencedirect.com/science/article/pii/S026635380500312X. Reliability and Life Prediction of Composite Structures 9th European-Japanese Symposium on Composite Materials.

[38] A. Matzenmiller, J. Lubliner, and R.L. Taylor. A constitutive model for anisotropic damage in fiber-composites. *Mechanics of Materials*, 20(2):125 – 152, 1995. ISSN

0167-6636. doi: http://dx.doi.org/10.1016/0167-6636(94)00053-0. URL http://www.sciencedirect.com/science/article/pii/0167663694000530.

[39] Tobias Kremer. *KLuB-VDI2014 v2.0*. TU Darmstadt, Fachgebiet Konstruktiver Leichtbau und Bauweisen, Petersenstraße 30, 64287 Darmstadt, January 2007.

[40] N. D. Dhurvey, Priyanka; Mittal. Study the effect of externally and internally ply drop-off in composite laminate analysis. *ARPN Journal of Engineering and Applied Sciences*, 8(4):153 – 164, 2013. ISSN 1819-6608. doi: http://connection.ebscohost.com/c/articles/89165864/study-effect-externally-internally-ply-drop-off-composite-laminate-analysis. URL http://www.arpnjournals.com/jeas/research_papers/rp_2013/jeas_0413_881.pdf.

[41] ISOVOLTA-GATEX GmbH. Gx 11.3309 gws / composite werkstoff mit hoher mechanischer festigkeit, September 2012.

[42] A. Schranzinger. 20140424_andritz_pressure plate_fea_design change. Technical report, AVL List GmbH, Hans-List Platz 1, April 2014.

[43] Gunter Erhard. *Konstruieren mit Kunststoffen*. VDI-Buch. Carl Hanser Verlag GmbH & Co. KG, 2008. ISBN 978-3-446-41750-2. doi: 10.3139/9783446417502. URL http://www.hanser-elibrary.com/isbn/9783446416468.

[44] Peter Linde and Henk de Boer. Modelling of inter-rivet buckling of hybrid composites. *Composite Structures*, 73(2):221 – 228, 2006. ISSN 0263-8223. doi: http://dx.doi.org/10.1016/j.compstruct.2005.11.062. URL http://www.sciencedirect.com/science/article/pii/S0263822305003910.